RCA REVIEW

a technical journal

RADIO AND ELECTRONICS
RESEARCH • ENGINEERING

VOLUME XVI JUNE 1955 NO. 2

RCA REVIEW, published quarterly in March, June, September, and December by RCA Laboratories, Radio Corporation of America, Princeton, New Jersey. Entered as second class matter July 3, 1950 at the Post Office at Princeton, New Jersey, under the act of March 3, 1879. Subscription price in the United States and Canada; one year $2.00, two years $3.50, three years $4.50; in other countries: one year $2.40, two years $4.30, three years $5.70. Single copies in the United States, $.75; in other countries, $.85.

RCA REVIEW

a technical journal

RADIO AND ELECTRONICS
RESEARCH • ENGINEERING

Published quarterly by
RCA LABORATORIES
in cooperation with all subsidiaries and divisions of
RADIO CORPORATION OF AMERICA

VOLUME XVI | JUNE, 1955 | NUMBER 2

CONTENTS

RCA REVIEW is regularly abstracted and indexed by *Industrial Arts Index, Science Abstracts* (I.E.E.-Brit.), *Electronic Engineering Master Index, Chemical Abstracts, Proc. I.R.E., and Wireless Engineer.*

RCA REVIEW

BOARD OF EDITORS

THE EFFECT OF INITIAL NOISE CURRENT AND VELOCITY CORRELATION ON THE NOISE FIGURE OF TRAVELING-WAVE TUBES*

By

Stanley Bloom

Research Laboratory, RCA Laboratories,
Princeton, N. J.

Summary—*The noise content in a single-velocity electron beam, and the noise figure of a traveling-wave tube, are discussed for the general case in which there may be correlation between the noise current and the noise velocity excitations existing near the virtual cathode. Whereas in the absence of correlation only two independent noise current space-charge waves exist in the beam as described in earlier analyses, finite correlation now introduces a third wave which results in the addition of a correction term to the previous expressions for beam "noisiness" and noise figure. As the initial correlation increases from zero to unity, the minimum noise figure decreases to unity. However, neither the amount of correlation nor the actual values of the initial noise excitations near the virtual cathode have any effect upon the conditions which minimize the noise figure. These optimizing conditions are stated in terms of only two variables, the standing-wave ratio of the resultant noise current wave and the position of the helix with respect to this wave. The values of these two variables are unique.*

The various formulas describing the conditions leading to the lowest noise figure are represented in terms of a new parameter which greatly simplifies the design curves.

Introduction

SEVERAL papers have recently appeared on the subject of the minimum noise figure of traveling-wave tubes.[1-3] These analyses proceed from the following model: Two independent space-charge waves of noise convection current exist on the electron beam, one wave being excited by a shot-noise current fluctuation I_a at or near the virtual cathode of the electron gun, the other wave being excited by

---

* Decimal Classification: R339.2.

[1] F. N. H. Robinson, "Microwave Shot Noise in Electron Beams and the Minimum Noise Factor of Traveling-Wave Tubes and Klystrons," *Jour. Inst. Radio Eng.* (Brit.), Vol. 14, p. 79, February, 1954.

[2] S. Bloom and R. W. Peter, "A Minimum Noise Figure for the Traveling-Wave Tube," *RCA Review*, Vol. 15, p. 252, June, 1954.

[3] J. R. Pierce and W. E. Danielson, "Minimum Noise Figure of Traveling-Wave Tubes with Uniform Helices," *Jour. Appl. Phys.*, Vol. 25, p. 1163, September, 1954.

a thermal-noise velocity (or "voltage") fluctuation V_a completely *uncorrelated* with I_a. Being statistically independent, these two noise-current waves add quadratically, the resultant current having the form of a constant plus a sinusoid. Since no r-f power is exchanged between the beam and external circuits in the region preceding the helix, the beam "noisiness"[4]—product of the resultant noise current minimum and maximum—is constant and independent of changes of beam voltage or geometry. This invariance of the beam noisiness results in the traveling-wave tube having a minimum noise figure, since any beneficial lowering of the current-wave maximum is accompanied by a deleterious increase of the wave minimum.

It is, however, not yet known whether the space-charge cushion in front of the cathode does produce some finite degree of correlation between the initial noise current and velocity fluctuations. To encompass this possibility, Haus[5] has generalized the theory in a rigorous fashion. Making use of correlation-function analysis, he has derived expressions for beam noisiness and minimum noise factor applicable for any degree of initial correlation.

It is one of the purposes of this paper to show how correlation can be included in the treatment of noise figure in a very simple manner without an appeal to the intricate mathematics of correlation-function theory. For this purpose a correlation factor, κ, is introduced into the transmission-line formalism of an earlier paper.[2]

On the basis of such a phenomenological treatment the physical situation becomes clearer; *there is now a third noise-current space-charge wave on the beam excited by the correlated portions of* V_a *and* I_a, *and this third wave is uncorrelated with the two waves arising from the uncorrelated parts of* V_a *and* I_a.

Fortunately for design purposes we shall see that neither the degree of correlation between the initial noise current and noise velocity nor the actual values of I_a and V_a have any effect upon the conditions for minimizing the amplifier noise figure, although, to be sure, they do affect the minimum value thus obtained. Thus the optimum noise-current standing-wave ratio in the helix region and the optimum position of the helix with respect to the current standing wave remain as given in the earlier paper,[2] even in the presence of finite initial correlation.

A convenient parameter will be described which greatly simplifies

---

[4] J. R. Pierce, "A Theorem Concerning Noise in Electron Streams," *Jour. Appl. Phys.*, Vol. 25, p. 931, August, 1954.

[5] H. A. Haus, "Noise in One-Dimensional Electron Beams," paper presented at *I.R.E. Conference on Electron Devices*, Orono, Maine, 1954.

the formulas and design curves relating the characteristic constants of a given traveling-wave tube to the optimum noise current standing-wave ratio and optimum helix position.

Total Noise-Current Standing Wave and the Beam Noisiness

The system being considered is the same as that described in the previous paper[2] and is shown schematically in Figure 1. The region between the initial plane a where the beam first begins to act as a whole, and plane c where the helix drift space starts is treated as a general impedance transformer whose properties are a function of the d-c accelerating voltages and the beam geometry. Thus the r-f noise current and voltage at plane c are obtainable from their values at plane a once the transformer is known.

The analysis is started by making use of the fact that at the initial plane a there is a noise current excitation I_a due to shot noise and a noise velocity, or voltage,[6] excitation V_a due to the Maxwellian thermal velocity distribution. In contrast to the previous treatment[2] an arbitrary amount of correlation of V_a with I_a is now assumed. This is taken into account by introducing a purely formal "correlation factor"

$$0 \leq \kappa \leq 1$$

such that $\kappa = 0$ for no correlation between I_a and V_a, and $\kappa = 1$ for full correlation. Three independent pairs of current and voltage noise waves are thus initiated at plane a:

$$\begin{aligned} I_{(1)}(a) &= 0 \\ V_{(1)}(a) &= (1-\kappa)\, V_a \\ I_{(2)}(a) &= (1-\kappa)\, I_a \\ V_{(2)}(a) &= 0 \\ I_{(3)}(a) &= \kappa I_a \\ V_{(3)}(a) &= \kappa V_a. \end{aligned} \tag{1}$$

In the helix drift region beyond plane c, the beam characteristic impedance,[6] $W = 2V_0\omega_p/I_0\omega$, is constant. The resultant noise current and noise voltage in this drift region consist of the quadratic sums of the three uncorrelated components;

---

[6] S. Bloom and R. W. Peter, "Transmission-Line Analog of a Modulated Electron Beam," *RCA Review*, Vol. 15, p. 95, March, 1954.

$$|I(\phi)|^2 = \Sigma_n |I_n(\phi)|^2$$
$$|V(\phi)|^2 = \Sigma_n |V_n(\phi)|^2, \quad n = 1, 2, 3 \tag{2}$$

where the impedance-transformer equations for the drift space are

$$V_n(\phi) = V_n(c) \cos\phi + jWI_n(c) \sin\phi$$
$$I_n(\phi) = jW^{-1}V_n(c) \sin\phi + I_n(c) \cos\phi. \tag{3}$$

Thus

$$W^2|I(\phi)|^2 = \Sigma_n |V_n(c) \sin\phi - jWI_n(c) \cos\phi|^2. \tag{4}$$

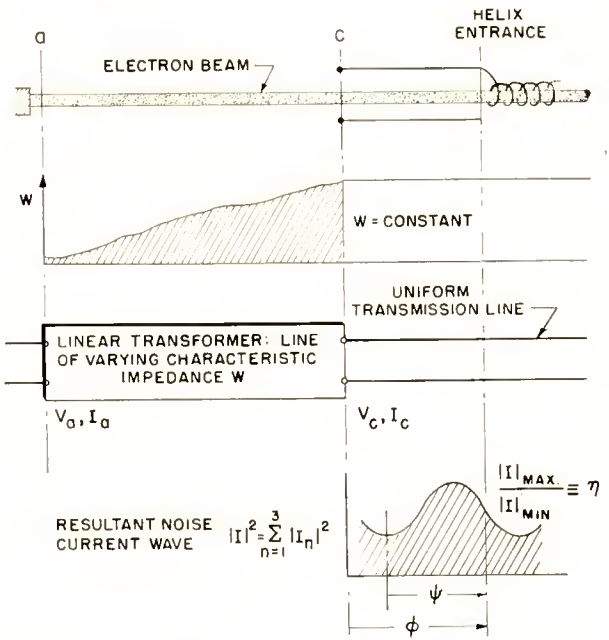

Fig. 1—The portion of the electron beam from plane a, near the virtual cathode, to plane c, where the helix drift-space begins, is represented by a lossless transmission line of varying characteristic impedance. The subsequent portion of the beam with constant characteristic impedance is represented by a uniform line. The three independent noise-current space-charge waves of Equation (1) add quadratically to produce a resultant wave with a standing-wave ratio of η and a current minimum lying ψ space-charge-wave radians from the helix entrance.

It will simplify notation if we now introduce two noise quantities corresponding to the real and imaginary parts of the noise power:

$$P_R(c) \equiv \frac{1}{2} \Sigma_n [I_n(c)\, V^*_n(c) + I^*_n(c)\, V_n(c)] \tag{5a}$$

$$P_R(c) \equiv \frac{1}{2} j\Sigma_n [I_n(c)\ V^*_n(c) - I^*_n(c)\ V_n(c)]. \tag{5b}$$

These two quantities are analogous to Haus'[5] real and imaginary parts, $H(c)$ and $\Lambda(c)$, of the "cross-power density."

Expanding Equation (4) and using Equation (5b),

$$W^2 |I(\phi)|^2 = |V(c)|^2 \sin^2 \phi + W^2 |I(c)|^2 \cos^2 \phi - 2WP_X(c) \sin \phi \cos \phi$$

so that finally the resultant noise current in the helix drift region at the angular position ϕ from plane c has the form of a constant plus cosine:

$$|I(\phi)|^2 = \frac{1}{2} [|I|^2_{\max} + |I|^2_{\min}] + \frac{1}{2} [|I|^2_{\max} - |I|^2_{\min}] \cos (2\phi + \Gamma) \tag{6}$$

where

$$\begin{aligned} W^2[|I|^2_{\max} + |I|^2_{\min}] &= |V(c)|^2 + W^2 |I(c)|^2 \\ W^2[|I|^2_{\max} - |I|^2_{\min}] &= \sqrt{[2WP_X(c)]^2 + [W^2 |I(c)|^2 - |V(c)|^2]^2} \end{aligned} \tag{7}$$

and the phase angle Γ obeys

$$\tan \Gamma = \frac{2WP_X(c)}{W^2|I(c)|^2 - |V(c)|^2}. \tag{8}$$

Equation (6) will be used shortly, but first consider the square of the beam *noisiness*, which is, by Equation (7),

$$W^2|I|^2_{\max}|I|^2_{\min} = |V(c)|^2|I(c)|^2 - P_X^2(c)$$

$$= [A^2|V(a)|^2 + B^2|I(a)|^2 + 2\,AB\,P_X(a)]$$
$$\times [C^2|V(a)|^2 + D^2|I(a)|^2 - 2CD\,P_X(a)]$$
$$- [(AD - BC)\,P_X(a) + BD|I(a)|^2 - AC|V(a)|^2]^2.$$

Here use has been made of the impedance-transformer equation between planes a and c:

$$\begin{aligned} V_n(c) &= AV_n(a) + jBI_n(a) \\ I_n(c) &= jCV_n(a) + DI_n(a), \end{aligned} \tag{9}$$

where elements A, B, C, D are real. On expanding the above expres-

sion and employing the fact that the transformer is lossless, i.e., that $AD + BC = 1$, we see that the beam noisiness is an invariant:

$$W^2|I|^2_{max}|I|^2_{min} = |V(a)|^2|I(a)|^2 - P_X^2(a). \tag{10}$$

This means that the product of the resultant noise-current minimum and maximum along a drifting beam, multiplied by the constant characteristic impedance of that drift region, is invariant to arbitrary impedance transformations preceding the drift region.

Introducing the three uncorrelated space-charge waves at plane a as given by Equation (1), the noisiness, Equation (10), becomes

$$W^2|I|^2_{max}|I|^2_{min} = [(1-\kappa)^2 + \kappa^2]^2|V_a|^2|I_a|^2 - [(j\kappa^2/2)(V^*_a I_a - V_a I^*_a)]^2. \tag{11}$$

In the absence of correlation between V_a and I_a ($\kappa = 0$) this reduces to the result previously obtained,[2]

$$W^2|I|^2_{max}|I|^2_{min} = |V_a|^2|I_a|^2, \tag{12}$$

whereas for full correlation ($\kappa = 1$),

$$W^2|I|^2_{max}|I|^2_{min} = \frac{1}{4}(V^*_a I_a + V_a I^*_a)^2 = P_R^2(a) \tag{13}$$

which is dependent upon the relative phases between V_a and I_a, and is zero when V_a and I_a are in quadrature.

General Expression for the Noise Figure of a Traveling-Wave Tube

The noise figure, F, of a traveling-wave tube is calculated in exactly the same way as in Reference (2) except that the contribution due to the third noise wave arising from the correlated portions of the initial excitations V_a and I_a must be added:

$$\frac{F-1}{k} = \Sigma_n |\alpha V_n(\phi) + j\beta W I_n(\phi)|^2, \quad n = 1, 2, 3$$

which, by Equations (3), becomes

$$\frac{F-1}{k} = \Sigma_n |(\alpha\cos\phi - \beta\sin\phi) V_n(c) + jW(\alpha\sin\phi + \beta\cos\phi) I_n(c)|^2. \tag{14}$$

Here, as before,[2]

$$\alpha \equiv \delta_2 + \delta_3$$
$$\beta \equiv (\delta_2\delta_3 - 4QC)/\sqrt{4QC}$$
$$k \equiv \sqrt{4QC}/2WKT\triangle f$$
$$\sqrt{4QC} \equiv \omega_p/\omega C = WI_0/2V_0C.$$

Equation (14), after expansion, can be simplified by use of Watkins'[7] f-function:

$$\begin{aligned} 2f(\phi) &\equiv 2|\alpha\cos\phi - \beta\sin\phi|^2 \\ &= (f_a + f_i) + (f_a - f_i)\cos(2\phi + \gamma) \end{aligned} \tag{15}$$

where

$$\tan\gamma = \frac{\alpha\beta^* + \alpha^*\beta}{|\alpha|^2 - |\beta|^2}, \qquad \pi \leq \gamma \leq \frac{3\pi}{2} \tag{16}$$

and f_a, f_i are the maximum and minimum values of f respectively, obeying

$$\begin{aligned} 2f_{\substack{a\\i}} &= |\alpha|^2 + |\beta|^2 \pm \sqrt{(|\alpha|^2 - |\beta|^2)^2 + (\alpha^*\beta + \alpha\beta^*)^2} \\ 2\sqrt{f_a f_i} &= -j(\alpha^*\beta - \alpha\beta^*). \end{aligned} \tag{17}$$

Thus Equation (14) becomes

$$\begin{aligned} \frac{F-1}{k} &= |V(c)|^2 f(\phi) + W^2 |I(c)|^2 f(\phi \pm \pi/2) \\ &\quad + W(f_a - f_i) P_X(c)\sin(2\phi + \gamma) - 2WP_R(c)\sqrt{f_a f_i} \\ &= \frac{1}{2}(f_a + f_i)\left[|V(c)|^2 + W^2|I(c)|^2\right] \\ &\quad - \frac{1}{2}(f_a - f_i)\sqrt{[2WP_X(c)]^2 + [|V(c)|^2 - W^2|I(c)|^2]^2} \\ &\quad \times \cos(2\phi + \gamma + \Gamma) - 2WP_R(c)\sqrt{f_a f_i} \\ &= \frac{1}{2}(f_a + f_i) W^2\left[|I|^2_{\max} + |I|^2_{\min}\right] - \frac{1}{2}(f_a - f_i) W^2\left[|I|^2_{\max} - |I|^2_{\min}\right] \\ &\quad \times \cos(2\phi + \gamma + \Gamma) - 2WP_R(c)\sqrt{f_a f_i}. \end{aligned} \tag{18}$$

[7] D. A. Watkins, "Noise Reduction in Beam Type Amplifiers," *Proc. I.R.E.*, Vol. 40, p. 65, January, 1952.

The quantity $P_R(c)$ in the above equation can be replaced by $P_R(a)$ since P_R, like the beam "noisiness", is an invariant.[5] By Equations (5a) and (9),

$$P_R(c) = \frac{1}{2}\Sigma_n \{[jCV_n(a) + DI_n(a)]\,[AV^*_n(a) - jBI^*_n(a)] + [-jCV^*_n(a) + DI^*_n(a)]\,[AV_n(a) + jBI_n(a)]\}$$

$$= \frac{1}{2}(AD + BC)\,\Sigma_n\,[I_n(a)\,V^*_n(a) + I^*_n(a)\,V_n(a)]$$

$$= P_R(a). \tag{19}$$

If, now, angles are measured not from plane c at the beginning of the helix drift region but from the minimum of the resultant noise-current wave, then by Equation (6)

$$\psi = \phi - \left(\frac{\pi - \Gamma}{2}\right)$$

and Equation (18) becomes

$$\frac{F-1}{k} = W^2|I|^2_{\max} f(\psi) + W^2\,|I|^2_{\min} f(\psi + \pi/2) - 2WP_R(a)\,\sqrt{f_a f_i}\,. \tag{20}$$

In the absence of initial correlation, $P_R(a) = 0$ and Equation (20) becomes

$$F - 1 = \frac{W\sqrt{4QC}}{2\,KT\,\triangle f}\left[\,|I|^2_{\max} f(\psi) + |I|^2_{\min} f(\psi + \pi/2)\,\right]. \tag{21}$$

It is interesting to note that this expression can also be derived quite simply as a logical extension of the noise figure formula for the case in which there is only one initial noise source, I_a *or* V_a. In the case of a single noise source

$$F - 1 = \frac{W\sqrt{4QC}}{2\,KT\,\triangle f}\,|I'|^2_{\max} f(\psi), \tag{22}$$

where $|I'|_{\max}$ is the amplitude of the standing wave in the helix region

and ψ is the angle from $|I'|_{\min} = 0$ to the helix. Suppose, now, that the resultant wave $|I|^2$ of Figure 1 is split into two independent components, $|I'|^2$ and $|I''|^2$, spaced $\pi/2$ radians apart with $|I'|_{\max} = |I|_{\max}$ and $|I''|_{\max} = |I|_{\min}$. Then the zero of $|I'|$ is ψ radians from the helix and the zero of $|I''|$ is $\psi + \pi/2$ radians from the helix. The total noise figure, which is the sum of the two independent noise figures, is then, by Equation (22),

$$F - 1 = \frac{W\sqrt{4QC}}{2KT\,\triangle f}\left[\,|I'|^2_{\max} f(\psi) + |I''|^2_{\max} f(\psi + \pi/2)\,\right],$$

which gives the same value for F as Equation (21).

Suppose, on the other hand, that the two independent components $|I'|$ and $|I''|$ are not $\pi/2$ radians apart but rather have a general separation, θ_d. Then, if the zero of $|I'|$ is $\theta + \theta_d/2$ radians from the helix and the zero of $|I''|$ is $\theta - \theta_d/2$ radians from the helix, the noise figure is, again by Equation (22),

$$F - 1 = \frac{W\sqrt{4QC}}{2KT\,\triangle f}\left[\,|I'|^2_{\max} f(\theta + \theta_d/2) + |I''|^2_{\max} f(\theta - \theta_d/2)\,\right]. \quad (23)$$

This is the expression used by Pierce and Danielson[3] and gives the same value as Equation (21), as is shown in the Appendix. The angle of separation θ_d appearing in Equation (23) is a dummy parameter and is swallowed-up when the form of Equation (21) is used.

Minimization of the Noise Figure

Because the beam noisiness $W|I|_{\max}|I|_{\min}$ is invariant, it is convenient to introduce the *noise-current standing-wave ratio*

$$\frac{|I|_{\max}}{|I|_{\min}} \equiv \eta \quad (24)$$

and write the noise figure as

$$\frac{F-1}{k} = W^2|I|_{\min}|I|_{\max}\,[\eta f(\psi) + \eta^{-1} f(\psi + \pi/2)] - 2WP_R(a)\sqrt{f_a f_i}. \quad (25)$$

This general noise figure expression is minimized by giving the bracketed term its lowest value, all other terms being constant for a given

traveling-wave tube. The minimization leads to unique values of the two, and only two, independent variables, η and ψ.

Since $\eta \geqslant 1$, the optimum angle from a current minimum to the beginning of the helix is that making $f(\psi)$ a minimum, f_i, and therefore also $f(\psi + \pi/2) = f_a$. This angle is

$$\psi_{\text{opt}} = (\pi - \gamma)/2 \tag{26}$$

whence

$$\frac{F-1}{k} = W^2 |I|_{\max} |I|_{\min} [\eta f_i + \eta^{-1} f_a] - 2WP_R(a) \sqrt{f_a f_i}.$$

We next optimize with respect to η. Differentiation yields

$$\eta_{\text{opt}} = \sqrt{f_a/f_i}. \tag{27}$$

Practically, this means that the characteristic impedance along the beam in the region between the cathode and the helix drift region is so altered, e.g., by adjusting the d-c accelerating voltages, that in the helix drift region the resultant current wave has the standing-wave ratio of η_{opt}.

Then the *minimum noise figure* is

$$F_{\text{MIN}} = 1 + [W|I|_{\max} |I|_{\min} - P_R(a)] \frac{\sqrt{4QC f_a f_i}}{KT\triangle f}. \tag{28}$$

In the absence of correlation ($\kappa = 0$), $P_R(a) = 0$, and Equation (28) is simply Equation (17) of Reference (2). For partial correlation the noise figure is lowered, until finally with full correlation ($\kappa = 1$), F_{MIN} is unity, by Equation (13).

It is important to note that the optimizing conditions of Equations (26) and (27) are independent of both the degree of initial correlation between V_a and I_a and the actual values of V_a and I_a.

Returning to Equation (25) suppose that the helix entrance is at its *worst* position. There $f(\psi) = f_a$, $f(\psi + \pi/2) = f_i$ so that

$$\psi_{\text{worst}} = -\gamma/2. \tag{29}$$

Thus, as the helix entrance is moved along the beam the noise figure goes through successive minima and maxima spaced $\pi/2$ radians apart. The ratio of worst to best noise figures, as far as angles are concerned, is

$$\frac{F_{MAX}-1}{F_{MIN}-1}=\frac{\frac{1}{2}W|I|_{max}|I|_{min}\,(\eta\eta_{opt}+\eta^{-1}\eta^{-1}_{opt})-P_R(a)}{\frac{1}{2}W|I|_{max}|I|_{min}\,(\eta\eta^{-1}_{opt}+\eta^{-1}\eta_{opt})-P_R(a)}$$

which is a function not only of the characteristic parameters (QC, d, b) of the particular traveling-wave tube but also of the beam conditions (V_a, I_a and κ) at the initial plane. However, in the absence of correlation $P_R(a)=0$, and we have

$$\left(\frac{F_{MAX}-1}{F_{MIN}-1}\right)_{\kappa=0,\ \eta=arbit}=\frac{\eta\eta_{opt}+\eta^{-1}\eta^{-1}_{opt}}{\eta\eta^{-1}_{opt}+\eta^{-1}\eta_{opt}} \tag{30}$$

which is *independent* of the initial noise values. If, in addition, the current-standing-wave ratio is optimized,

$$\left(\frac{F_{MAX}-1}{F_{MIN}-1}\right)_{\kappa=0,\ \eta=\eta opt}=\frac{1}{2}\,(\eta^2_{opt}+\eta^{-2}_{opt}). \tag{31}^*$$

Parameterization of Formulas

It can easily be shown from the secular equation[8] for the traveling-wave tube,

$$\delta^2=(j\delta+jd-b)^{-1}-4QC,$$

that the incremental propagation constants of the three forward-traveling circuit waves obey the following equations:

$$\alpha\equiv\delta_2+\delta_3=-(\delta_1+d+jb)$$
$$\sqrt{4QC}\,\beta\equiv\delta_2\delta_3-4QC=\delta_1\,(\delta_1+d+jb)=-\alpha\delta_1 \tag{32}$$

where QC is Pierce's space-charge factor, d is the loss parameter, and b the velocity parameter. Here $\delta_1=x_1+jy_1$ refers to the gaining wave.

If, now, we suppose that the tube is operated at the helix voltage yielding maximum gain of the growing wave (i.e., $b=b_{max.\ x_1}$), differentiating the secular equation and setting $dx_1/db=0$, gives

$$4QC=-2y_1|\delta_1|-|\delta_1|^2. \tag{33}$$

Thus, from Equations (32) and (33), there result

---

* This equation replaces Equation (33) of Reference (2), which is incorrect.

[8] J. R. Pierce, *Traveling-Wave Tubes*, D. Van Nostrand Company, Inc., New York, N. Y., 1950.

$$\beta/\alpha + \beta^*/\alpha^* = -2\sqrt{\frac{1-\bar{y}^2}{2\bar{y}-1}}$$

$$|\beta/\alpha|^2 = \frac{1}{2\bar{y}-1} \tag{34}$$

where, as a new parameter, the normalized imaginary part of the incremental propagation constant has been introduced:

$$\bar{y} \equiv -y_1/|\delta_1|$$
$$1/2 \leq \bar{y}\ (QC,d) \leq 1. \tag{35}$$

This parameter greatly simplifies many of the formulas and curves. For, from Equations (16), (17), (26), (27),

$$\eta^2_{\text{opt.}} = \frac{1 + |\beta/\alpha|^2 + \sqrt{(1-|\beta/\alpha|^2)^2 + (\beta/\alpha + \beta^*/\alpha^*)^2}}{1 + |\beta/\alpha|^2 - \sqrt{(1-|\beta/\alpha|^2)^2 + (\beta/\alpha + \beta^*/\alpha^*)^2}}$$

$$\tan\gamma = \tan(-2\psi_{\text{opt.}}) = \frac{\beta/\alpha + \beta^*/\alpha^*}{1-|\beta/\alpha|^2},$$

which, by Equations (34), become simply

$$\eta^2_{\text{opt.}} = \frac{1+\sqrt{2(1-\bar{y})}}{1-\sqrt{2(1-\bar{y})}} \tag{36a}$$

$$\cos(-2\psi_{\text{opt.}}) = \sqrt{(1-\bar{y})/2y^2}. \tag{36b}$$

The parameter $\bar{y}$ is shown in Figure 2 as a function of space-charge factor QC and loss factor d. The optimum standing-wave ratio, $\eta_{\text{opt.}}$, and helix position, $\psi_{\text{opt.}}$, are shown in Figure 3 as functions of $\bar{y}$. Both $\eta_{\text{opt.}}$ and $\psi_{\text{opt.}}$ can be represented by a single curve on a Smith chart, Figure 4, the $\bar{y}$ values running along the curve.

If we call the *normalized r-f impedance*[2] of the beam $Z(\psi)/W \equiv V(\psi)/WI(\psi) = r(\psi) + jx(\psi)$, then instead of using $\eta_{\text{opt.}}$ and $\psi_{\text{opt.}}$, an alternative way of expressing the optimizing conditions is to specify the optimum value of r-f "resistance" and "reactance" at the helix entrance. These are easily found to be (see Equation (38a) of Reference (2))

$$r_{\text{opt.}} = \bar{y}/\sqrt{2\bar{y} - 1}$$
$$x_{\text{opt.}} = \sqrt{(1 - \bar{y}^2)/(2\bar{y} - 1)}. \tag{37}$$

and appear as the coordinates of the curve in Figure 4.

Expression (31) for the noise figure ratio in the absence of correlation, as a function of the parameter $\bar{y}$, is simply

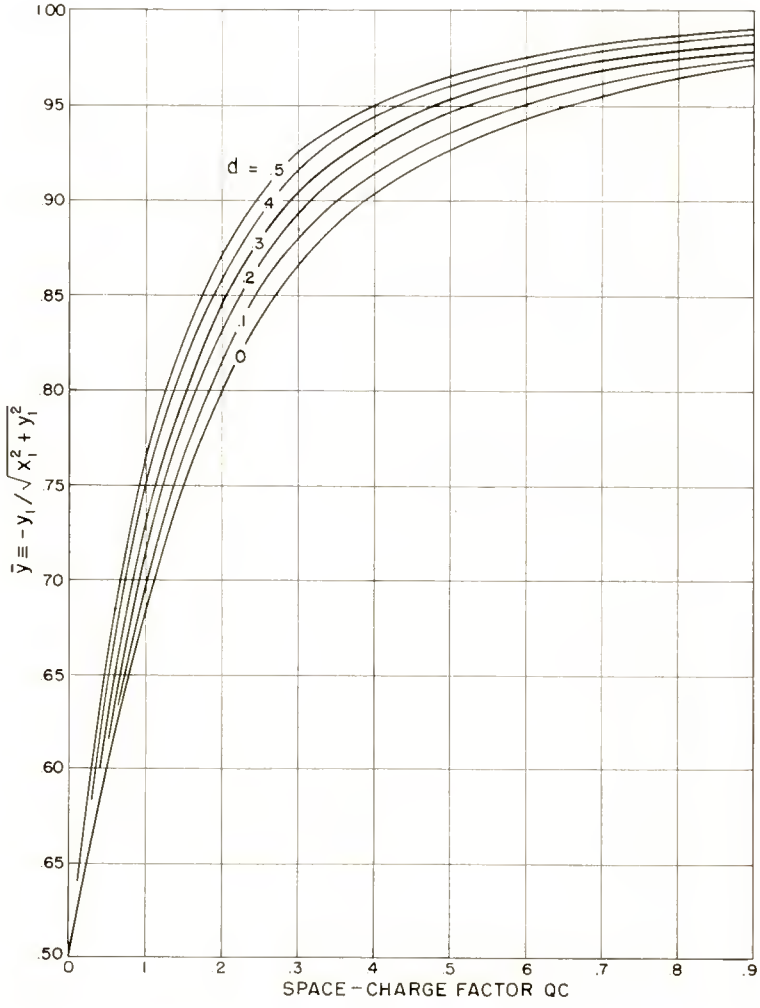

Fig. 2—The parameter $\bar{y} \equiv -y_1/\sqrt{x_1^2 + y_1^2}$ as a function of the space-charge factor QC and the loss factor d of a traveling-wave tube operating at maximum gain of the growing wave.

$$\frac{F_{MAX}-1}{F_{MIN}-1}=\frac{3-2\bar{y}}{2\bar{y}-1} \tag{38}$$

and is shown as the dashed curve in Figure 3.

The formula for the minimum noise figure, Equation (28), can also be simplified. From Equations (17) and (32),

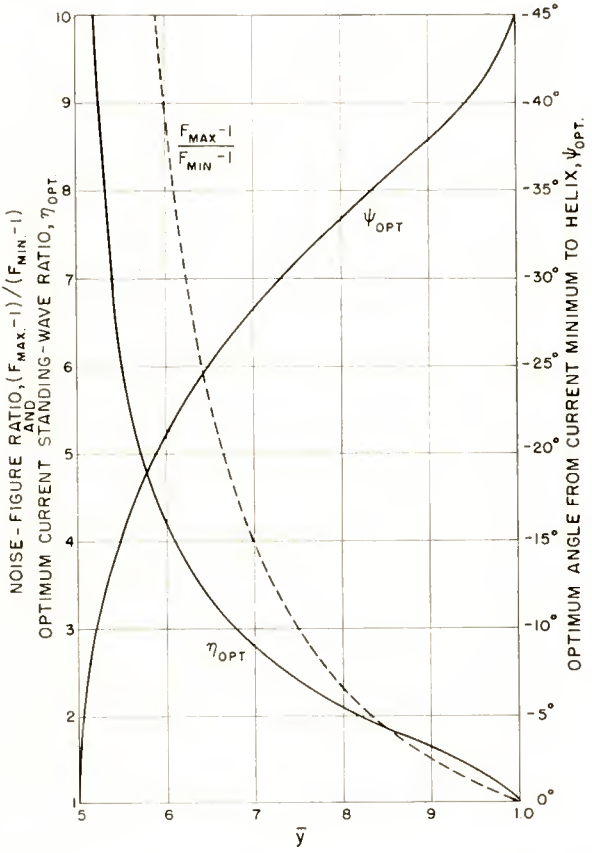

Fig. 3—Suppose the traveling-wave tube is being operated at maximum gain and has known value of QC and d. Then y is read from Figure 2. To obtain the minimum noise figure the impedance transformation between cathode and helix must be adjusted until the noise-current wave in the helix drift region has a standing-wave ratio of $\eta_{opt.}$ and, the helix position must also be adjusted so that a wave minimum lies $\psi_{opt.}$ space-charge-wave radians from the helix entrance. Negative values of $\psi_{opt.}$ indicate that the optimum helix positions are on the gun side of the wave minima. Also, when the impedance transformation is optimal but the helix entrance is moved along the beam, the noise figure goes through successive minima and maxima, spaced $\pi/2$ radians apart. In the absence of initial correlation, the ratio of excess noise figures is then $(F_{MAX}-1)/(F_{MIN}-1)$.

$$\sqrt{4QC\,f_a f_i} = -j|\alpha|^2\sqrt{QC}\,(\beta/\alpha - \beta^*/\alpha^*) = -y_1|\alpha|^2$$
$$= -y_1[(x_1 + d)^2 + (y_1 + b)^2].$$

If the δ-secular equation is split into its real and imaginary parts and QC eliminated there results

$$\sqrt{4QCf_a f_i} = (x_1 + d)/2x_1,$$

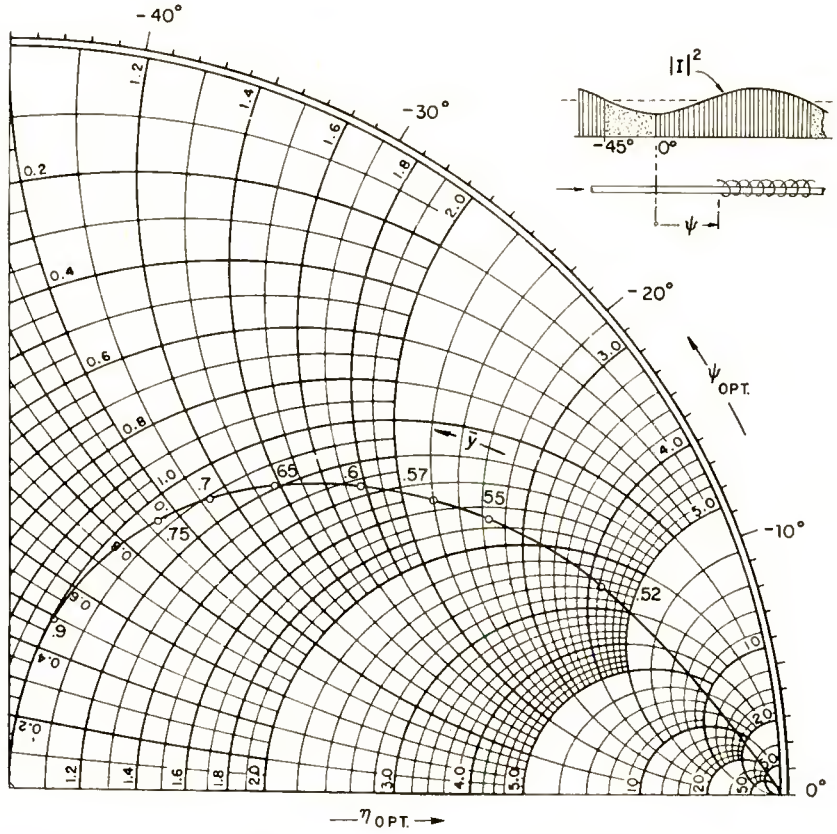

Fig. 4—A Smith-chart representation of $\eta_{opt.}$ and $\psi_{opt.}$ as functions of the parameter $\bar{y}$. Alternatively, this curve also gives the normalized r-f resistance $r_{opt.}$ and r-f reactance $x_{opt.}$ of the noise wave at the helix entrance.

which has also been obtained by Harrison.[9] The minimum noise figure thus takes on the explicit form

[9] S. W. Harrison, "On the Minimum Noise Figure of Traveling-Wave Tubes," *Proc. I.R.E.*, Vol. 43, p. 227, February, 1955.

$$F_{\text{MIN}} = 1 + \frac{[W\,|I|_{\max}\,|I|_{\min} - P_R(a)\,]}{K\,T\,\Delta f}\left(\frac{x_1 + d}{2x_1}\right) \qquad (39)$$

Equation (39) shows that the minimum noise figure is lowest at that value of the velocity parameter b (i.e., helix voltage) which gives maximum x_1 (i.e., maximum gain). The factor $(x_1 + d)/2x_1$ is shown in Figure 5 as a function of QC for various values of d and for b of maximum gain of the growing wave.

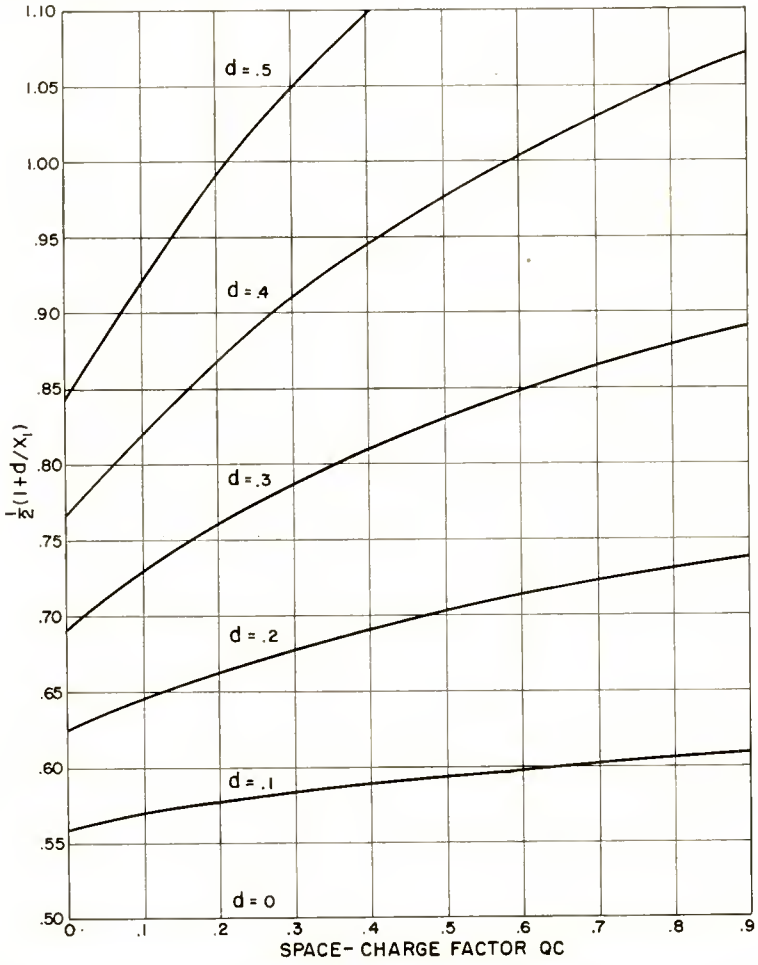

Fig. 5—The minimum noise figure is proportional to the factor $(1 + d/x_1)/2$ which is a function of space charge QC, loss d and the velocity parameter b. When, however, the helix voltage is such as to produce the maximum gain of the growing wave, the factor $(1 + d/x_1)/2$ has the values shown in the figure.

Equation (39), which predicts minimum noise to occur at maximum gain, is one means for testing experimentally whether or not a given tube has truly been optimized for lowest noise figure. Then, an agreement between Equation (38) and experiment would indicate that no correlation exists between the initial excitations V_a and I_a.

Acknowledgment

The author wishes to thank R. W. Peter for many enlightening discussions.

Appendix

It will be shown here that the general expression for the noise figure in the absence of initial correlation, Equation (21), is identical to the Pierce and Danielson[3] expression, Equation (23).

The total current in the helix drift region is the quadratic sum of the two uncorrelated currents:

$$\begin{aligned} |I(\theta)|^2 &= |I'(\theta)|^2 + |I''(\theta)|^2 \\ &= |I'|^2_{\max} \sin^2 (\theta + \theta_d/2) + |I''|^2_{\max} \sin^2 (\theta - \theta_d/2) \\ &= \frac{1}{2}(a+b) - \frac{1}{2}\sqrt{a^2 + b^2 + 2ab\cos 2\theta_d}\cos(2\theta + \zeta) \end{aligned} \tag{A-1}$$

where

$$\begin{aligned} a &\equiv |I'|^2_{\max}, \qquad b \equiv |I''|^2_{\max} \\ \tan\zeta &= \left(\frac{a-b}{a+b}\right)\tan\theta_d \\ &= \left(\frac{a-b}{a+b}\right)\left(\frac{1-\cos 2\theta_d}{1+\cos 2\theta_d}\right)^{1/2} \end{aligned} \tag{A-2}$$

Thus (21) becomes

$$\begin{aligned} &|I|^2_{\max} f(\psi) + |I|^2_{\min} f(\psi + \pi/2) \\ &= \left[\frac{1}{2}(a+b) + \frac{1}{2}\sqrt{a^2 + b^2 + 2ab\cos 2\theta_d}\right] f(\psi) \\ &+ \left[\frac{1}{2}(a-b) - \frac{1}{2}\sqrt{a^2 + b^2 + 2ab\cos 2\theta_d}\right] f(\psi + \pi/2) \\ &= \frac{1}{2}(a+b)(f_a + f_i) + \frac{1}{2}(f_a - f_i)\sqrt{a^2 + b^2 + 2ab\cos 2\theta_d}\cos(2\psi + \gamma) \end{aligned} \tag{A-3}$$

by use of Equation (15).

Since, in Equation (21), ψ is the angle from the resultant current minimum $|I|^2_{\min}$ to the helix, then from Equation (A-1),

$$\psi = \theta + \zeta/2$$

and therefore $\cos(2\psi + \gamma) = \cos\zeta \cos(2\theta + \gamma) - \sin\zeta \sin(2\theta + \gamma)$. This, together with Equation (A-2), puts Equation (A-3) into the form

$$\begin{aligned}
&|I|^2_{\max} f(\psi) + |I|^2_{\min} f(\psi + \pi/2) \\
&= \frac{1}{2}(a+b)\left\{ f_a + f_i + (f_a - f_i)\left[\cos\theta_d \cos(2\theta+\gamma) - \left(\frac{a-b}{a+b}\right) \right.\right. \\
&\qquad \left.\left. \times \sin\theta_d \sin(2\theta+\gamma) \right] \right\} \\
&= a\left[\frac{1}{2}(f_a + f_i) + \frac{1}{2}(f_a - f_i)\cos(2\theta + \theta_d + \gamma) \right] \\
&\quad + b\left[\frac{1}{2}(f_a + f_i) + \frac{1}{2}(f_a - f_i)\cos(2\theta - \theta_d + \gamma) \right] \\
&= |I'|^2_{\max} f(\theta + \theta_d/2) + |I''|^2_{\max} f(\theta - \theta_d/2),
\end{aligned}$$

which is Equation (23).

The above expression can also be written as

$$\begin{aligned}
&\frac{1}{2}(f_a + f_i)\,|I'|^2_{\max}\,[1 + \beta\cos(2\theta + \theta_d + \gamma)] \\
&\qquad + \frac{1}{2}(f_a + f_i)\,|I''|^2_{\max}\,[1 + \beta\cos(2\theta - \theta_d + \gamma)]
\end{aligned}$$

where $\beta \equiv (f_a - f_i)/(f_a + f_i)$. In the particular case of $QC = 0$ the angle $\gamma = \pi$ and so $+\beta$ becomes $-\beta$ in the above expression. This expression is then equivalent to Equation (8) of Pierce and Danielson, thus indicating that their analysis of the optimizing conditions is limited to the $QC = 0$ case.

THE RADECHON, A BARRIER GRID STORAGE TUBE*

By

ARTHUR S. JENSEN

Research Laboratory, RCA Laboratories,
Princeton, N. J.

Summary—*The Radechon is a developmental barrier grid storage tube of simplified design intended for use in systems requiring one or a few electrical reproductions of the original signal with random access, half-tone rendition of about 30 gray levels, and limiting resolution of 400 lines per target diameter. Characteristic curves and resolution curves are given along with a discussion of their use in computing the tube operation in any system.*

In the Radechon, information is stored in the form of an electric charge pattern on a dielectric target. The same electron beam is used for both writing and reading, the distinction of operations being made by a 20-volt switching signal applied at the target. Since the removal of charge from the target constitutes the reading signal, erasure occurs simultaneously. The concept of discharge factor, which is the efficiency of discharging the target per sweep of the beam, is discussed in relation to writing and reading. Discharge factor curves are given, and it is shown that, since the discharge factor is proportional to the slope of the chord to the characteristic curves, it may be measured directly on the characteristic curve at the operating point for any system.

Since storage devices act like low-pass filters, resolution is presented as a curve, showing the dependence of maximum output signal amplitude on the number of signal pulses stored per target diameter. Beam spot size and screen mesh limitations to resolution are discussed.

INTRODUCTION

IN the several years that have elapsed since the initial report on the barrier grid storage tube[1,2] considerable experience has been accumulated in its use. The early version of the tube was complicated by an electron-optical system for separating input and output signals. It was soon recognized that the tube must be simplified both to facilitate its manufacture and to make it easier to operate in equipment. This was desirable even though it meant making the associated

---

* Decimal Classification: R138.31.

[1] Arthur S. Jensen, J. P. Smith, M. H. Mesner, and L. E. Flory, "Barrier Grid Storage Tube and Its Operation," *RCA Review*, Vol. IX, pp. 112-135, March, 1948.

[2] The research on this tube has been a team project lasting over several years and credit must be given to the earlier workers, particularly R. L. Snyder, U. S. Patents 2,470,875, 2,548,405, and 2,563,500; and A. Rose, U. S. Patent 2,563,488. The early work on this tube was performed under Contract W28-003-sc-1541 with the U. S. Army Signal Corps Engineering Laboratories, Evans Signal Laboratory.

circuits more complicated so that signal separation could be accomplished externally. Such a simplified developmental tube has been designed and manufactured, and has been operated in many experimental systems applications with success.

There are several fertile fields of application for a storage tube that provides one or several reproduced copies of the originally impressed signal with random access and reasonable half-tone rendition. Simple analog signal reproduction, binary digit storage with high speed random access,[3] signal-to-noise ratio improvement by integration of repetitive signals,[4] picture storage and reproduction with random access to parts of the picture, and coordinate transformation of stored pictures are a few of the applications in which the Radechon (Figure 1), as such a storage tube, has proved successful.

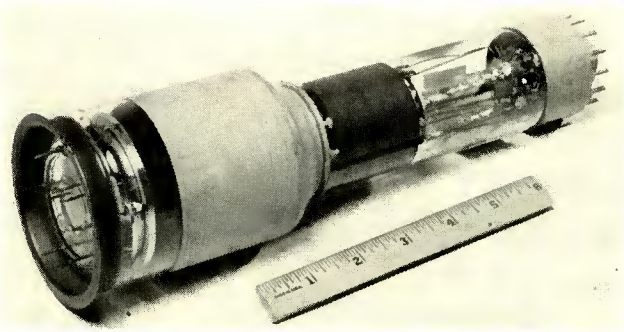

Fig. 1—Radechon.

The essential storage target structure is the same in both the present Radechon and the previous barrier grid tube. Storage time, considerations of storage action and electron optics at the target, and relationships between discharge factor, resolution, signal-to-disturbance ratio, signal output, bandwidth, etc. are all considered in the previous report,[1] and all pertain equally well to the present tube. This paper presents a more complete understanding of the tube that has been obtained through experience with its use.

The Radechon

As seen in the schematic diagram of Figure 2, the Radechon has an electron gun of relatively conventional design, chosen to provide a

[3] E. W. Bivans and J. V. Harrington, "An Electronic Storage System," *Proc. I.R.E.*, Vol. 38, No. 2, p. 205, February, 1950.

[4] J. V. Harrington and T. F. Rogers, "Signal-to-Noise Improvement Through Integration in a Storage Tube," *Proc. I.R.E.*, Vol. 38, pp. 1197-1203, October, 1950.

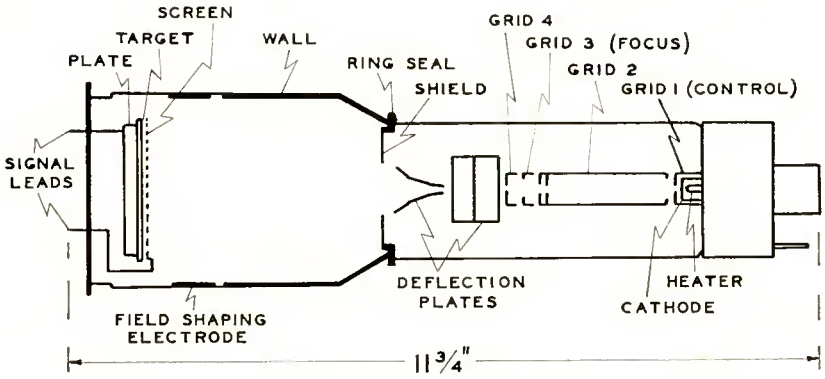

Fig. 2—Radechon construction.

high current density in a relatively small spot, with electrostatic focusing and deflection. Some experimental tubes have been made with magnetic deflection with some increase in resolution, but most applications have required electrostatic deflection to provide rapid and random access to all portions of the target. A shield is provided at the ring seal to attenuate the capacitive coupling of large high-frequency signals on the deflection plates or control grid to the target structure which is used as an output signal electrode. The primary beam from the electron gun is deflected to strike the target at the desired region where it generates secondary electrons both from the screen and the target insulator. An accelerating electric field between the screen and the collector wall (electrically connected to the shield and ring seal) causes these secondaries to go quickly to the wall where they are collected.

The target (Figure 3 shows one of several construction designs used) comprises a thin sheet of insulator, one side of which is coated with a metal layer *plate*, the other side of which is in contact with a fine mesh *screen*. In most tubes this screen is 230-mesh woven wire stainless steel of 1 mil wire diameter. Recent experimental tubes have been made with 500-mesh electroformed copper or nickel. In this target structure the surface of the insulator is one element of a

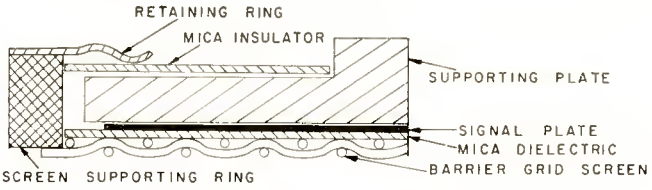

Fig. 3—Target structure.

capacitor, the other element of which is the plate and the screen (schematically shown for one small area of the target in Figure 4). The target as a whole forms a continuum of such capacitors.

Signals are stored as electrostatic energy either by the deposition of electrons on, or the removal of electrons from, the surface of the insulator (the *target*) as determined by control of the secondary electrons by the screen. Usually, input signals are applied to the electron gun control grid, and the storage target discharging current constitutes the output signal current.

Operation

Target Behavior

Most investigators agree that the probability distribution per unit

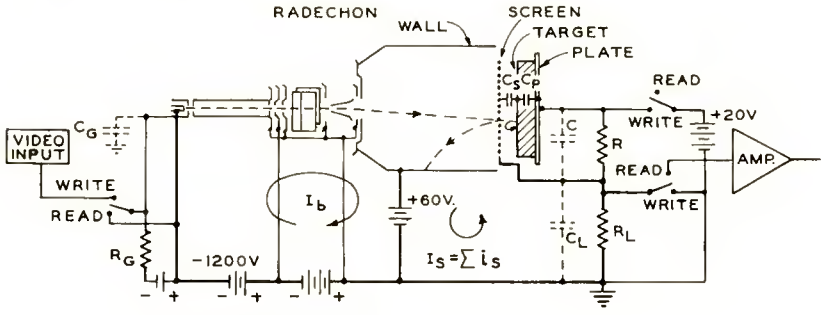

Fig. 4—Schematic simplified tube circuit.

energy interval of secondary electrons is Maxwellian. For the plane parallel plate geometry that most closely fits the conditions of the Radechon storage target this is illustrated in Figure 5. The total integral under this curve is the product of the secondary emission ratio and the beam current. Since the tube is operated with the screen voltage about 1200 volts positive with respect to the cathode, the secondary emission ratio of the target is greater than unity (storage data indicates that it is close to 3.0) so that if the target is at screen potential, there is a net flow of electrons away from the target (secondary electron current minus the primary beam current) thus charging the target positively. As this continues, a retarding electric field is set up between the target and the screen such that slow secondaries

are energetically unable to reach and pass through the screen. Since the screen is in contact with the target, these slow secondaries are constrained to return to the target within a mesh spacing from whence they came. Thus the screen prevents redistribution over the target such as occurs in many other storage tubes. Fast secondaries are still able to penetrate the screen and be accelerated to the wall. This continues until the target reaches an *equilibrium potential* for which the current of fast secondaries that escapes through the screen to the wall is just equal to the primary beam current.

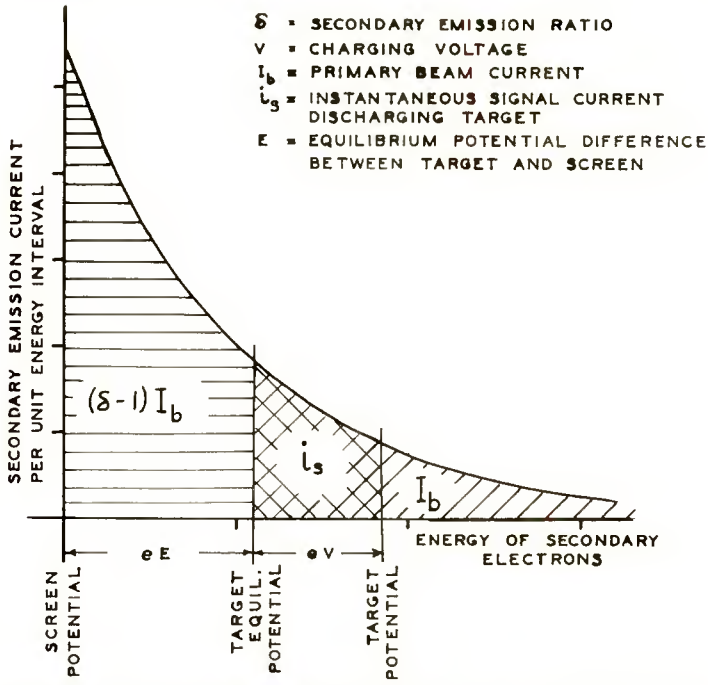

Fig. 5—Maxwellian energy distribution of secondary electrons.

The potential of the target may be changed by the application of a *charging voltage* across the capacitive divider (all the C_s and C_p in series) formed by the screen, the target and the plate (Figure 4). Since C_s is much smaller than C_p, the potential of the target is changed by nearly the entire charging voltage. With the instantaneous target potential thus different by an amount V from the equilibrium target potential (Figure 5), the net secondary electron current leaving the target is different from the primary beam current by an amount i_s, the instantaneous signal current by which the *target capacitance* (the parallel capacitance of C_p and C_s) is discharged to equilibrium poten-

tial. For a scanning beam, elemental portions of the target under the beam are at different states of discharge. Therefore, the *total signal current*, I_s, flowing in the external circuit impedance comprising C_L and R_L, is the sum, for the width of the beam along the scanning path, of the instantaneous signal currents from these target elements. This total signal current constitutes the *output signal* of the tube, particularly during the reading operation.

Characteristic curves[5] showing the relationships between the output signal current, the charging voltage, and the beam current for an

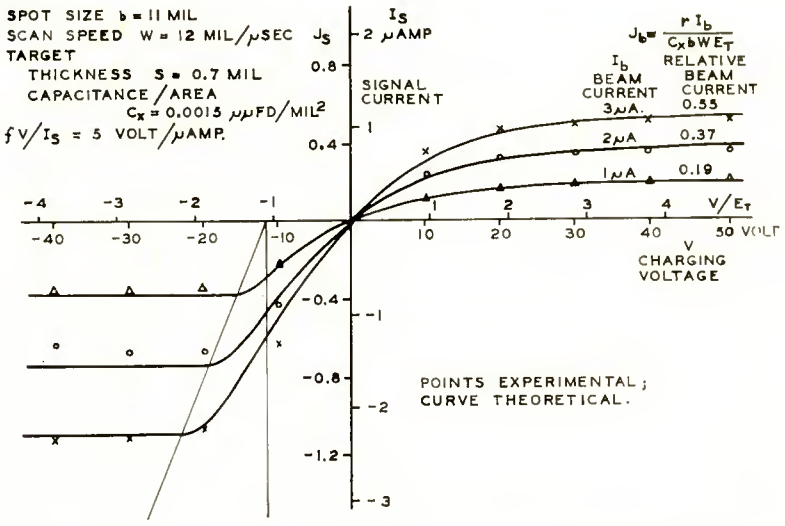

Fig. 6—Target characteristics of developmental ttype Radechon.

average developmental tube are plotted in Figure 6. In this figure the points plotted are experimentally measured data, while the curves are derived from the target-action theory.[6] Note that this figure together with Figure 6 of Reference (6) gives two views of the characteristic surface of operation of the Radechon. The shape of the curves changes somewhat with scan speed. To account for this and to provide a set of universal curves, scales for J_s, relative signal current, and V/E_T, relative charging voltage, are provided.[6]

---

[5] From data taken by M. D. Harsh and W. H. Sandford, Jr. of the Tube Division, Lancaster, Pa. This work was done under contract DA-36-039-SC-42505 with the U. S. Army Signal Corps Engineering Laboratories, Evans Signal Laboratory.

[6] A. S. Jensen, "Discharging an Insulator Surface by Secondary Emission Without Redistribution," *RCA Review*, Vol. XVI, pp. 216-233, June, 1955.

Writing

Assuming that, by scanning, the entire target has been brought to equilibrium potential while the plate and screen were held at the same potential, writing is usually accomplished by one of two methods.

Method A: While the screen is held at a fixed potential, a fixed charging voltage (about 20 volts) is applied to the plate, positive to the screen. The video signal to be written is applied to the electron gun control grid, usually clamped to cutoff, while the beam is scanned

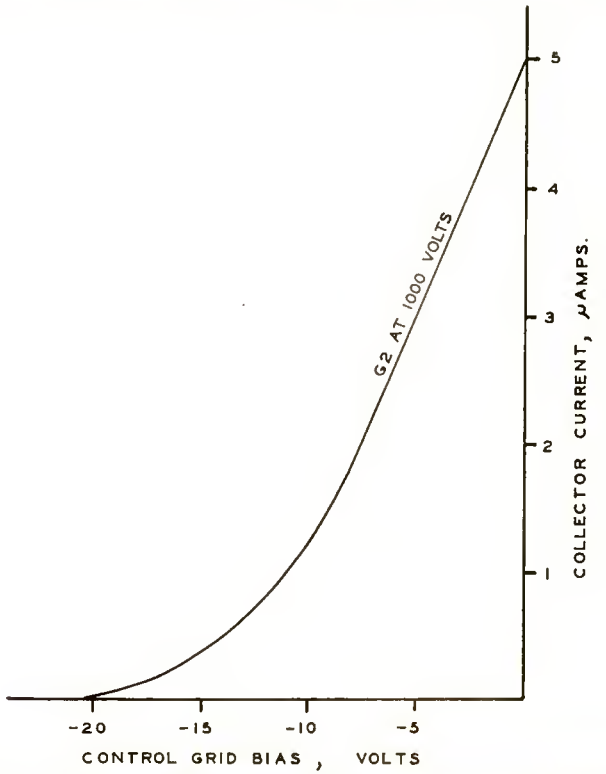

Fig. 7—Control grid characteristic of developmental Radechon.

across the target in the desired pattern or raster. This operates the tube along the reasonably linear current characteristic of Figure 6 of Reference (6) for which the plate potential is a constant. Since the electron gun control grid characteristic (Figure 7) is also reasonably linear, the entire writing process is linear. Furthermore, the high-frequency video signal amplifier need only drive the relatively small 7.4-micromicrofarad control-grid capacitance, while the relatively high 1000-micromicrofarad plate-to-screen capacitance is driven by the

usually lower frequency switching between write and read conditions. This preferred method of writing is that diagrammed in Figure 4.

Method B: While the screen is held at a constant potential, and the control grid is also held at a constant potential to produce a constant beam current, the video signal is applied to the plate as a varying charging voltage. This operates the tube along a target characteristic curve of Figure 6 for which the beam current is constant. In addition to the unfavorable capacitance driving, this method inherently is unable to charge the target as fully for linear operation, and therefore is not to be favored over Method A except in special applications. However, this method does provide the very important advantage, when the tube is operated at high discharge factor, of writing the newly impressed signal on the target practically independent of previously written signals; that is, erasure of old information is accomplished simultaneously with writing of new information.

Discharge Factor

It must be remembered that the storage target is a capacitor, and that capacitors are never completely charged to the voltage applied. With a scanning beam, the beam is incident upon an elemental area of the target only for the time interval required for it to advance one beam width. For a stationary beam, it is usually pulsed on for a limited time interval. Therefore, the time during which signal current flows to discharge the target capacitor is limited by the system procedure. To facilitate the discussion of such discharging a very important concept has been evolved. The *discharge factor* is defined as the ratio between the voltage difference through which the target capacitance has been discharged by one passage of the beam and the target's initial voltage difference from equilibrium.

$$f \equiv \frac{V - V_b}{V} \tag{1}$$

where f = discharge factor; V = charging voltage applied to target, the initial potential difference of target from equilibrium; V_b = potential difference of target from equilibrium after one passage or application of beam.

Quite conveniently, this quantity is proportional to the slope of the chord of the target characteristic (Figure 6) drawn from the origin to the curve at the charging voltage applied.

$$fV/I_s = 5 \text{ volts per microampere} \tag{2}$$

for Figure 6, and

$$fV/I_s = 1.4 \text{ volts per microampere} \tag{3}$$

for Figure 4 of Reference (6). Using these relationships, one may compute the potential V_b, to which the target has been discharged by one passage of the beam.

The discharge factor varies inversely with scan speed since the shape of the target characteristic varies in that way. Figure 8 shows three curves of discharge factor for an average developmental tube. It will be observed that since the discharge factor cannot be 100 per cent there is never saturation, and the simple term "writing speed"

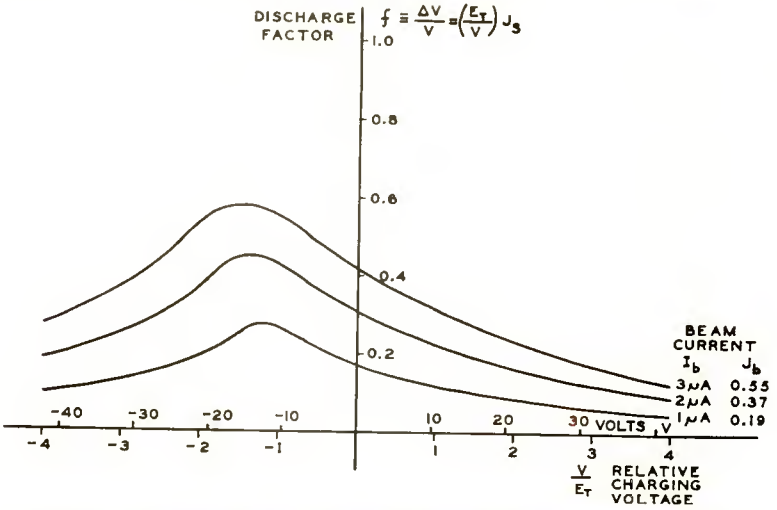

Fig. 8—Discharge factor curves for developmental type Radechon.

has no meaning unless it is simultaneously related to the discharge factor or the signal-to-disturbance ratio (See Equation (8)).

Reading

Following the writing process, reading is accomplished by first removing the charging voltage from the plate so that plate and screen are at substantially the same potential (a d-c voltage difference, constant during the entire reading process, is allowable). Now all parts of the target that were not written upon are back at equilibrium potential, whereas those portions that were written upon are negative with respect to equilibrium potential by the potential difference through which they were discharged during writing, to wit:

$$V_r = -fV = -(V - V_b). \tag{4}$$

This negative voltage V_r is the charging voltage for the reading process, and the same characteristic curves (Figure 6) can be used to compute the operation. Now both plate and screen are placed at a relatively high impedance from ground, and the reading output signal is taken from the screen (although it appears at the plate, as well) through a conventional preamplifier containing high-peaking and aperture-correction networks and stages in a manner well known in the television camera art. The beam current is held steady, usually at zero bias for one copy read-out, or at lower values to obtain several but not many copies.

Note that the tube is a high impedance device (over 100 megohms) for which the output is essentially a current. The output voltage[6] is then dependent upon the load resistor which in turn depends upon the bandwidth required, the plate and screen to collector capacitance of 5 micromicrofarads, and the output wiring capacitance (taken as 15 micromicrofarads in calculating the constant in Equation (9) below).

Reading, then, is accomplished along one of the relatively linear target characteristics of Figure 6 for which beam current is a constant and the origin is zero signal. The reading output signal can be computed from the target characteristics and four equations given. For the developmental tube, the reading output current I_{sr}, after a single writing operation in the manner described, is approximately[6]

$$\frac{I_{sr}\, W_w}{I_{bw}\, I_{br}} = 0.83 \frac{\text{mil}}{\text{microsecond microampere}} \tag{5}$$

where I_{bw} is the writing beam current, I_{br} is the reading beam current, and W_w is the writing scan speed. The reading discharge factor is taken as 0.5 or less, and this relation is valid as long as the reading beam current, I_{br}, is adjusted so that

$$\frac{I_{br}}{W_r} \leqq 0.23 \frac{\text{microampere microsecond}}{\text{mil}} \tag{6}$$

where W_r is the reading scan speed.

Erasing

Since reading is accomplished by the removal of electrons from the target and consequent discharge of it from the reading charging voltage toward equilibrium, reading is also an erasing action. Often the discharge factor during reading is sufficiently high that further erasing is unnecessary. However, in critical applications a second or several

subsequent reading processes at high discharge factor may be necessary to return the target sufficiently close to equilibrium potential prior to the next writing.

Resolution

In storage tubes with continuous storage area designed to reproduce picture signals with halftone response, one cannot refer to discrete target elements. Instead, it is more sensible to discuss resolution in the manner used in dealing with television pickup tubes or storage devices such as magnetic tape. For a given scan speed (or instantaneous writing speed) both the writing and reading processes appear as low-pass filters, and the customary frequency characteristic may be plotted by writing in a sine-wave signal, measuring its reading output, and plotting relative output as a function of frequency. For a more general curve, the abscissa chosen is the ratio of frequency to scan speed which has the dimensions sine-wave cycles per unit length of scan on the target. However, since the scan is never visible in the storage tube and cannot be measured, it is more meaningful to use the useful target diameter as the unit of length. (In a like manner, it is better to quote the deflection factor for the tube as 230 volts per target diameter, than to use other units of length.) In television practice it is customary to use square waves and to count both the peak *and* the trough so that

$$2 \text{ lines} = 1 \text{ sine-wave cycle}, \tag{7}$$

the unit of resolution then being *lines per target diameter*. Such resolution curves for both the developmental[5] and the experimental tubes are plotted in Figure 9.

Limitations to resolution

Spot size: The target area under bombardment by the primary beam at any instant is finite in extent but is not sharply defined. A graph of beam current density as a function of distance from the center of the beam is approximately Gaussian in shape (Figure 10, top). The effect of this variation in current density is to produce a step-function current to a conducting ribbon as the beam is scanned across it (Figure 10, bottom); this current increases slowly and continuously. By this means *spot size*, or beam diameter, is often defined arbitrarily as the distance the center of the beam moves while the current to the ribbon increases from 10 to 90 per cent of maximum. This can be measured on an oscilloscope as soon as the scale of length

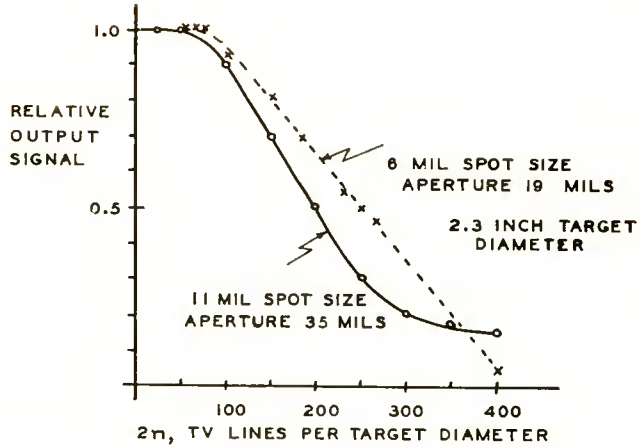

Fig. 9—Radechon resolution; solid curve for developmental-type tube, dashed curve for experimental tube.

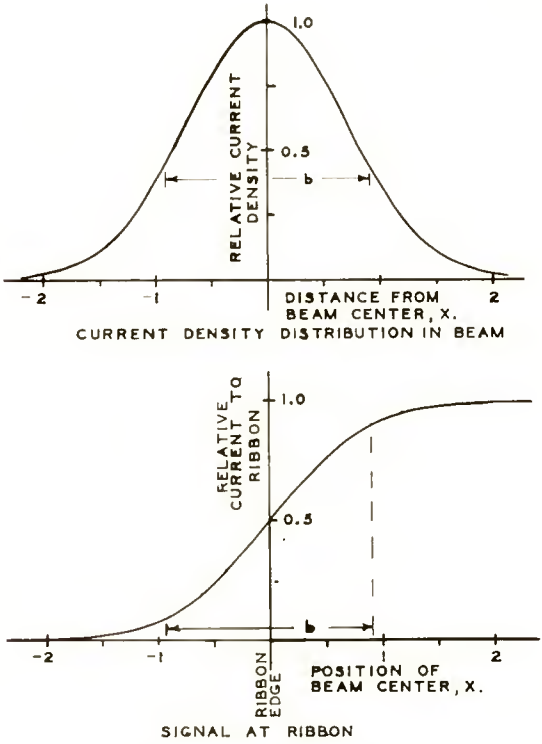

Fig. 10—(*Top*) Current-density distribution in beam; (*bottom*) signal at ribbon.

is determined from the known width of the ribbon placed on the screen for this purpose in experimental tubes. The *effective* spot size, however, must be defined in terms of the charge stored on the target. For low discharge factor this is the same as the arbitrarily defined spot size, but for high discharge factor the edges of the beam are more efficient than the center in storing charge so there is an effective increase in spot size and consequent reduction in resolution.

Furthermore, it must be remembered that a storage tube must be used in both writing and reading before a useful output is obtained. Any pulse stored on the target by a scanning beam will result in a deposition of charge one spot size longer than the distance the center of the beam moved during the pulse. Upon reading, the output signal will appear from the instant the leading edge of the spot reaches the stored charge until the trailing edge leaves it, thus effectively increasing the length of the output signal by the time required for the beam to move another one spot size. Thus the spot size enters twice to limit the resolution.

It is well known that increasing the distance between the gun lens and the target increases the spot size approximately linearly. Essentially, the "spot" should be considered as a solid angle with its apex at the gun lens. Thus to a first approximation the only way to increase the number of spots per total target area is to increase the deflection angle. The increase in number of spots per target area obtained by this method is almost independent of target size.

The measurements given here and in Reference (6) were taken with a maximum of 1200 volts between cathode and screen. However, since the secondary emission ration is about 3, which is higher than necessary, it might be sacrificed somewhat by increasing the voltage to 2000 volts or even more with the advantage of a smaller spot, better resolution and higher beam current.

Deflection stability and astigmatism: Resolution of the system can be impaired by instabilities in either the voltage supply or the deflection circuits. In addition to the usual limitations on hum and signal stability, the potentials of the cathode, the gun anodes, and the screen must be kept constant, and no signals applied to them, since they affect the deflection sensitivity, variations of which appear as a loss of resolution at the target edges. The deflection plates should be driven in push-pull with their average potential equal to that of the last gun anode to prevent their introducing excessive astigmatism.

The screen: The major purpose of the screen is to prevent redistribution of secondary electrons across the target with its consequent reduction in resolution and signal output. In order to accomplish this

the screen must be in contact with the target with no spacings through which secondaries might find a way to reach other parts of the target. Ideally, the screen should be fastened to the insulator over the entire target. Redistribution within a mesh sets the lower limit to the fineness of the mesh required at about 2 to 3 meshes per spot size. This is actually a lower limit to the effective spot size. In the developmental tube having a woven screen with 530 meshes per target diameter, this and the true spot size are roughly equally limiting to the resolution. The experimental tube with 900 meshes per target diameter is limited in resolution only by spot size.

An important function of the screen is the electrostatic shielding of adjacent portions of the target from each other. In order to accomplish this, the ratio of mesh opening to screen thickness must be less than 2 (a slightly greater ratio is satisfactory if signals are small). It was for this reason that woven wire screen was used until recently when thick electroformed screen was made available. When thin screen of higher ratio is used, negative charges on the target set up electric fields extending outside the screen to inhibit secondary emission from adjacent portions of the target, a phenomenon referred to as *coplanar grid effect*. A schematic diagram of the equipotentials of such a field, Figure 11, indicates how this is brought about. Note how the relative potentials along a path normal to a point on the target may go through values negative with respect to the potential of the target at that point. This type of interaction between adjacent large areas is apparent as a loss of resolution in regions of large signal differences.

Disturbance: This has been discussed previously,[1,6] but it is important to emphasize that screen disturbance depends primarily on the ratio of screen wire diameter to spot size and is only weakly related to transmission ratio. The electroformed screen used in the experimental Radechon[6] has finer wires (0.7 mil) which enable the use of a smaller spot to obtain better resolution with no loss in signal-to-disturbance ratio. This screen disturbance, or modulation of the beam while it scans over the screen, is the most important disturbance other than shading. It is about 7 times as large as thermal noise at the input of the pre-amplifier and 100 times as large as the shot noise. The required signal-to-disturbance ratio, D, is the real limitation to useful writing speeds since, for the recommended tube operation, they are related according to:

$$\frac{D\, W_w\, n}{I_{bw}} = 15 \frac{\text{cycles}}{\text{microsecond microampere}} \tag{3}$$

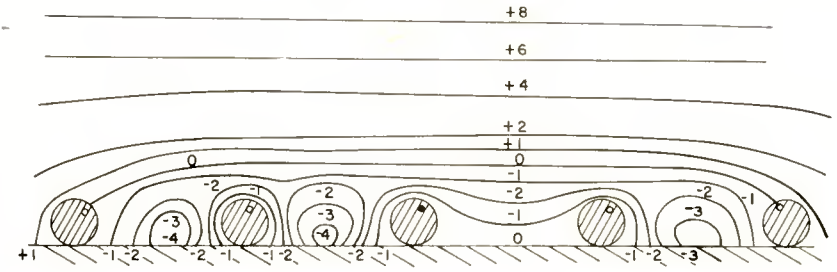

Fig. 11—Equipotentials showing coplanar grid effect with open mesh (schematic).

where n is the resolution, in cycles per unit length of scan on target, for which the system is designed. The signal-to-noise ratio, (S/N), is somewhat of a limitation to the reading conditions also since:

$$\frac{(S/N)\ W_w W_r n}{I_{bw}\, I_{br}} = 420\ \frac{\text{mil cycles}}{\text{microsecond}^2\ \text{microampere}^2}. \qquad (9)$$

Both signal-to-disturbance ratio and signal-to-noise ratio are inversely dependent on the designed resolution of the system. The constants in both Equations (8) and (9) are for the output circuit bandwidth being properly chosen for $2n$ lines per target diameter resolution in the developmental type Radechon operated in the recommended mode (Method A).

In the present Radechon, since the signal is taken from the screen and not a particular collector, shading from variation in collection efficiency is greatly reduced compared to that in earlier tubes (Figure 12).

Results

Experimental Procedure

The measurements from which the characteristic curves were plotted were taken by writing a few pulses on the target fourteen times along a single line to charge the target nearly completely, then reading off this charge fourteen times. In Figure 13 the top line is

Fig. 12—(*left*) Input square waves; (*right*) Output showing shading.

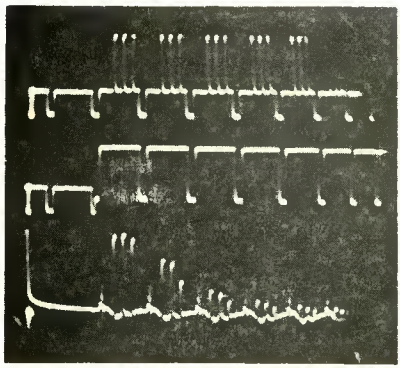

Fig. 13—(a) Writing input to G1; (b) Reading input to G1; (c) Reading output at screen.

the input to the control grid during the writing of several of these lines, the positive-going pulses turning the beam on for writing, the negative-going pulses blanking the beam during the horizontal retrace. The peaks of the writing pulses are clamped to zero bias. The second line is the input to the control grid during reading; the peak value of these reading pulses can be adjusted independent of the writing signal. The bottom line is the reading output signal.

If vertical deflection is applied so the signals are written on and read off the target in five groups of fourteen lines each, the output appears on a kinescope as in Figure 14, the target being overscanned purposely so that its outline can be seen in this picture. In this picture, each pulse was written once and read once in each frame. Their vertical spacing is such as to permit roughly 250 pulses per target diameter.

Ordinarily the wall and ring seal are operated about 60 volts positive with respect to the screen and act as a collector of secondary electrons, the only screen current being the difference between its second-

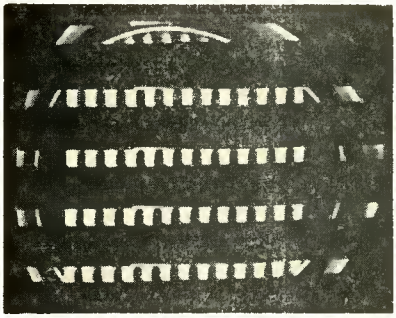

Fig. 14—Stored signal output of pulses displayed on kinescope with target ring overscanned. Five groups of 14 lines each.

aries and the primary beam current it intercepts. However, it is interesting to know how this varies with wall potential, particularly in that range where the screen also collects secondaries from the target. Such a curve is shown in Figure 15.

The slope of this curve is exactly the "plate resistance" of the tube — over 100 megohms at the operating point. Furthermore, its becoming quite flat at negative wall potentials indicates that the screen can collect all the primary beam. But this screen current, when pulsed, as it is by the blanking signals, appears as a video signal through the output amplifier onto the oscilloscope where it can be directly compared with the output reading signal independent of amplifier gain. Measurement of the d-c beam at the clamp reference bias then provides the scale factor to measure the output reading signal directly in current. Once the scale factor has been determined this means may be used to measure reading and writing beam currents at other biases without recourse to further d-c beam measurements. In Figures 13 and 16 all the signals were actually observed in this manner at the output of the pre-amplifier so that writing beam current, reading beam current, and reading output signal current are all on the same scale and can be compared directly.

Halftones

Figure 16 is a direct demonstration of the halftone rendition of the Radechon. The bottom line is the beam current during writing, while the top line is its reproduction 1/150 second later, read out with maximum constant beam current.

Target Life

One experimental Radechon[7] was in operation in systems application for 3000 hours over a period of 2 years with no appreciable degradation of signal. Although this was one of the earlier types of tube with collector output, it is considered to be representative since the target was similar to that used in the later tubes.

The only effect observed so far that limits the life of a target is the permanent marking of the screen when the raster is so small that the average beam current per unit length of scan is greater than 0.5 microampere per inch. This changes the secondary emission ratio of the screen and that area then appears as a disturbance signal.

Storage Time

For most applications, milliseconds of storage is sufficient. One

[7] Personal communication from J. V. Harrington, E. W. Bivans, and T. F. Rogers of the Air Force Cambridge Research Laboratories, Cambridge, Mass.

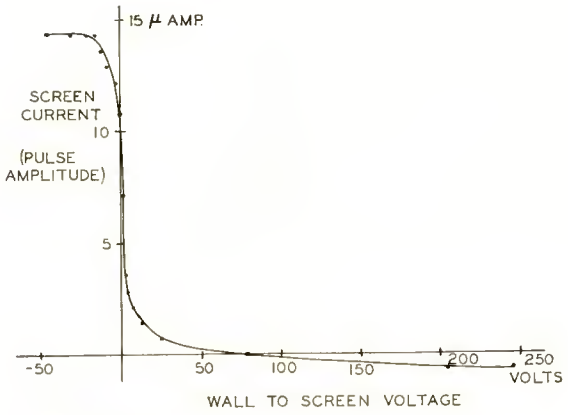

Fig. 15—Screen current versus wall storage.

measure of storage time is the length of time required for a charge on a given element of the target to decay to one half of its initial value. With the beam current continuously operating at maximum, either reading or writing on *other* portions of the target, the figure for this storage time is about 5 seconds (accumulated time if the beam is not on continuously), the decay being due to scattered electrons. With the beam turned off, however, this storage time is about 100 hours.

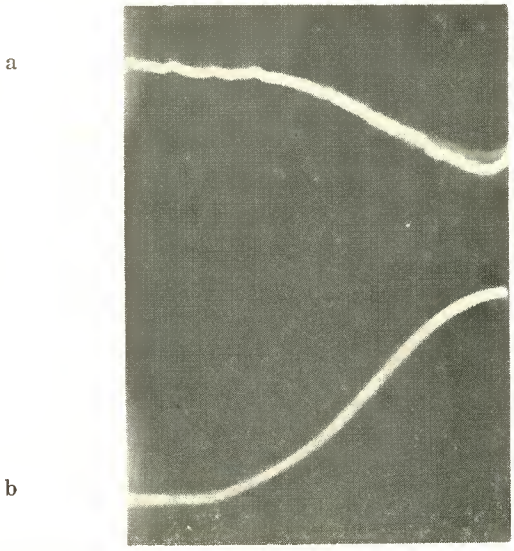

Fig. 16—Halftone storage. (a) Stored output at screen 1/150 second after writing; (b) Writing input to grid 1.

Conclusions

While the Radechon is not a universal storage tube, there are many applications in digit storage, integration, aperiodic access, and two dimensional reproductions of halftone pictures where it is finding increasing application. Its simplicity and freedom from spurious effects together with its relatively high signal output make it attractive from a circuit standpoint.

Acknowledgment

The author is indebted to L. E. Flory of these Laboratories for many stimulating discussions and continued encouragement in this series of investigations.

DISCHARGING AN INSULATOR SURFACE BY SECONDARY EMISSION WITHOUT REDISTRIBUTION*

By

Arthur S. Jensen

Research Laboratory, RCA Laboratories,
Princeton, N. J.

Summary—*The equations for the complete characteristic curves and discharge factor curves for the developmental Radechon storage tube are derived assuming a Maxwellian energy distribution of secondary electrons, a rectangular uniform beam cross section, and simple target geometry. Comparison of these theoretical curves with measured values is made for several representative tubes with reasonable determination of secondary emission parameters.*

Output signal amplitude and signal-to-disturbance ratio equations are derived from aperture theory and the limitations of electron beam cross section, screen mesh and tube output capacitance, again with good agreement with experimental data. These limitations are discussed in a manner that indicates quantitatively the considerations of interest in connection with the design of circuits and systems utilizing the Radechon.

Introduction

SEVERAL storage tubes[1-3] depend in their operation upon the discharging of an insulator surface by secondary emission in the absence of redistribution. A knowledge of the manner in which this discharge occurs enables one to understand better the operation of such tubes. In particular, the operating characteristic curves of the Radechon can be computed and are in reasonable agreement with experimentally determined curves. Several authors[4-6] already have reported on certain aspects of this problem. Its complexity pre-

---

* Decimal Classification: R138.31.

[1] A. S. Jensen, J. P. Smith, M. H. Mesner, and L. E. Flory, "Barrier Grid Storage Tube and Its Operation," *RCA Review*, Vol. IX, pp. 112-135, March, 1948.

[2] A. S. Jensen, "The Radechon, a Barrier Grid Storage Tube," *RCA Review*, Vol. XVI, pp. 197-215, June, 1955.

[3] R. B. DeLano, Jr., "Large Capacity Storage Tube for Digital-Computer Application," *Proc. I.R.E.*, Vol. 42, p. 626, March, 1954.

[4] J. V. Harrington, "Storage of Small Signals on a Dielectric Surface," *Jour. Appl. Phys.*, Vol. 21, pp. 1048-1053, October, 1950.

[5] C. V. Parker, "Charge Storage in Cathode-Ray Tubes," *Proc. I.R.E.*, Vol. 39, pp. 900-907, August, 1951.

[6] W. W. Weinstock, "An Analysis of Storage Tube Target Action," Master's thesis submitted to the Moore School of Electrical Engineering, University of Pennsylvania, June, 1953.

cludes a complete solution in closed form, and this attempt at solution will make simplifying assumptions also.

The barrier grid target structure of the Radechon consists of a thin sheet of insulator with a fine mesh screen in contact with one side and a metallized plate on the other side. The primary electron beam is incident upon this screen and the surface of the insulator, which surface is usually referred to as the *target* (Figure 1). The screen is relatively thick, the width of an opening being less than twice the thickness of the screen.

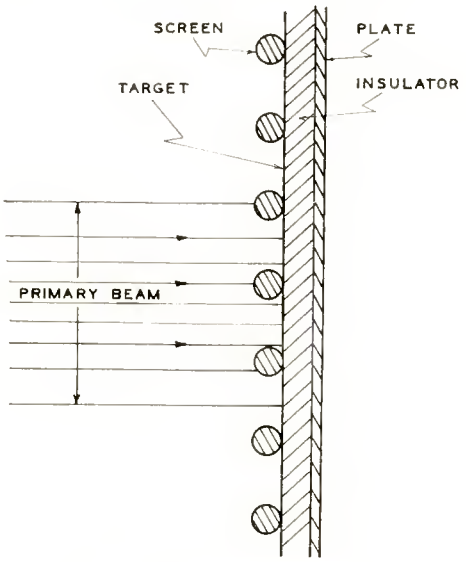

Fig. 1—Target structure.

A schematic diagram of the developmental tube and simplified associated circuits appears in Figure 4 of Reference (2). When the primary beam is incident upon the target surface, secondary electrons are emitted, some of which escape through the screen to the wall as a collector, while the others return to the target. The secondary electron current that escapes to the wall depends upon the relative potential of the target with respect to the screen, upon the energy distribution of the secondaries and upon the secondary emission ratio. The beam current, I_b, flows in the circuit loop as indicated, from the gun via the target to the wall and return. In addition, whenever the capacitance of the target to other electrodes (the sum of all the C_s and C_p in parallel) is being discharged, a discharging current, I_s, flows in the circuit loop as indicated from the target to the wall through the load impedance, R_L and C_L, to return to the screen and plate. Variations of this dis-

charging current through the load impedance constitute the output signal during reading in the Radechon.

Basis of Analysis

To simplify the problem sufficiently to enable its solution in analytical form, the following assumptions have been made:

1. The effect of the screen on the electron optics in front of the target can be approximated by an equipotential plane closely spaced to the target and parallel to it, thus reducing the problem to that of plane, parallel plate geometry.

2. The particular distribution of current in the primary beam is unimportant so that a negligible error results from assuming a rectangular cross section within which the current density is constant.[4]

3. The energy distribution of the secondary electrons is a Maxwellian distribution.[7]

4. Redistribution of secondary electrons is sufficiently restricted by the presence of the screen that those secondaries that return to the insulator return to practically the same point from which they originated.

5. Redistribution within a screen mesh, high velocity primary electrons reflected from edges of screen wires, etc., serve to discharge areas of the target insulator otherwise hidden by the screen from the beam so that the entire target area is involved in the storage process. The screen used in the experimental tubes is a woven mesh with round wires. This assumption was found to be necessary in order to make reasonable values of target capacitance per unit area agree with the experimental data. The final computation of dielectric constant supports this view.

6. The percentage of the primary beam that reaches the insulator and the percentage of the secondaries that reach the wall are constants.

7. Variation in screen transmission ratio, efficiency of collection of secondaries, variations in secondary emission ratio of either insulator or screen, and other uneveness or nonuniformity, all of which generally contribute to the shading and other disturbance signals, are ignored.

8. The secondary emission ratio of the insulator is constant and greater than unity.

9. The switching transient that occurs when the plate voltage is switched from write to read condition or vice versa is ignored, and

[7] K. G. McKay, "A Pulse Method of Determining the Energy Distribution of Secondary Electrons from Insulators," *Jour. Appl. Phys.*, Vol. 22, pp. 89-94, January, 1951.

it is assumed that at all other times the difference in potential between screen and plate is constant.

10. The beam is scanning the target with a constant scan speed.

11. During reading, the beam current is constant.[8]

12. Space-charge effects are ignored; in particular, since the primary beam current density is only about 750 microamperes per square millimeter and the effective screen spacing is about 0.02 millimeter, no space-charge-induced potential minimum is expected between target and screen.[9]

Analysis

Discharging Current Density

For a Maxwellian energy distribution, the current density of secondary electrons leaving the target surface with z-directed energies between eE_z and $e(E_z + dE_z)$ can be expressed in the general form as:

$$\frac{d\rho}{dE_z} = A \exp(-aE_z) \qquad \text{for } 0 \leq E_z. \tag{1}$$

The constants of this expression are evaluated such that the total secondary electron current density from the target is $\delta r \rho_b$, and the average secondary electron energy is eE_T. The transmission ratio, r, of the screen enters into this expression since not all of the primary beam reaches the target, some being intercepted by the screen.

$$\frac{d\rho}{dE_z} = \frac{\delta r \rho_b}{E_T} \exp\left(-\frac{E_z}{E_T}\right) \qquad \text{for } 0 \leq E_z. \tag{2}$$

This expression is plotted in Figure 2. The total integral under this curve from zero to infinity is just equal to the total secondary electron current density. Of those that leave the target, only those with sufficient energy to reach the screen and penetrate it can escape to the wall (there always being a collecting field between the screen and the wall). This is the integral under the curve between the target potential and infinity, namely:

---

[8] As a result of this assumption, this paper omits the transient response that occurs when the beam current is changed. This transient response is represented by the last term of Equation (12) in Reference (5).

[9] G. C. Sponsler, "Potential Distribution and Prevention of a Space-Charge-Induced Minimum Between a Plane Secondary Electron Emitter and Parallel Control Grid," *Jour. Appl. Phys.*, Vol. 25, pp. 282-287, March, 1954.

$$\rho_w = \int_{E_z}^{\infty} \frac{d\rho}{dE_z} dE_z. \tag{3}$$

This gives

$$\rho_w = \delta r \rho_b \exp\left(-\frac{E_z}{E_T}\right) \quad \text{for } 0 \leq E_z \tag{4a}$$

$$\rho_w = \delta r \rho_b \qquad \text{for } E_z \leq 0. \tag{4b}$$

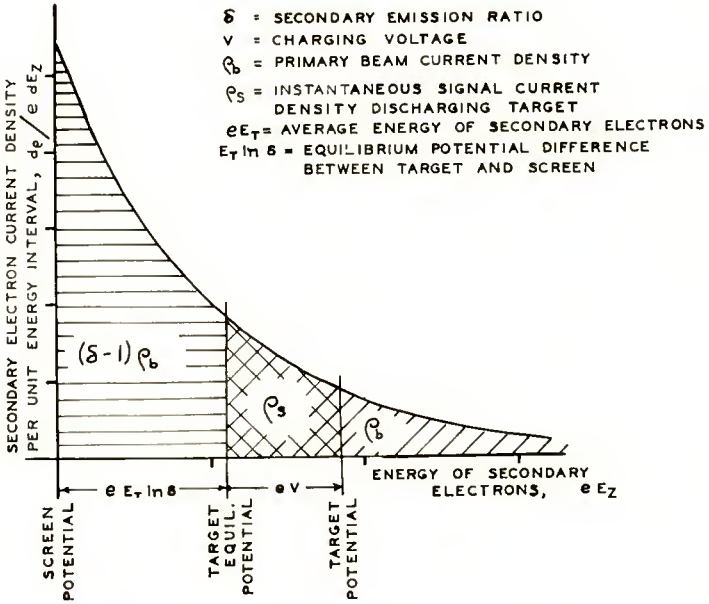

Fig. 2—Energy distribution of secondary electrons.

The remaining secondary electrons, those that do not escape through the screen, fall back again to the target, being restricted by the screen to return to virtually the same points from which they originated. It is evident from the circuit of Figure 4 of Reference (2) that the difference between the primary current density that reaches the target and the current density escaping to the wall is available to discharge the target capacitance.

$$\rho_s = r\rho_b - \rho_w. \tag{5}$$

Again, the screen transmission ratio enters the calculation since only that fraction of the beam can contribute towards discharging the

target. There is a target potential for which there is no further discharging, for which the current density escaping to the wall is just equal to the primary current density. This is known as the *equilibrium potential.* From Equation (4) this is seen to be

$$E_z = E_T \ln \delta \qquad \text{for } \rho_s = 0 \text{ and } \rho_w = r\rho_b. \tag{6}$$

It is important to note that the electron beam can only discharge the target toward this equilibrium potential. Changes in potential of the target away from equilibrium can only be made by applying a signal to the plate. This equilibrium potential makes a convenient choice for an axis, with respect to which target potentials are expressed as

$$V = E_z - E_T \ln \delta. \tag{7}$$

With this choice of axis, the discharging current density becomes

$$\rho_s = r\rho_b \left[1 - \exp\left(-\frac{V}{E_T} \right) \right] \qquad \text{for } -E_T \ln \delta \leq V \tag{8a}$$

$$\rho_s = r\rho_b \,(1-\delta) \qquad \text{for } V \leq -E_T \ln \delta. \tag{8b}$$

Final Potential after Discharge

A particular elemental target area can be discharged only while under bombardment by the primary beam. The total effect of this

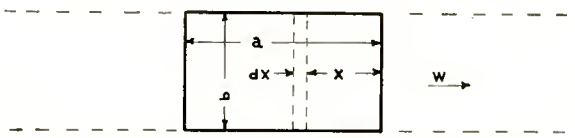

Fig. 3—Assumed scanning beam cross section.

discharging can be evaluated by integrating the changes in potential as the beam scans over the element, as in Figure 3. The potential of the target elements as a function of their position, x, with respect to the scanning beam can be computed by solving the equation

$$\int_{V}^{V_x} dV = -\int_{0}^{x/W} \frac{\rho_s}{C_x}\, dt \tag{9}$$

while the beam is scanning at speed W. (Here x is measured from the front edge of the sharply defined assumed beam shown in Figure 3.

Later, in connection with Figure 10 of Reference (2), the same letter is used as a measure from the center of a real spot.)

There are three different cases, each resulting in a different solution for Equation (9). In Case I, when the target potential is always positive with respect to the screen, Equation (8a) may be substituted in Equation (9), and the integration made directly. Similarly, in Case III, when the target potential is always negative with respect to the screen, Equation (8b) is substituted before integration. However, in Case II, when the target potential is initially negative to that of the screen but ultimately is positive, the problem must be broken into two parts, using Equations (8b) and (8a) respectively. The solutions are

Case I $[-E_T \ln \delta \leq V]$

$$V_x = V + E_T \ln\left\{\left[1 - \exp\left(-\frac{V}{E_T}\right)\right] \exp\left(-\frac{r\rho_b x}{C_x W E_T}\right) + \exp\left(-\frac{V}{E_T}\right)\right\} \tag{10a}$$

Case II $[J_b E_T(1-\delta) - E_T \ln \delta \leq V \leq -E_T \ln \delta \leq V_x]$

$$V_x = V + E_T \ln\left[\exp\left(-\frac{V}{E_T}\right) + (1-\delta) \exp\left\{-\frac{r\rho_b x}{C_x W E_T} + \frac{\delta}{1-\delta}\left(\frac{V}{E_T} + \ln \delta\right)\right\}\right] \tag{10b}$$

Case III $[V \leq J_b E_T(1-\delta) - E_T \ln \delta]$

$$V_x = V - \frac{r\rho_b(1-\delta)x}{C_x W}. \tag{10c}$$

The relative beam current

$$J_b \equiv \frac{r\rho_b a}{C_x W E_T} \equiv \frac{\gamma a}{W} \equiv \frac{rI_b}{C_x b W E_T}. \tag{11}$$

One can write the expressions for the final target potential after the complete passage of the beam in the form[10]

[10] Equations (12a) and (15a) of this paper are identical respectively to Equations (5) and (10) of Reference (5).

Case I $[-E_T \ln \delta \leq V]$

$$V_b = V + E_T \ln \left\{ \left[1 - \exp\left(-\frac{V}{E_T} \right) \right] \exp\left(-J_b\right) + \exp\left(-\frac{V}{E_T} \right) \right\} \tag{12a}$$

Case II $[J_b E_T(1-\delta) - E_T \ln \delta \leq V \leq -E_T \ln \delta \leq V_b]$

$$V_b = V + E_T \ln \left[\exp\left(-\frac{V}{E_T} \right) + (1-\delta) \exp\left\{ -J_b + \frac{\delta}{1-\delta} \left(\frac{V}{E_T} + \ln \delta \right) \right\} \right] \tag{12b}$$

Case III $[V \leq J_b E_T(1-\delta) - E_T \ln \delta]$

$$V_b = V - J_b(1-\delta) E_T. \tag{12c}$$

Signal Current

The signal current observed at the output of the tube is the sum of all the discharging currents from the target elements under bombardment. Referring to Figure 3,

$$I_s = \int_0^a b \rho_s dx, \tag{13}$$

the integration being over the entire spot area in accordance with assumption (5). Again, there are three cases for solution, and substituting Equations (8) and (10), writing for the relative signal current,

$$J_s = \frac{I_s}{C_s b W E_T} \tag{14}$$

which is similar to Equation (11), one obtains[10]

Case I $[-E_T \ln \delta \leq V]$

$$J_s = -\ln \left\{ \left[1 - \exp\left(-\frac{V}{E_T} \right) \right] \exp\left(-J_b\right) + \exp\left(-\frac{V}{E_T} \right) \right\} \tag{15a}$$

Case II $[J_b E_T(1-\delta) - E_T \ln \delta \leq V \leq -E_T \ln \delta]$

$$J_s = -\ln \left[\exp\left(-\frac{V}{E_T} \right) + (1-\delta) \exp\left\{ -J_b + \frac{\delta}{1-\delta} \left(\frac{V}{E_T} + \ln \delta \right) \right\} \right] \tag{15b}$$

Case III $[V \leq J_b E_T(1-\delta) - E_T \ln \delta]$

$$J_s = (1-\delta)\, J_b. \tag{15c}$$

Characteristic Curves

Since this signal current constitutes the output signal for the tube, curves plotted from these equations are the characteristic curves for the tube's operation.[11] Families of such curves are plotted in Figures 4 and 5 and also in Figure 6 of Reference (2) for three different Radechons; measured values are plotted for comparison.[12] The three regions of the curves corresponding to the three cases of solution are marked on the graph. Note in particular that for higher J_b the point

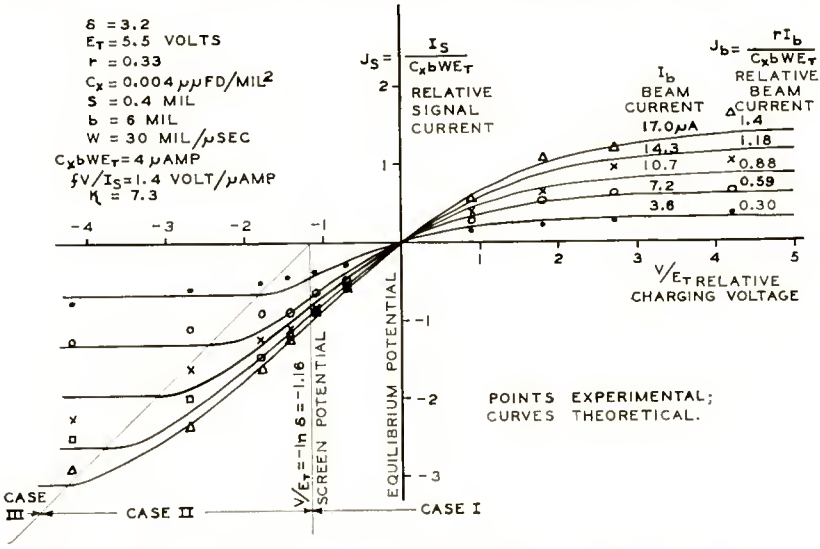

Fig. 4—Target characteristics of an experimental Radechon.

on the negative portion of the curve where the tangent becomes horizontal moves out to the left according to

$$V/E_T = (1-\delta) J_b - \ln \delta \tag{16}$$

and the region over which the curve is tolerably straight increases, particularly in the negative direction.

Note also, that for a given value of relative charging voltage,

[11] In plotting these curves, V is taken as the charging voltage applied to the plate with respect to the screen, ignoring the capacitive divider effect of C_s and C_p, since this effect is not significantly large.

[12] Operating data for the developmental tubes was obtained by M. D. Harsh and W. H. Sandford, Jr. of the Tube Division, Lancaster, Pa.

V/E_T, the output signal is a decreasing function of J_b, becoming more linear with respect to J_b as V increases. Such current characteristic curves are essentially cross sections of the above figures and are plotted, together with measured values for comparison, in Figures 6 and 7. This indicates that for simple signal storage operation in which a signal is written at one time and read out later, it is desirable to write with variable beam current (signal applied to the control grid) while a charging voltage of approximately 20 volts is applied on the plate with respect to the screen, and to read with a large steady beam current after the plate has been returned to the same potential as the screen.

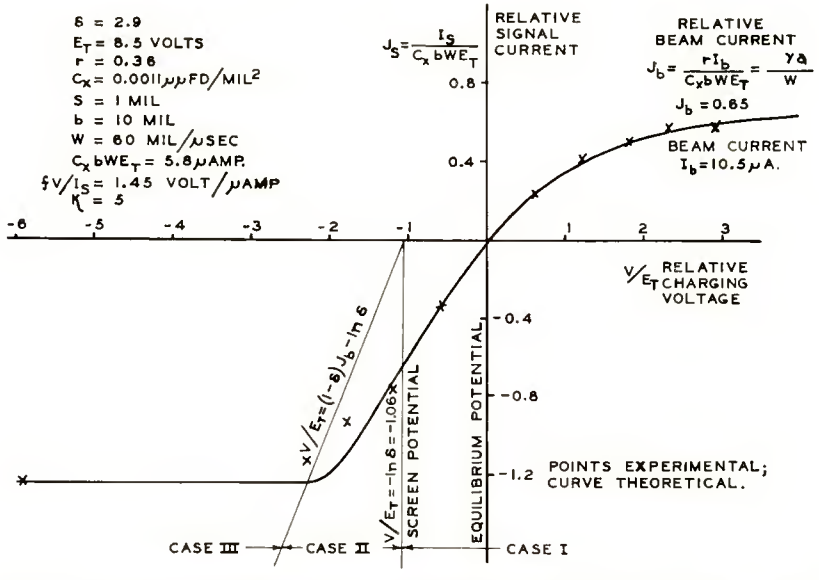

Fig. 5—Target characteristics of an STE-S type experimental Radechon.

The charging voltage of the target during reading is determined by the charge deposited during writing.

The theoretical curves plotted in the preceding figures were fitted to the measured values by an appropriate choice of four parameters: secondary emission ratio of the insulator (δ), average energy of secondary electrons (eE_T), screen transmission ratio (r), and target capacitance per unit area (C_x). The reasonableness of the fit lends credence to the values chosen for these parameters so that this plotting of the curves becomes a means for their measurement. It is of special interest that the secondary emission ratio of mica at 1200 volts, with contamination normally expected from standard tube construction, is close to 3.0, and that the average energy of secondary electrons from

the mica is about 8 electron-volts, which is somewhat higher than that for metals and possibly somewhat higher than its true value, since the target does not actually have the plane, parallel plate geometry assumed in the derivation.

It is possible to compute the dielectric constant of the mica target from the value of target capacitance per unit area that had to be assumed and the known target thickness. For the three tubes, this was 5, 7, and 5 respectively, encouragingly close to the published value for mica (5.66 to 5.97, Elsas, 1891).

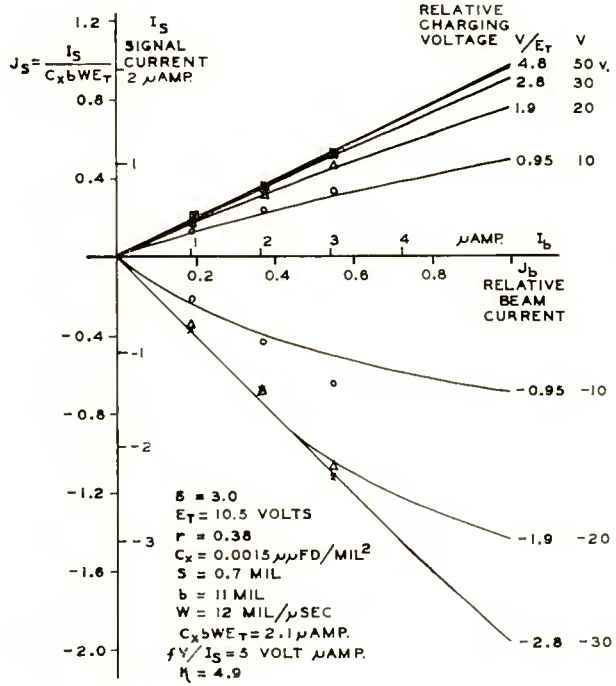

Fig. 6—Current characteristics of the developmental type Radechon.

Discharge Factor

It is evident from Equations (12) that, since the beam is incident upon any small area of the target for only a limited time, this target area cannot be completely discharged. To facilitate the discussion of such discharging, an important concept has been evolved. The *discharge factor*, f, is defined as the ratio between the voltage difference through which the target capacitance has been discharged by one passage of the beam and the target's initial voltage difference from equilibrium.

$$f \equiv \frac{V - V_b}{V}. \tag{17}$$

From this definition and Equations (12) and (15), it follows that for all three cases

$$f = \frac{E_T J_s}{V}. \tag{18}$$

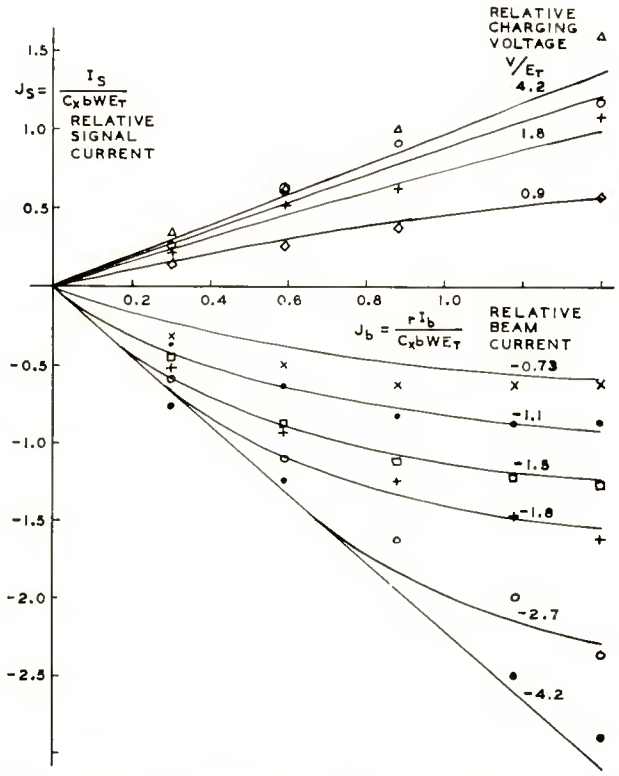

Fig. 7—Current characteristics of an experimental Radechon.

Thus the discharge factor is the slope of the chord of the target characteristic (Figures 4 and 5) drawn from the origin to the curve at the relative charging voltage applied. Therefore, a curve of discharge factors can be computed graphically for a tube once a target characteristic is available. Figure 5 is the target characteristic of an early experimental tube for which many measurements of discharge factor were made. These experimental values, slopes of the chords to the experimental points on the target characteristic, and values com-

puted from Equation (18) are all plotted in Figure 8 for comparison. Their mutual agreement indicates the firmness of the theory.

The discharge factor depends on the relative beam current in much the same way as does the relative signal current. A family of discharge factor curves for the developmental tube is plotted in Figure 8 of Reference (2).

Output Signal Amplitude

Resolution: Output Current For Varying Signal

The output signal current, I_s, discussed so far and plotted in the graphs is that for a quasi-static or slowly varying signal. In any real case, the signals vary in amplitude rapidly and the charge pattern

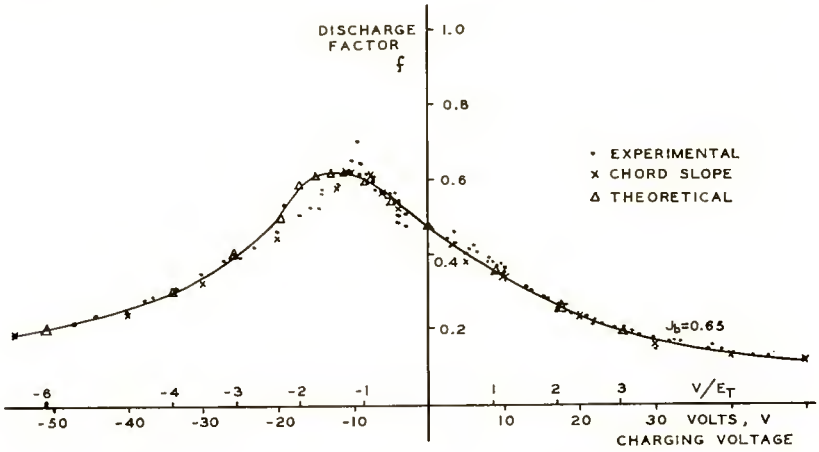

Fig. 8—Discharge factor for the STE-S type experimental Radechon.

stored on the dielectric target has dimensions not greater than a few beam spot widths. In this case errors in writing and reading this charge pattern are introduced by the finite size of the spot, which acts as a scanning aperture.[13] Any particular signal must both be written and read so that the storage tube actually comprises two such apertures in cascade. Therefore, the effective aperture is $b\sqrt{2}$ where b is the spot size (Equation (29) of Reference (13)). This results in a decrease in output signal current amplitude with increased number of signal cycles per target diameter in a manner described in Figures 14 and 15 of Reference (13). These curves are analogous to the transient response of low-pass electrical networks with sharp cutoff.

[13] O. H. Schade, "Electro-Optical Characteristics of Television Systems, Part II," *RCA Review*, Vol. IX, pp. 245-286, June, 1948.

Aperture correction networks,[14] comprising, for example, two cascaded R-C stages in the output amplifier, can compensate for this low-pass effect in much the same manner that high-peaking circuits are used in standard television camera practice to compensate for a large R-C constant at the image-orthicon output, at the expense of both high-frequency noise and disturbance.

This correction to account for the signal variations must be applied to I_s in all the equations in this paper.

Resolution: Spot Size Measurement

In every discussion of resolution, it must be remembered that real electron beam spots do not have sharp boundaries; therefore, any specification of spot size should include the method of measurement. In the method employed here, a sharp-edged metal ribbon 40 mils wide was placed on the target structure. The strip was then scanned and the output signal observed on an oscilloscope using a wide-band amplifier (Figure 10, Reference (2)). The length of the transient response of this unit step function was measured from the 10 to the 90 per cent amplitude response points and compared with the total width of the signal from the ribbon. This is roughly equivalent to measuring the spot width at the 44 per cent current density level, or at $x = 0.9$ for a beam whose current density varies as $\exp(-x^2)$. This differs somewhat from the definition used in Reference (13) which took $x = 2$. Making this correction and introducing the factor for cascading two apertures, one obtains the effective aperture given in the resolution curves[12] of Figure 9 of Reference (2), which in turn agree, both in the value of resolution at which the curve begins to fall off and in the slope of that fall off, with Figure 15 of Reference (13). (Schade's value of relative line number (N/N_δ) is approximately our $(4nb\sqrt{2}/x)$ and is equal to unity at 70 lines per target diameter for the developmental Radechon.)

This method of scanning the edge of a metal ribbon measures the current distribution across the spot. Actually, the pertinent quantity is the charge deposited on the target. But, since the charging of a capacitance is nonlinear, those portions of the beam that discharge the target most completely, operate at the least efficiency. This means that as the discharge factor is increased, the center of the beam becomes less efficient in discharging; the edges become more important and the spot effectively flattens out and becomes larger. Thus, as the

[14] Further references and better circuits can be found in R. C. Dennison, "Aperture Compensation for Television Cameras," *RCA Review*, Vol. XIV, pp. 569-585, December, 1953.

discharge factor is increased, particularly above 0.5, the resolution is decreased.

Signal Output

The storage tube is essentially a high-internal-impedance current generator, so that the simplified equivalent output circuit is that of Figure 9, in which the signal current, I_s, is determined by the tube characteristics as described above and V_s is the voltage signal appearing on the grid of the first amplifier tube.

$$V_s = \frac{I_s}{C_L\sqrt{\omega_L^2 + \omega^2}} \tag{19}$$

where

$$\frac{\omega_L}{2\pi} = \frac{1}{2\pi R_L C_L} \tag{20}$$

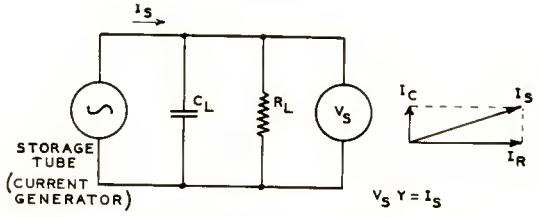

Fig. 9—Equivalent output circuit.

is the output bandwidth and $\omega/2\pi$ is the reading signal frequency. For a well-designed system, $\omega = \omega_L$ for the highest expected signal frequency. Taking n as the number of stored signal cycles per unit length of scan,

$$\omega_L = 2\pi W_r n \tag{21}$$

and

$$V_{sr} = \frac{I_{sr}}{2\pi W_r n C_L\sqrt{2}} \tag{22}$$

as the value of the stored signal input to the amplifier, where the subscripts r indicate that this is during reading.

Disturbance Signal

For the beam currents and current densities used to obtain a high discharge factor, the most serious disturbance is that generated by

scanning across the screen wires. This signal can be shown to be about 7 times as large as the thermal noise at the input of the preamplifier and about 100 times the shot noise. The maximum amplitude of the disturbance signal, I_d, is determined by that fraction of the beam which is intercepted by one screen wire so that

$$I_d = \frac{(\sigma - 1)\, u I_{br}}{a} \tag{23}$$

where σ is the secondary emission ratio of the screen wires (measured to be between 0.98 and 1.1), and u is the wire diameter. With $N = 1/\lambda$, where N is the screen mesh per unit length and λ the distance from center to center of the wires, the maximum screen disturbance frequency is

$$\omega_d = 2\pi N W_r, \tag{24}$$

and the disturbance signal becomes, from Equation (19),

$$V_d = \frac{(\sigma - 1)\, u I_{br}}{2\pi a W_r C_L \sqrt{n^2 + N^2}}, \tag{25}$$

the subscript r denoting reading. Typical values are $u = 1$ mil, $\sigma = 1.1$, and $N = 230$ per inch. The signal-to-disturbance ratio is then,

$$D \equiv \frac{V_{sr}}{V_d} = \frac{I_{sr}}{I_{br}} \frac{a}{(\sigma - 1)\, u} \frac{\left[1 + \left(\frac{N}{n}\right)^2\right]^{1/2}}{\sqrt{2}}. \tag{26}$$

This ratio is the number of gray levels reproducible as halftones in a signal. In agreement with Equation (26), this ratio has been about 30 for a resolution of about 300 lines per target diameter and a relative writing-beam current of 0.37. Note that this relation indicates that signal-to-disturbance ratio is a negative function of the system design resolution.

Simple Storage Operation

For simple signal storage in which a signal is written and then read out later, writing should be done with $V/E_T \simeq 2.5$ for which, from Equations (12), the change in voltage accomplished by depositing charges on the target is

$$\Delta V = V_b - V = -E_T J_{bw}, \tag{27}$$

the subscript w denoting the writing operation. Reading is accomplished at a fixed beam current for which $J_{br} \simeq 0.5$. The reading discharge factor is practically constant for all values of signal used; in this region $f_r \simeq J_{br} \leq 0.50$. From Equations (18) and (27) we obtain: $J_{sr} = -f_r J_{bw}$ and, dropping the minus sign, $J_{sr} = J_{bw} J_{br}$, or $I_{sr} = r J_{bw} I_{br}$,

$$V_{sr} = \left(\frac{r^2}{2\pi C_s b E_T C_L \sqrt{2}} \right) \frac{I_{bw} I_{br}}{W_w W_r n} \tag{28}$$

this being the value of the first reading signal output following a single writing. The linearity of this signal with writing- and reading-beam currents is noteworthy, since it indicates that the Radechon can reproduce halftone signal values.

Both the signal-to-disturbance ratio (D) and the signal-to-noise ratio (S/N) are limitations to the use of the tube. In particular, when the tube is operated as recommended in the preceding paragraph

$$\frac{D W_w n}{I_{bw}} = \left(\frac{r^2 N}{C_s E_T (\sigma - 1) u \sqrt{2}} \right). \tag{29}$$

This indicates that the maximum writing speed is inversely proportional to both the signal-to-disturbance ratio and the resolution required.

Likewise the signal-to-noise ratio, while usually considerably greater than the signal-to-disturbance ratio, may limit the reading conditions since,

$$(S/N) \equiv \frac{V_{sr}}{V_n} = \left(\frac{r^2}{4 C_s b E_T \sqrt{\pi C_L k T}} \right) \frac{I_{bw} I_{br}}{W_w W_r n} \tag{30}$$

where V_n is the thermal noise in the output resistor. When chosen for the desired bandwidth,

$$V_n = \left(\frac{2kT}{\pi C_L} \right)^{1/2} \tag{31}$$

Conclusions

When many simplifying assumptions must be made to enable the analytical solution of a problem, and when some of the parameters

such as the secondary emission ratio, the average energy of the secondary electrons, and even the target thickness are not well known and may vary from tube to tube, one cannot depend entirely upon theoretical calculations. However, the number of instances in which measured results have agreed with the foregoing theory have been sufficient to be very encouraging. In this respect these equations have value in indicating the manner in which the Radechon should be used in storage applications and the limitations to be expected in its operation.

RADECHON STORAGE TUBE CIRCUITS*

By

Arthur S. Jensen and George W. Gray

Research Laboratory, RCA Laboratories,
Princeton, N. J.

Summary—*Since a signal of about 20 volts must be applied to the storage target of the developmental Radechon either as a means for switching from write to read condition or, in a less preferred mode of operation, as an input writing video signal, this signal must be separated from the much smaller (about 30 millivolt) reading output signal. In the older barrier grid storage tube design, these signals were separated by taking the output from a collector of the secondary electrons from the target. However, experience has shown that separation in the external circuit is simpler in over-all operation. Several circuits have been used in the many applications of the tube. For applications in which switching time is available, relays are best. In special cases, short-time-constant clipping circuits suffice. Radio-frequency (r-f) signal separation provides short access time for the operation of a few tubes. Crystal diode switches are simple, and a self-balanced double cathode follower circuit provides very linear output. Each of these methods is described.*

The Signal Separation Problem

THE Radechon, a developmental barrier grid storage tube,[1,2] comprises a single electron gun and a storage target. In its operation during writing, either the input video writing signal is impressed upon the plate at about 10 volts peak to peak, or it is applied to the control grid while a 20-volt square pulse is applied to the plate. In either case, the screen must be held at a fixed potential.[3] The reading output signal is a current of which about 2 microamperes is modulated so that for the usually required 5-megacycle bandwidth, the input capacitance of the output amplifier, and ten to one high peaking, the output voltage is about 30 millivolts. Several methods that have been used to keep this low-level output signal separate from the high-

* Decimal Classification: R138.31.

[1] A. S. Jensen et al., "Barrier Grid Storage Tube and Its Operation," *RCA Review*, Vol. IX, No. 1, pp. 112-135, March, 1948.

[2] Arthur S. Jensen, "The Radechon, a Barrier Grid Storage Tube," *RCA Review*, Vol. XVI, pp. 197-215, June, 1955.

[3] As far as the writing and reading processes are concerned, the signal need only be applied between screen and plate irrespective of how the potential of either changes with respect to ground. However, if the screen potential is allowed to change, there is a small but perceptible change in deflection sensitivity that reduces the resolution.

level signals that are on the plate and the deflection plates are described below.

In all these circuits, it is important that the output circuits be well shielded. For this purpose a shield electrode, designed to provide adequate electrostatic shielding within the tube between the target structure and the electron gun with its deflection plates, is brought out on a ring seal.

Secondary Emission Method

The earlier tube designs[1] solved this signal separation problem by collecting the secondary electron current on a well-shielded collector,

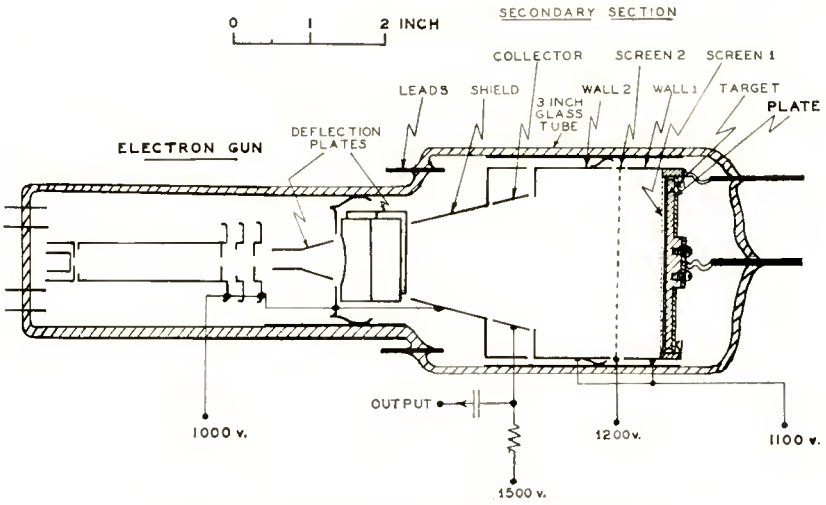

Fig. 1—STE-S type Radechon storage tube.

which then was the output electrode. The output amplifier measured the modulation which was impressed by the stored charge pattern upon this secondary electron current. However, this posed a difficult shading problem. It was difficult to design an electron optical system that collected the secondary electrons equally well from all areas of the target and yet used a small collector with little capacitance to other electrodes. A second screen improved the shading but made the adjustment of electrode potentials even more critical. It became evident that the complication might be better located in the external circuits.

Relay Circuit

In certain applications which do not require rapid switching from write to read and vice versa, the relay circuit of Figure 2 has proven

the most satisfactory. During writing, the load impedance (R_L, C_L) is shorted out so that the screen is held firmly at ground potential, while the switching voltage is developed across R and the target input capacitance C, the sum of all the C_s and C_p in series (about 1000 micromicrofarads). The resistor R is chosen so that this time constant is smaller than the allowable switching time. Video input is applied to the control grid. During reading, the plate is disconnected from the switching voltage source, the load impedance is placed between the target structure and ground, and the target structure is connected to the output amplifier. The load impedance time constant is chosen to match the required output bandwidth, except that increased low-frequency signal-to-noise ratio[1] can be obtained by using a large time constant at the input and high peaking later in the amplifier.

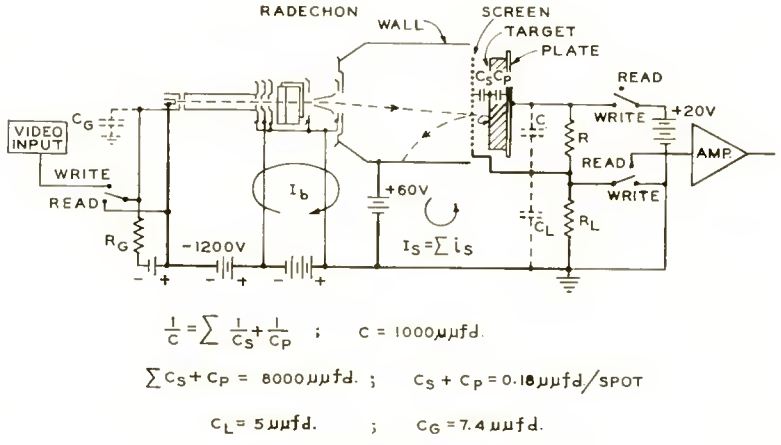

Fig. 2—Schematic relay circuit.

During writing, the average voltage of the target structure is one half the applied switching voltage. Upon switching back to the read condition, this appears as a large transient across the load impedance. An improved circuit (Figure 3) balances the impedance of R and the target input capacitance by the equivalent network R_2C_2, but requires another relay and additional switching power, and adds to the load capacitance. However, even with fixed circuit values, this reduces the switching transient to the order of magnitude of the stored output signal.

[1] For disturbances and noise not generated by the beam, and at the expense of high frequency disturbance and noise.

Radio-Frequency Signal Separation System

A method of signal separation identical to that used in some other storage tubes[5-8] has been applied successfully to the Radechon.[9,10] In this system, writing is accomplished as before with either a steady beam and the video applied to the plate, or a switching signal on the plate and the video applied to the control grid. During reading, the beam is keyed on by driving it above cutoff with an r-f oscillator. The stored charge pattern on the target modulates the r-f variations of the beam which are amplified by the output band-pass r-f amplifier, the stored signal modulation being detected, as in any receiver following the i-f amplifier. However, the lower frequency switching or video

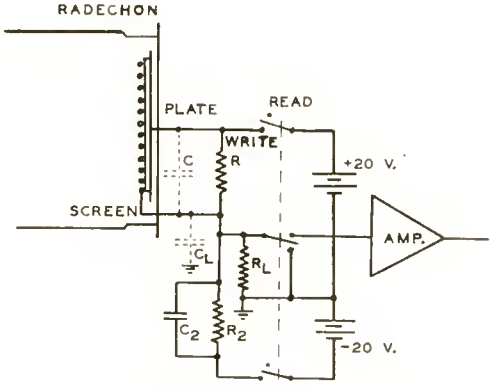

Fig. 3—Improved relay circuit.

signals applied to the plate are rejected by the output amplifier. Appropriate filters are required at the plate, and shielding around the target section of the Radechon and the output amplifier is extremely important. The ring seal internal shield has proven satisfactory in this method of operation.

---

[5] L. Pensak, "The Graphechon—A Picture Storage Tube," *RCA Review*, Vol. IX, p. 59, March, 1949.

[6] L. E. Flory, J. E. Dilley, W. S. Pike, and R. W. Smith, "A Storage Oscilloscope," *RCA Review*, Vol. XII, pp. 220-229, June, 1951.

[7] S. H. Dodd, H. Klemperer, and P. Youtz, "Electrostatic Storage Tube," *Elec. Eng.*, Vol. 69, pp. 990-995, November, 1950.

[8] A. J. Lephakis, "An Electrostatic-Tube Storage System," *Proc. I.R.E.*, Vol. 39, pp. 1413-1415, November, 1951.

[9] Personal communication from F. M. Gager, E. N. Zettle, and G. K. Jensen of the Naval Research Laboratory, Washington, D.C.

[10] Personal communication from N. I. Korman and W. V. Goodwin of Engineering Products Division, RCA, Moorestown, N. J.

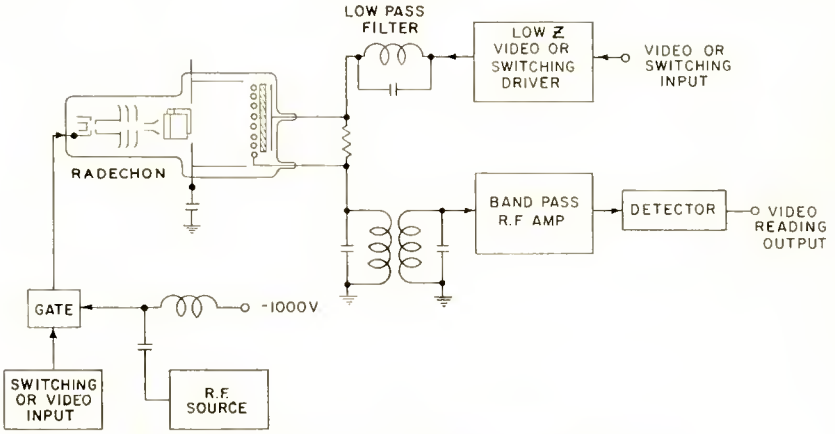

Fig. 4—Radio-frequency signal separation system.

Crystal Diode Circuit

Crystal diodes may be used as switches in the place of the relays of Figure 2 with a considerable gain in the speed of operation, but somewhat of a loss in efficiency of signal separation because the front resistance of the diode is not less than 25 ohms. One of several[11]

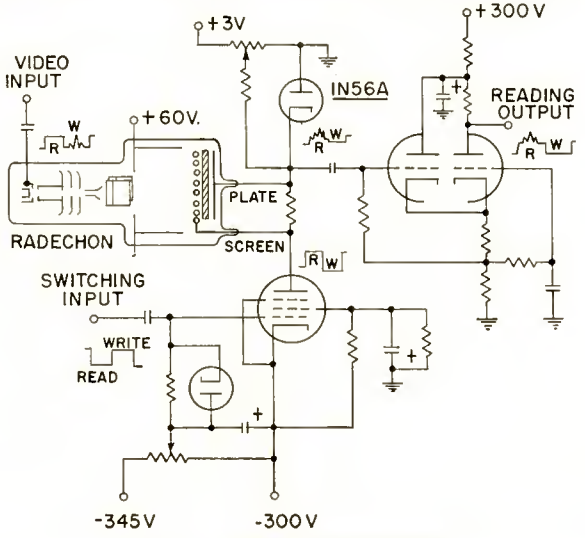

Fig. 5—Crystal output circuit.

[11] E. W. Bivans and J. V. Harrington first devised and used this and similar circuits in their investigations in connection with a binary digit storage system at the Air Force Cambridge Research Laboratories, Cambridge, Massachusetts: E. W. Bivans and J. V. Harrington, "An Electronic Storage System," *Proc. I.R.E.*, Vol. 38, No. 2, p. 205 (Conv. abstract No. 118), February, 1950.

successful circuits of this type is shown in Figure 5. During writing the pentode and crystal diode are both conducting, holding the target structure at a low impedance while the switching voltage is applied across it. Some of this switching voltage does appear on the input of the amplifier, however, since the crystal diode's forward resistance forms an appreciable part of the potential divider in the pentode's plate circuit. During reading, the pentode is driven beyond cutoff, the crystal diode is not conducting, and the entire target structure and the amplifier input are at a high impedance from ground so that current signals from the tube may be amplified. Ordinarily, the simple back resistance of the crystal diode is not sufficient, but, at the expense of adding a small pedestal to the output signal, the crystal diode may be back biased as shown and its resistance increased. It is advisable to have clipping circuits in later stages to remove this injected pedestal and the residual switching signal. If the time is available in the system's application, it is well to have a keyed clamp set the zero signal level after the reading switch has operated and before the reading beam is turned on.

The version of the circuit shown here is undesirable in some applications since it applies the switching voltage to the screen instead of the plate, thus reducing the tube resolution somewhat.[3] Furthermore, the nonlinear characteristic of the crystal diode is a distinct disadvantage if absolute measurements are to be made on the output signal. Fortunately, the majority of practical applications do not require this.

Double Cathode Follower Circuit

The search for an output circuit with a linear characteristic which would enable the measurement of reliable tube data for publication led to a circuit whose steady and reliable operation with good signal separation recommends it for more general use. In the double cathode follower circuit (Figure 6) the screen is dynamically held at a fixed potential. The lower pentode cathode follower feeds electrons into the screen as fast as they are taken out by the upper pentode. This operation is satisfactory even during the rise of the switching signal since both tubes are being operated over their transfer characteristic in the same direction at the same time. This feature is more important than the matching of the tubes. Unmatched tubes have been used with good results for separating the output signal from the switching signals, but it has not been successful in the separation from video input signals applied to the plate. The switching signal transient is about the same size as the output stored signal (Figure 7).

In the circuit shown the switching signal is applied to the grids

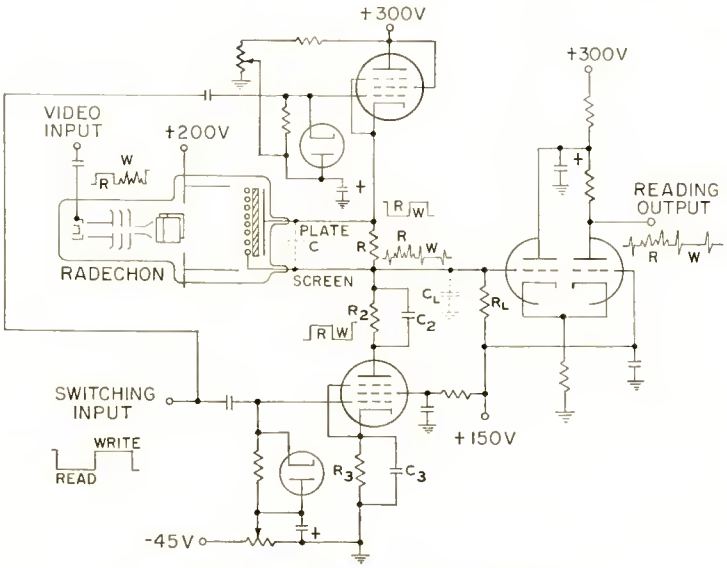

Fig. 6—Double cathode follower circuit.

of both upper and lower cathode followers to turn them on during writing. The switching voltage is then developed across the Radechon target structure. The network R_2C_2 balances that of the resistor R and the Radechon input capacitance C so that, upon cutting off of the cathode followers at the beginning of the reading period, there will be no large switching transient before C discharges. The network R_3C_3 in the cathode of the lower pentode is necessary to provide the same cathode feedback to it as the resistor R and the Radechon target input capacitance C provides to the upper pentode so that both tubes have the same dynamic operating characteristic. A similar network should be in the plate circuit of the upper pentode to balance R_2C_2, but its effect is negligible. All these resistors and capacitors respectively have the same value.

If no switching signal is to appear at the screen during writing, the currents through the two pentodes must be accurately the same. This is accomplished by adjusting their biases as indicated in the diagram. It is obviously impractical to do this manually, but a feedback loop from the output of the amplifier back to the bias source

Fig. 7—Six copies of output stored signal following switching transient.

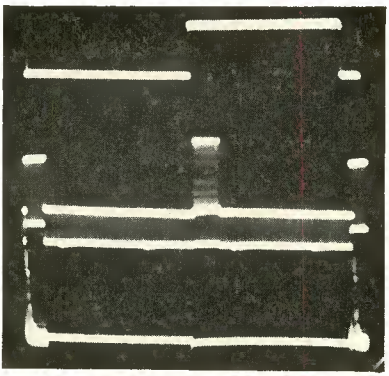

Fig. 8—(*Top*) Switching signal at plate. (*Center*) Input to control grid. First and last bursts are reading gates. Center burst is groups of writing pulses. Blanking applied during fly back. (*Bottom*) Stored output signal from double cathode follower circuit.

for either pentode easily accomplishes this balance. A wide-band feedback loop automatically operates only during writing time since the pentode it controls is cut off thus reducing the loop gain to zero during reading. A slow speed feedback loop, providing essentially d-c bias control must be keyed so that it measures only the writing output otherwise it will respond to the output reading signals. Both types of circuits of conventional design have been operated successfully, both separately and simultaneously. Figure 8 illustrates the balance that can be maintained. The bottom line is the stored signal output of fourteen reading copies following the writing of a group of pulses fourteen times on one single line scan. The output pulses appear very much compressed at the edges. A small discontinuity at the center is the switching transient. Note that the baselines during reading and writing are at approximately the same level, showing good separation of the input switching signal from the output signal.

During the reading period, while the pentodes are cut off, the Radechon load impedance consists of R_L, a known linear resistor which is the grid resistor of the amplifier, and C_L, which is the capacitance to ground of the Radechon target structure, the plate of the lower pentode, the cathode of the upper pentode, the amplifier input and wiring. In all these circuits a cathode-coupled input stage has been used to eliminate Miller-effect capacitance. The heaters of the pentodes were on a d-c supply to prevent hum pick-up at the cathode of the upper pentode. This circuit was used for the measurement of all the data given[2,12] on the Radechons.

[12] A. S. Jensen, "Discharging an Insulator Surface by Secondary Emission Without Redistribution," *RCA Review*, Vol. XIV, pp. 216-233, June, 1955.

A NEW METHOD FOR MAGNIFYING ELECTRON BEAM IMAGES*

By

W. R. Beam

Research Laboratory, RCA Laboratories,
Princeton, N. J.

Summary—*In the development of electron guns for kinescopes, cathode-ray tubes, and similar devices, it is desirable to measure the exact size and shape of the spot illuminating the phosphor screen. The direct method of visual observation is inadequate because of the effects of stray light and secondary electrons. This paper describes a method whereby an undistorted magnified image of the spot may be produced on a phosphor screen, magnified electronically up to forty times. A single deflection yoke sweeps the electron beam across a tiny resolving aperture at the point where the spot analysis is to be made. The current passed by the aperture forms a tiny beam which is swept further to "paint" an enlarged image of the beam on a fluorescent screen. The method permits the use of an auxiliary phototube to measure spot current and current density quantitatively. Electron beams having a wide range of spot size and beam power can now be studied, using this simple apparatus.*

Introduction

In order to obtain optimum brightness and resolution in a cathode-ray-tube display, it is essential that the beam be focused to a small, sharp spot at the screen. One aspect of electron gun development is the measurement of the size and shape of the illuminated spot produced by an unswept beam. At currents used in large kinescopes, it is impossible to stop sweeping the beam without "burning" the phosphor screen. Operation at a current low enough for safe undeflected operation usually results in a major change in spot size, due to the change of electrode voltages and space-charge effects. An alternative is low-duty-cycle pulsed operation. When a low-current or a pulsed spot is observed through a high power microscope, stray light, secondary electrons, and the coarseness of the phosphor all make it difficult to judge the approximate spot size. In the pulsed method, measurements are further complicated by the requirement of pulse voltages of one hundred volts or more; measurement of peak current at low duty cycles also poses a problem.

A method which has seen some practical use is that described by Jacob.[1] The current is measured in a Faraday cage behind a narrow

---

* Decimal Classification: R138.3.

[1] L. Jacob, *An Introduction to Electron Optics*, Wiley, 1951, pp. 127-129.

resolving slit (see Figure 1). The beam is deflected across the slit by a deflecting system, synchronized to the deflection of a cathode-ray oscilloscope. The part of the beam current which passes through the slit is received in the Faraday cage and then flows through an external resistor, producing a voltage which is displayed by proportional vertical deflection on the oscilloscope. The result is a fairly accurate representation of the current in a strip through the beam.

It seems much more desirable to measure the current density point by point; this requires a small hole instead of the slit. The greatest difficulty encountered in this method is determination of the exact position of the spot, and knowing whether the spot is in good focus. If the spot is not axially symmetrical, it is impossible to gain an impression of the types of aberration from which the gun may be suffering. The greatest practical problem associated with a measure-

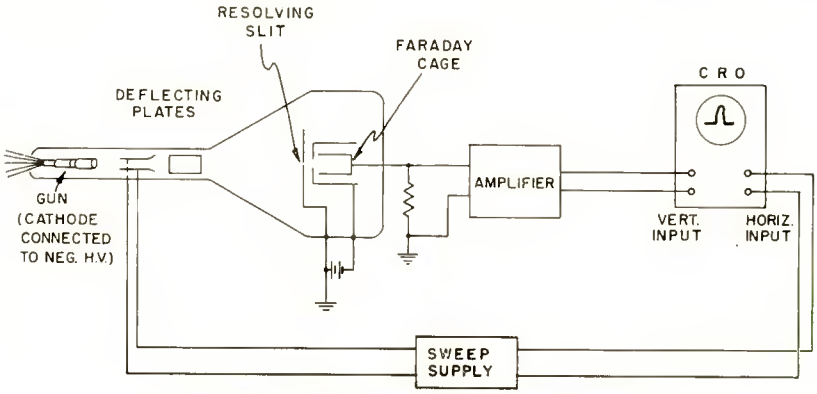

Fig. 1—Schematic diagram of Jacob's method.

ment of this type is in maintaining the cathode and focusing electrodes at potentials far below ground. In tubes requiring high second-anode voltage, battery supplies must be used for control grid, first anode, and other electrodes. If the cathode were operated at ground, the ripple in the second-anode voltage would be picked up in the Faraday cage circuit.

A problem common to all methods involving the measurement of small currents is that of secondary electrons. The measured current is usually an extremely small part of the total beam current. The secondary electron current produced by the main beam is large, and unless a properly constructed Faraday cage is used, these secondaries may find their way to the output. Even the secondary electrons produced by the measured part of the beam may cause trouble if potentials are not properly adjusted and electrodes properly shaped.

The Deflection Spot Magnifier

Because great difficulty was encountered with prior methods, a new method was devised, whereby an electronically magnified image of the spot is produced. The principle is illustrated in Figure 2. The component parts are the tube, which includes the gun to be tested, a plate with a tiny aperture, and a phosphor viewing screen; a deflection yoke of the type commonly used with television kinescopes, together with horizontal- and vertical-sweep circuits; and an auxiliary deflection yoke used for obtaining rough centering and for calibrating the magnification.

The electron beam is ordinarily brought to a focus in the plane of the aperture. In the absence of the aperture, the main deflecting yoke would deflect the entire beam through an arc. At the aperture plane,

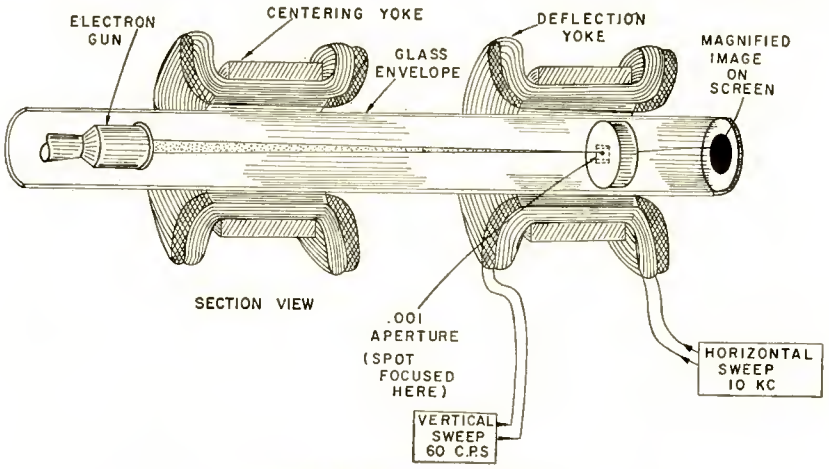

Fig. 2—Spot magnifier.

the deflected position of the beam is considerably less than at the screen. With the aperture plate in position, only a small part of the beam current passes through the hole and is deflected to the screen. The part of the beam from which this small current is taken is a function of the deflection current in the yoke. The position on the screen where this current falls is likewise a function of the yoke current. Thus, every point on the screen has a one-to-one relationship to a point on the cross section of the beam. To a good approximation, this relation is linear; the deflection of the current passing the aperture gives a magnification which is limited only by the presence of stray a-c magnetic fields. In use, the deflection yoke is operated with deflection currents similar to those employed in a television set, and a clear magnified image of the electron spot is viewed on the phosphor screen.

The finest details may be observed, such as lens aberrations and spot asymmetry. Resolution is limited by two factors—the aperture size, and spread of the beam passing through the aperture. The first limitation may be reduced by use of a small aperture, and the second is negligible at suitably large magnification. While, in the Jacob method, variations of electrode voltages may completely confuse the picture, here they merely defocus or shift the spot—conditions which may be readily recognized and corrected.

The size of the magnified spot is sufficient to carry out any qualitative and semiquantitative measurements visually. A ruler may be placed against the face of the tube to measure the magnified spot size to reasonable accuracy. While viewing of the magnified spot is sufficient for some purposes, the use of this technique to obtain precise quantitative data on characteristics of a gun or focusing system requires the addition of a few refinements.

An extra deflection yoke is mounted near the gun, at some distance from the swept yoke. Direct current in this yoke centers the beam on the resolving aperture. It may also be used to determine accurately the degree of magnification. This is carried out as follows: a deflection of the beam by this centering yoke will shift the beam with respect to the aperture. This shift is magnified on the phosphor screen by the magnification ratio of the system. It is convenient to begin with no sweep on the main yoke. By means of the centering yoke, the spot is moved a known distance (an inch or more) at the aperture. This distance can be scribed on the aperture plate, the beam's position being observed by means of a phosphor dusted on the aperture plate. The current required in the centering yoke for this motion is recorded. With the sweep turned on and the magnified image in view, the current in the centering yoke is changed to shift the image a fixed distance on the screen. By taking the ratio of the deflection currents for equal deflections at the screen and at the aperture, the magnification is obtained.

An alternate method of calibration would be to use two resolving apertures, a known distance apart. Two images of the spot would appear. The ratio of their spacing on the screen, to the known aperture spacing, is the magnification. This method of calibration is not good when extremely large magnifications are desired or when the spot is large. In the former case, images from both apertures may not appear at the same time on a small screen. In the latter case, the images may overlap, making observation of spot shape more difficult.

Characteristics and Limitations

One of the important features of this technique is that magnifica-

tion is, for fixed geometry, solely a function of the beam voltage. In fact, to a first approximation, it is even independent of beam voltage. It is readily seen that magnification is the ratio of deflection after the aperture to deflection before the aperture. If the deflection yoke produces substantially linear deflection versus current, the distortion of the image will be negligible. The magnification and distortion are entirely independent of the amplitude of sweep. It is therefore possible to decrease the brightness of the magnified image by increasing the amplitude of sweep. For this reason it is convenient to derive sweep currents from two independent adjustable sources. Vertical sweep at 60 cycles was obtained from a variable auto transformer and step-down transformer, while horizontal sweep at 10 kilocycles came from an audio-signal generator.

It is not necessary that the sweeps be sawtooth in form. If photometric measurements are desired, sawtooth sweep insures that the beam will spend equal times on equal areas of the image. With sinusoidal sweep, the outer edges of the image will be slightly brighter than the center. With sinusoidal sweep of large amplitude, the departure from uniformity is entirely negligible.

If available, a 60-cycle vertical sawtooth sweep is further to be preferred because it lessens the image distortion caused by ripple in the various electrode voltages. With a 60 cycle sawtooth, each part of the beam is imaged once each cycle. With sine sweep, each part is imaged twice each cycle. It is instructive to operate the vertical sawtooth slightly off line frequency. The "wiggling" of the image at the difference frequency indicates the severity of ripple distortion.

The range of beam power over which this method has been successfully used is about .25 to 25 watts. The maximum power is determined by the heating which the aperture plate can stand. The minimum power (or beam current) is largely determined by the size of the resolving aperture and of the beam. At 25 kilovolts, assuming that .001-inch resolution and a magnification of ten is desired, the minimum spot current density giving a useful image is about eight milliamperes per square centimeter.

The only precaution which need be taken when assembling apparatus is to make certain that the horizontal and vertical coils of the deflection yoke do not have different centers of deflection. The result would be slightly different horizontal and vertical magnifications. While in itself not disastrous, two calibrations are needed to establish magnification, one along each axis. It appears, however, that standard deflection yokes designed for use in television receivers are entirely adequate for this application.

Photometric Measurements

While the method as described does not lend itself immediately to quantitative current density measurements, the relation between current and screen illumination at the magnified image is sufficiently linear to allow photometric measurements.

Two types of measurements have been performed. In the first, the object was to determine how much of the beam current overlapped a particular region (round, or of arbitrary shape) on the screen. The measurement is made in two steps. With the image of the spot on the screen, the total screen illumination is read with a photometer. A mask is placed over the image, and the photometer measures the light emerging from the edges of the spot which protrude. The second reading is divided by the first and the result is a "stray current" factor. If a round mask is used, the measurement indicates the relative amount of light emanating from a region outside a circle represented by the mask.

This measurement is affected adversely by light dispersion. For a more accurate measurement, the screen may be coated with two colored phosphors, one in the shape of the desired mask. With proper filters on the photometer, the two contributions can be measured independently. A variation is to leave an uncoated region on the screen in the desired mask shape. The spot is first moved away from this area, to read total light, then moved into the uncoated region to get a minimum light reading. All of these methods give results which are adequate for determining the approximate spot size. (It is convenient to define the spot size as that region which will encompass some specified part of the total light produced.)

The photometer can also be used to measure current density at each point in the spot. First the magnified image is produced. As a guide, the outline of the image can be drawn on the viewing screen. Static deflection replaces the sweep, and the spot can be moved statically to various positions within the outline of the image. At each point, the photometer reading is proportional to the current density. If exact coordinates on the spot are desired, they can be measured from the deflection currents required.

Another type of photometric measurement is made by sweeping along one axis only. The light output is displayed on an oscilloscope whose horizontal sweep is synchronized with that of the deflection coil. The traces are similar to those observed by Jacob;[1] the resolving aperture is round, hence the current *density* as a function of position is measured. Figure 3 shows a trace obtained in this fashion. The double trace near the ends is caused by the decay characteristic of the

phosphor. For this work a short-decay phosphor is best; that used in the tube from which Figure 3 was taken had a rather long decay time. In addition to the elimination of coupling and ripple voltage problems, this method has a further advantage over that of Jacob. It is possible to observe, prior to taking oscilloscope readings, the axis on the spot across which the sweep will be taken. The spot may first be brought to optimum focus and examined for nonuniformities. When the horizontal sweep amplitude is reduced slowly to zero, the vertical sweep continues along the desired axis. By adjustment of centering currents various sections of the spot may be investigated.

Although no attempt was made to correct the readings for nonlinear current–light output characteristics of the phosphor, this would allow more accuracy in these photometric methods.

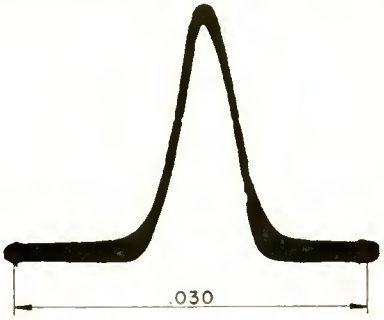

Fig. 3—Current density distribution in focused electron beam, 100 microamperes at 25 kilovolts.

Experimental Setup

Figure 4 illustrates the complete equipment setup for visual observation of the magnified spot. The gun under test is mounted in a tube of uniform 2-inch diameter (see Figure 5). This tube is about 6 inches longer than the tube in which the gun is used, the additional length providing space for deflection of the beam after passing the aperture. The .001-inch diameter aperture in a .005-inch molybdenum sheet is mounted on a cylindrical assembly, loose within the tube. Although 1-mil-diameter apertures were found to give adequate resolution, it is not difficult to produce even smaller holes. To produce the small holes, a hardened steel pin is ground to a fine point. The included angle of the point should be about 60°. The point is pressed a prescribed distance into the molybdenum sheet, which is backed up by a copper or soft steel plate. The resulting boss on the reverse side is ground down until the aperture thus presented is of the desired size.

The aperture assembly can be moved (by shaking the tube) to any

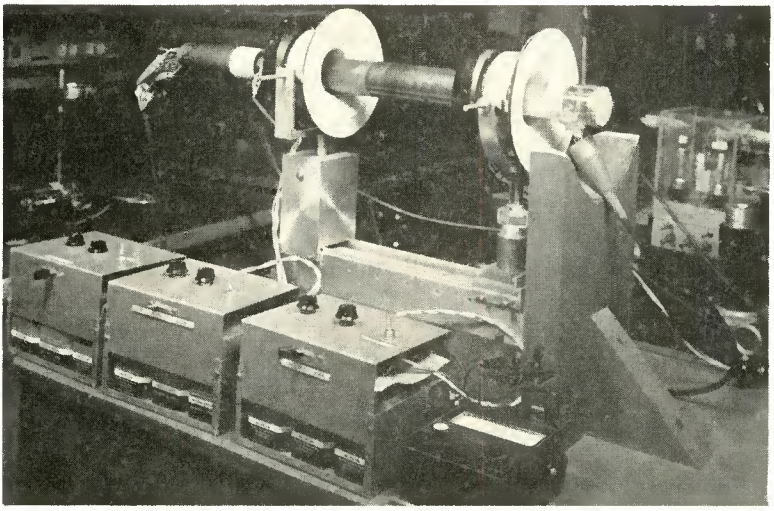

Fig. 4—Spot magnifier set up for operation.

desired distance from the screen. This motion permits coarse adjustment of the magnification while fine adjustment is made by axial movement of the sweep yoke. By the combination of these two adjustments, magnifications from 7 to 40 are obtained. There is no real limit on the magnification, except perhaps that set by stray a-c magnetic fields. An additional feature of the tube is the ability to drop the aperture plate to the side of the bulb, leaving an opening more than an inch in diameter. Such a feature is of considerable utility in examining the spot at normal size.

Photometric measurements were made with a type 6199 end-on multiplier phototube enclosed in an electrically insulated, light-tight tube which could be slipped over the 2-inch viewing screen of the tube under test.

Conclusions

The spot magnifying system described has proved to be a most

Fig. 5—Standard spot magnifier envelope.

useful instrument in high-resolution electron-gun research. Electron beam power up to 25 watts can be handled without resort to pulsing schemes, and resolution depends only upon the size of the resolving aperture. The magnification system requires the most elementary of equipment, and constant magnification is obtained even with unregulated power and sweep supplies. It is not necessary to operate the tube with the cathode below ground potential, nor to use high-voltage coupling circuits.

Calibration is performed with four simple measurements, two of current and two of sweep distance. Magnification may be made as large or as small as desired, in a single tube; once calibrated, it is not necessary to recalibrate unless the tube is moved.

Photometric measurements, while somewhat more questionable than current measurements, are simple to perform. The uncertainty of spot shape and position in the Jacob method has been eliminated, since the spot can be observed before photometric data is taken.

By using this method of gun testing, more quantitative data can be obtained than through the use of larger, more complicated testing tubes. Because each gun can be sealed into its own small, cheap, simply constructed envelope, it is possible to test, store, and retest guns with ease.

A NOVEL ULTRA-HIGH-FREQUENCY HIGH-POWER-AMPLIFIER SYSTEM*†

By

L. L. Koros

Engineering Products Division, Radio Corporation of America, Camden, N. J.

Summary—*A novel type of power amplifier, especially developed for high-power ultra-high-frequency monochrome and color television transmitters, but also applicable to other services such as scatter-propagation, is described. The amplifier employs type 6448 beam-power tubes for class-B service up to 15 kilowatts peak of sync output with an amplification factor of 15 at 6 megacycles bandwidth (.5 decibel points) and, for class-C service with a power amplification factor of 50. The amplifier design is applied in the TTU-12A transmitter.*

The plate-cavity construction is unconventional. It is believed that the cavity design which is described in connection with the type 6448 beam power tube can also be adapted to other, higher powered ultra-high-frequency tubes which may follow in the future.

An open-circuited half-wavelength plate-cavity is used which consists essentially of one high-impedance and one low-impedance quarter-wavelength section. No conventional load-coupling element is used; the output transmission line is directly connected to the power-tube plate through a d-c blocking condenser. The grid circuit operates in three-quarter-wavelength mode.

A computation method is presented to predict the bandwidth and other cavity-design data, such as the loading resistance reflected to the power-tube and the voltage distribution in the cavity. The practical application of the analytical expressions is demonstrated in an example.

An analytical method and a graph are presented in the Appendix for the determination of the stored wattless power in transmission-line elements which form part of resonant cavities.

Introduction

THE problem of producing high power at ultra-high-frequencies (UHF) for television transmitters has been attacked in several ways. Paralleling of small tubes[1,2] led to transmitters for up to

---

* Decimal Classification: R355.7 × R583.4.

† A paper on the amplifier was presented at the Fourth Annual Broadcast Symposium of the I.R.E. Professional Group on Broadcast Transmission Systems, Cleveland, Ohio, on September 24, 1954, and was published in the *I.R.E. Transactions* PGBTS-1, pp. 18-26, March, 1955.

[1] G. H. Brown, W. C. Morrison, W. L. Behrend and J. G. Reddeck, "Method of Multiple Operation of Transmitter Tubes Particularly Adapted for Television Transmission in the UHF Band," *RCA Review*, Vol. X, pp. 161-172, June, 1949.

[2] L. S. Lappin and J. R. Bennett, "A New Ultra-High-Frequency Television Transmitter," *RCA Review*, Vol. XI, pp. 190-211, June, 1950.

one kilowatt. An efficient one-kilowatt power tetrode,[3] type 6181, was developed later and attempts were made to attain a substantial increase in the operating level of higher powered grid-controlled tubes. Also, the application of radio-frequency (r-f) power tubes, previously successfully used for shorter wavelengths, was considered for the UHF region. It was shown that magnetrons, frequency and phase controlled by an r-f injection source[4-6] might be suitable. Klystron amplifiers[7,8] were demonstrated later as useful high-power tubes in this region. Finally, continuous developmental work resulted in a 15-kilowatt UHF beam-power tube.[9] Circuit development work was carried out concurrently with the tube development, and early in 1953 the 15-kilowatts peak of sync power-output was obtained. A report on the practical aspects of the amplifier system was presented elsewhere.[10] The present paper describes the result of the circuit-development work which adapts the 6448 high-power tetrode to monochrome and color UHF television transmitters.

Special Problems

Some of the problems which arose in the development of the UHF high-power amplifier differed from those encountered at lower carrier frequencies. Whereas the power and voltages in the input circuit are of moderate level and consequently do not require the application of basically new techniques, the output-circuit design must solve the following problems:

(a) The space available in the cavity to apply conventional load-coupling elements is inherently small due to the short wave-

---

[3] W. P. Bennett and H. K. Kazanowski, "One-Kilowatt Tetrode for UHF Transmitters," *Proc. I.R.E.*, Vol. 41, pp. 13-19, January, 1953.

[4] L. L. Koros, "Frequency Control of Modulated Magnetrons by Resonant Injection System," *RCA Review*, Vol. XIII, pp. 48-57, March, 1952.

[5] J. S. Donal, Jr. and K. K. N. Chang, "An Analysis of the Injection Locking of Magnetrons Used in Amplitude-Modulated Transmitters," *RCA Review*, Vol. XIII, pp. 240-257, June, 1952.

[6] L. L. Koros, "Measurements of Some Operational Characteristics of an Amplitude-Modulated Injection-Locked UHF Magnetron Transmitter," *Proc. I.R.E.*, Vol. 41, pp. 4-10, January, 1953.

[7] D. H. Priest, C. E. Murdock, and J. J. Woerner, "High-Power Klystron at UHF," *Proc. I.R.E.*, Vol. 41, pp. 20-25, January, 1953.

[8] Norman Hiestand, "High-Power UHF Klystron-Amplifier Design," *Convention Record of the I.R.E., 1953 National Convention*, Part 4, *Broadcasting and Television.*

[9] W. P. Bennett, "A Fifteen-Kilowatt Beam-Power Tube for UHF Service," *I.R.E. Transactions* PGBTS-1, pp. 11-17, March, 1955.

[10] L. L. Koros, "High-Power UHF-TV Uses Grid-Control Tube," *Electronics*, pp. 130-134, April, 1955.

lengths involved. High d-c and r-f voltages, due to the high output power, increase the difficulties.

(b) The stored wattless power must be kept low in the plate cavity in order to obtain the required bandwidth with an adequate plate-loading resistance. Furthermore, the power losses in the cavity due to circulating currents must be kept low.

(c) A wide tuning-range must be covered with a minimum of component changes in the cavity.

All three requirements are satisfied by a novel type of cavity design which, as a consequence of properly selected line-impedance combinations, acts as a voltage step-down transformer between the tube and load. Inherently, this type of cavity stores only the minimum amount of wattless power. The same type of plate cavity can be applied for class-B linear r-f amplifiers and for high-level-modulated class-C amplifiers and also for the class-C amplifiers for FM sound-channel application. The experimental work was done on a class-B linear amplifier system in which the r-f exciter, a one-kilowatt type 6181 tetrode stage, was cathode modulated with the video signal. A class-C stage was employed to amplify frequency-modulated sound transmission.

Basic Design of the Plate Cavity

The type 6448 tube is a grid-driven, grounded-cathode, grounded-screen-grid amplifier. A half-wavelength resonator was selected for the plate. It is not feasible to build a quarter-wavelength plate cavity for the UHF range with the 6448 tube, because the first low-voltage plane is within the plate-seal region of the tube. Figure 1 represents a typical form of the cavity. An important element of the cavity is a sliding line section which acts as a tuner and also as a coupling reactance between the tube and antenna. This work was based in part on work with cavities including sliding capacitors as tuning elements done by L. W. Haeseler and S. A. Watson[11] and by T. M. Gluyas, Jr., and on L. S. Nergaard's studies[12] on cavities.

The oversimplified schematic representation of the basic circuit is shown in Figure 2. The cavity, like the tube, is built from coaxial transmission-line elements. Figure 2 shows the cavity elements as two-wire transmission-line sections for clearer representation only.

---

[11] U.S. Patent No. 2,421,784, filed February, 1943.

[12] L. S. Nergaard, "A 5031 as a Wide-Band 520 MC Power Amplifier," presented at the *I.R.E. Electron-Tube Conference*, Cornell University, June 28, 1948.

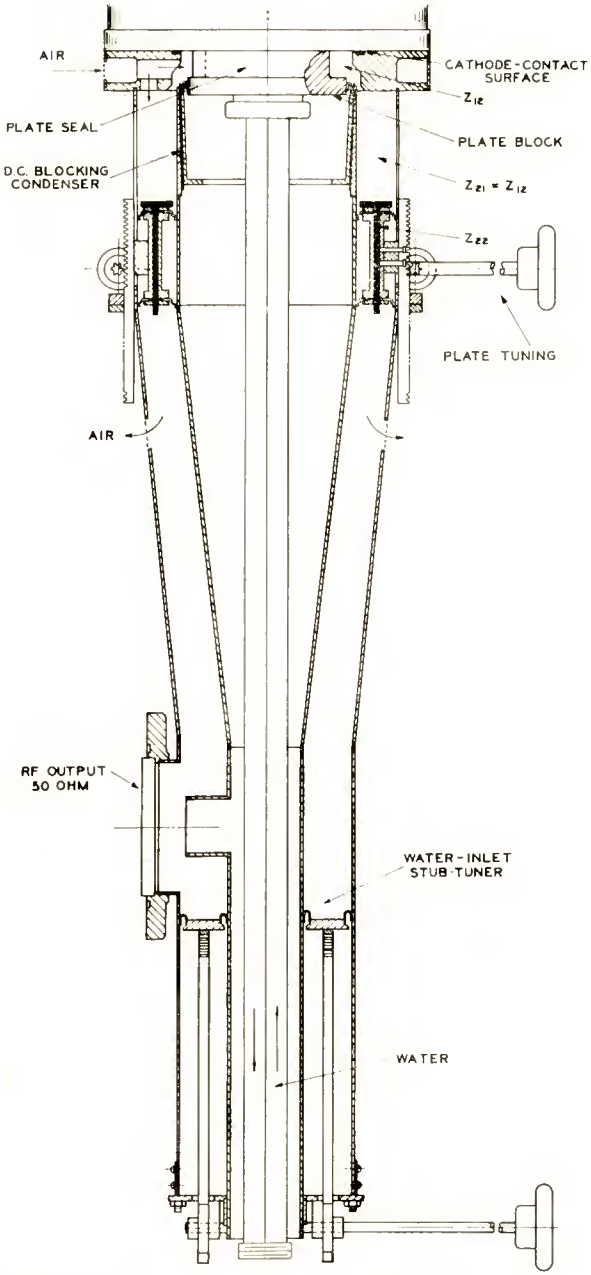

Fig. 1—Plate Cavity. The tuning section, Z_{22}, is at low-frequency position.

The condenser C is the plate end capacity of the tube-anode block. The first quarter-wavelength cavity section begins in the tube. In the over-simplified representation, the first part of the first $\lambda/4$ coaxial cavity section, which is in the tube, has a uniform Z_{11} surge-impedance up

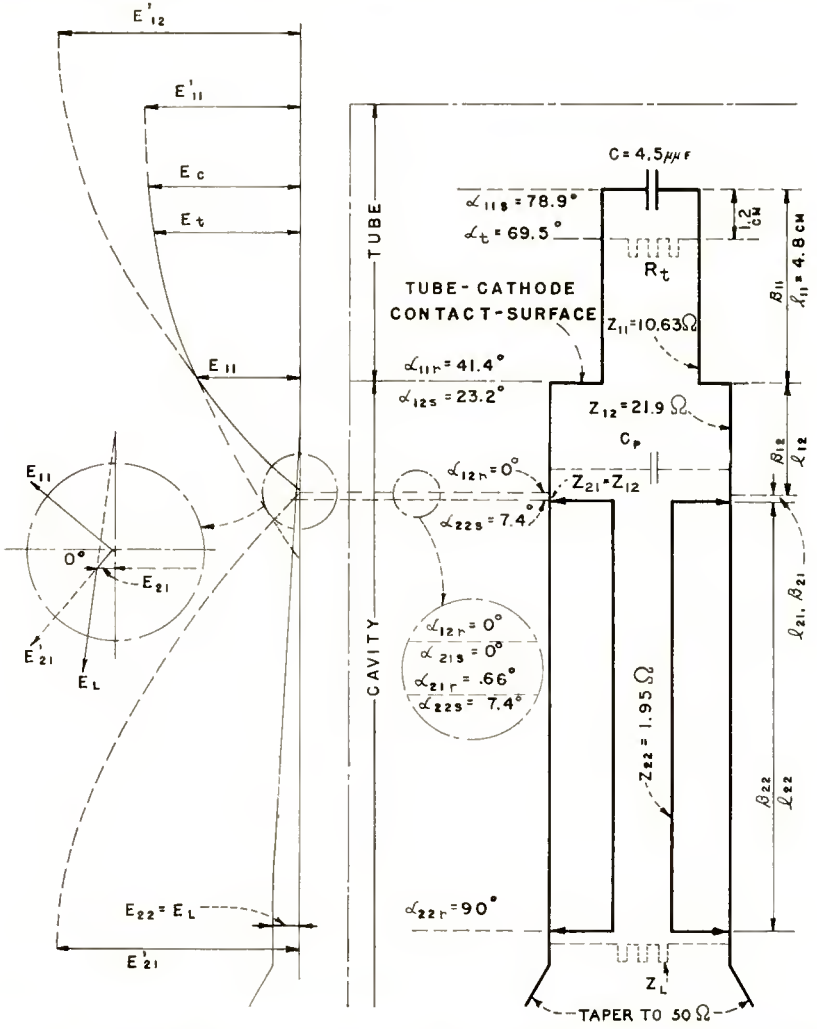

Fig. 2—Length of the line elements and voltage distribution in the plate cavity.

to the r-f cathode contact surface (Figure 2). The second part of the first $\lambda/4$ section, with Z_{12} surge impedance, is in the cavity. The high standing-wave ratio section of the cavity (Figure 1) is built from two line sections each of which is uniform electrically: Z_{12} and the

sliding element, Z_{22}. Mechanically, the Z_{12} line element is composed of two sections. In the first section the inner conductor of the coaxial cavity is the tube-anode block; in the second section the inner conductor is the cavity line which contacts the tube plate. To assure an equal surge impedance in both sections, the external conductor of the cavity follows the diameter changes of the inner conductor. There are two discontinuities, however, in the Z_{12} section. One is the d-c blocking condenser for the plate voltage. This condenser, with Teflon* dielectric, is built into the cavity center conductor; consequently, it is in series with Z_{12}. This condenser shows a very low reactance for the Z_{12} line, and thus can be neglected in the computation. The other discontinuity is a capacitance (C_p in Figure 2) which is parallel with the Z_{12} line. C_p is formed between the tube-plate contacting edge and the external conductor of the cavity. It can be considered as a lumped capacitor with the value of several micro-microfarads. It will be shown in a practical computation that C_p is close to the low-voltage plane, and thus has only a negligible effect.

The second $\lambda/4$ section starts with a line section of Z_{21} surge impedance, but it is substantially confined into a low-surge impedance line section, Z_{22}. This Z_{22} section slides on contact springs in the Z_{21} impedance section. Z_{21} is a constant-impedance extension of the first $\lambda/4$. The position of the sliding line section determines the length of the half-wavelength resonator, and tunes the carrier frequency. The surge impedances of the sliding section and of the section in which it slides are selected to obtain at the load end of Z_{22} the necessary voltage, which must be applied on the Z_{21} line surge impedance to produce the rated power output, P_o. In this ideal case $Z_{21} = Z_L$, which is the load reflected at the end of the cavity. The effect of deviation from the ideal is discussed later. The impedance Z_{21} is transformed by a tapered section into 50 ohms, which is the surge impedance of the antenna line. The tapered section, if it is sufficiently long, introduces negligible reflection. The application of the tapered section is shown in Figure 1.

Length of the Cavity Components and Tuning

The lengths of the coaxial line elements are determined from the resonance requirement of an electrical half-wave resonator, open circuited at the tube end and at the cavity (load) end. The dimensions of the tube determine the length and surge impedance of one part of the plate network which, as an oversimplification, is replaced by a

* Registered trade mark of the E. I. DuPont Co.

uniform line element. This line element has a length $l_{11} = 4.8$ centimeters, $Z_{11} = 10.63$ ohms, and $C = 4.5$ micromicrofarads, which are representative of a typical tube. The rest of the line elements are in the cavity and can be selected by the designer.

The computation of the cavity is based on some further approximations. It is supposed that the loaded Q of the cavity is high, and consequently the minimum voltage in the cavity can be considered as substantially zero. Furthermore, the cavity is considered to be lossless. The array of the forty tube units, which together form the type 6448 beam-power tube,[5] is considered as one generator. This generator is concentrated on the circle connecting the vertical centers of the forty tube elements. This center-line is 1.2 centimeters from the end of the plate block and is designated the α_t plane in Figure 2. The limiting planes of the cavity sections are designated by α combined with a subscript which is composed of the section number and s for the sending (tube) end and r for the receiving (load) end. As an example, the condenser plane is the sending end of the first section of the first $\lambda/4$, thus it is designated α_{11s}. The lengths of the line elements in centimeters are designated by l; the corresponding lengths in degrees are designated by β, in both cases with a subscript indicating the section.

We may write

$$\tan \alpha_{11s} = \frac{1}{2\pi f C Z_{11}} \tag{1}$$

$$\beta_{11} = \frac{l_{11}}{\lambda} 360^\circ = \frac{4.8}{\lambda} 360^\circ \tag{2}$$

$$\alpha_{11r} = \alpha_{11s} - \beta_{11} \tag{3}$$

$$\alpha_t = \alpha_{11s} - \frac{1.2}{\lambda} 360^\circ. \tag{4}$$

At the joint plane of the line elements of Z_{11} and Z_{12} surge impedance, which is the joint plane of the tube and cavity, the reactance must be the same looking toward the generator and the load. Consequently

$$\tan \alpha_{12s} = \frac{Z_{11}}{Z_{12}} \tan \alpha_{11r}. \tag{5}$$

The zero-volt plane is at the end of the Z_{12} line element; thus $\alpha_{12r} = 0$. At this plane the first $\lambda/4$ portion of the cavity joins the second $\lambda/4$ portion. This second $\lambda/4$ portion is composed of a relatively short line element of $Z_{21} = Z_{12}$, and of a sliding line section of Z_{22}. As a rule,

$$Z_{22} << Z_{12} < 50 \text{ ohms.} \tag{6}$$

The length of the Z_{22} section, β_{22}, is selected to cover a predetermined frequency range. It is assumed first that the sliding tuning section is shorter than $\lambda/4$. This is, however, not essential. For resonance, the reactance of the Z_{22} section must match the reactance of the Z_{21} section; thus

$$\tan \beta_{21} = \frac{Z_{22}}{Z_{21}} \cot \beta_{22} \tag{7}$$

$$\beta_{21} = \alpha_{21r} \tag{8}$$

and

$$\alpha_{22s} = \alpha_{22r} - \beta_{22} = 90^\circ - \beta_{22}. \tag{9}$$

The length β_{21} determines the distance of the tuning element Z_{22} from the zero-volt plane in the cavity:

$$l_{21} = \frac{\beta_{21}}{360^\circ} \lambda. \tag{10}$$

If the length of the sliding tuning element selected is longer than 90°, the resonance position of the tuning element brings the sending-end edge of the sliding line to the generator side of the zero-voltage plane. The zero-voltage plane is on the sliding element. This is an acceptable condition, provided the zero-voltage plane is not too far away from the sending end of the tuning element. The minimum amount of energy is stored in the unique case of a 90° tuning element. It is assumed for our computation that the receiving-end plane of Z_{22} ($\alpha_{22} = 90^\circ$) is loaded with a resistance, Z_L. It is further assumed that Z_L is selected to be equal to Z_{21}; thus it is transformed by the tapered section (Figure 1) into 50 ohms (the surge impedance of the output transmission line) without producing standing waves, and thus the end of the high standing-wave ratio section of the cavity is at the α_{22} plane.

The Z_{22} section is built with Teflon dielectric. The surge impedance of such a Teflon-dielectric line section can be selected as low as necessary, without fear of breakdown. Care should be taken when selecting the diameters of the d-c plate blocking condenser and of the sliding section that they do not support a $TE_{1,1}$ mode resonance in the output frequency region. Figures 3, 4, and 5 are photographs of the main components of the plate cavity.

Sample Tuning Calculations

The lengths of a plate cavity will be computed for a carrier frequency of 650 megacycles ($\lambda = 46.2$ centimeters), with the following tube data: $C = 4.5$ micromicrofarads, $Z_{11} = 10.63$ ohms, and $l_{11} = 4.8$ centimeters. Circuit values: $Z_{12} = 21.9$ ohms, $Z_{22} = 1.95$ ohms, $\beta_{22} =$

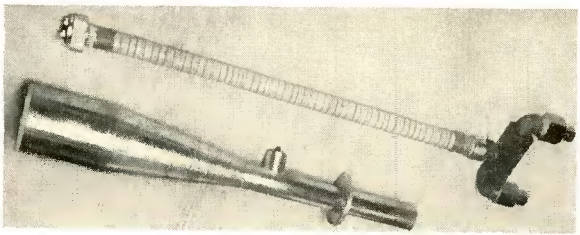

Fig. 3—Inner conductor of the plate cavity and insulated water pipe. The pipe is inserted into the inner conductor in operating condition.

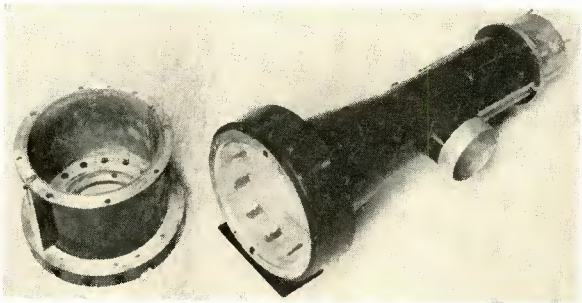

Fig. 4—External conductor of the plate cavity. The cylindrical and tapered parts are disassembled.

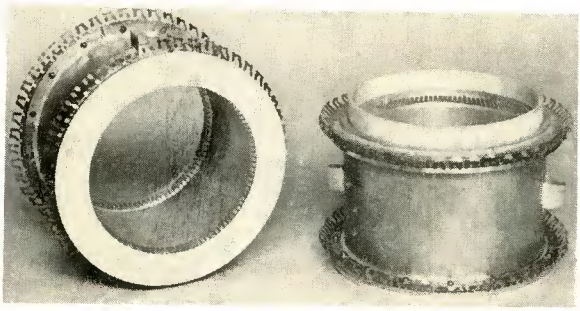

Fig. 5—Teflon-insulated sliding tuning line section. Two identical units are shown in different positions; only one is inserted into the plate cavity in operating condition.

82.6°. The mechanical length of β_{22} is (82.6°/360°) 46.2 = 10.6 centimeters in air line, which is $10.6/\sqrt{2} = 7.5$ centimeters in Teflon-insulated line. Experiments indicate that the stray capacity at the line ends is equivalent to 0.5 centimeter line length. The physical length of the 82.6° sliding section becomes, therefore, 7 centimeters. From Equation (1)

$$\tan \alpha_{11s} = \frac{1}{2\pi \times 650 \times 10^6 \times 4.5 \times 10^{-12} \times 10.63}$$

and $\alpha_{11s} = 78.9°$ (See Figure 2).

From Equations (2) and (3)

$$\beta_{11} = \frac{4.8}{46.2} \times 360° = 37.5°$$

$$\alpha_{11r} = 78.9° - 37.5° = 41.4°.$$

The position of the idealized generator plane from Equation (4) is

$$\alpha_t = 78.9° - \frac{1.2}{46.2} \times 360° = 69.5°.$$

The position of the joint plane of Z_{11} and Z_{12} line elements in the Z_{12} line, from Equation (5), is

$$\tan \alpha_{12s} = \frac{10.63}{21.9} \tan 41.4°,$$

$$\text{thus } \alpha_{12s} = 23.2°.$$

The position of the sliding line for tuning of 650 megacycles will be, from Equation (7),

$$\tan \beta_{21} = \frac{1.95}{21.9} \cot 82.6°$$

$$\beta_{21} = \alpha_{21s} = 0.66°$$

and the distance of the Z_{22} sliding section from the 0-volt line becomes

$$l_{21} = \frac{.66°}{360°} \times 46.2 = 0.085 \text{ centimeters.}$$

The distance of the 0-volt line from the tube contact surface is

$$l_{12} = \frac{23.2^\circ}{360^\circ} \times 46.2 = 2.98 \text{ centimeters.}$$

The position of the sending end of the Z_{22} line section, from Equation (9), is

$$\alpha_{22s} = 90^\circ - 82.6^\circ = 7.4^\circ.$$

Voltage Distribution in the Cavity

The "tube" is considered to be concentrated in the α_t plane. A fictitious loading resistor, R_t, is reflected into this tube plane by the antenna. The antenna resistance is reflected at the end of the $\lambda/2$ cavity, at the $\alpha_{22r} = 90^\circ$ plane as another fictitious resistor, Z_L. Between the load, Z_L, and R_t, the cavity is interconected as a transformer. The transformer ratio is determined by the selected surge impedances, Z_{12} and Z_{22}, and by the electrical length of the Z_{22} line, β_{22}. The transformer ratio will be obtained by computing the voltage distribution in the different planes in the cavity.
The output, P_o, produces

$$E_t = \sqrt{P_o R_t} \tag{11}$$

voltage in the α_t plane of the cavity. The fictitious high voltage in the first $\lambda/4$ section becomes

$$E'_{11} = \frac{E_t}{\sin \alpha_t}. \tag{12}$$

E'_{11} is the voltage which would be built up if the first $\lambda/4$ section were not terminated with a condenser C at the α_{11s} plane ($\alpha_{11s} < 90^\circ$), and the Z_{11} line section were extended to 90°. The voltage at the end of the anode block of the tube becomes

$$E_c = E'_{11} \sin \alpha_{11s}. \tag{13}$$

The voltage at the end of the Z_{11} line,

$$E_{11} = E'_{11} \sin \alpha_{11r}. \tag{14}$$

The fictitious high voltage in the Z_{12} line section becomes

$$E'_{12} = \frac{E_{11}}{\sin \alpha_{12s}} = E'_{11} \frac{\sin \alpha_{11r}}{\sin \alpha_{12s}}. \tag{15}$$

The standing wave in the cavity has a 0-volt plane at the end of the Z_{12} line section. The cavity current at the 0-volt plane becomes

$$I_0 = \frac{E'_{12}}{Z_{12}}. \tag{16}$$

The surge impedances Z_{12} and Z_{21} are equal in this case. Consequently, the fictitious high voltages, E'_{12} and E'_{21}, are also equal in the relevant line sections. The voltage at the joint of the Z_{21} surge-impedance line and the sending end of the sliding Z_{22} tuning line section becomes

$$E_{21} = E'_{21} \sin \alpha_{21r} \tag{17}$$

and at the end of the cavity, in the $\alpha_{22} = 90°$ plane,

$$E_{22} = \frac{E_{21}}{\sin \alpha_{22s}} = E'_{21} \frac{\sin \alpha_{21r}}{\sin \alpha_{22s}} = E'_{12} \frac{\sin \alpha_{21r}}{\sin \alpha_{22s}}. \tag{18}$$

The voltage computed from Equation (18) determines the necessary load, Z_L, which absorbs the power output, P_o:

$$Z_L = \frac{E_{22}^2}{P_o}. \tag{19}$$

Considering Equations (19), (18), (15), (12), and (11), one may write

$$Z_L = R_t \left(\frac{\sin \alpha_{11r} \times \sin \alpha_{21r}}{\sin \alpha_t \times \sin \alpha_{12s} \times \sin \alpha_{22s}} \right)^2 \tag{20}$$

The voltage step-down ratio of the cavity from the tube plane to the Z_L plane, which is independent from the selection of R_t and depends only on the tube and cavity geometry, becomes

$$n = \frac{\sin \alpha_t \times \sin \alpha_{12s} \times \sin \alpha_{22s}}{\sin \alpha_{11r} \times \sin \alpha_{21r}}. \tag{21}$$

Experimental data, analyzed with the help of the equations described here, demonstrated that the optimum load for the 6448 tetrode in

class-B, television picture-channel operation is $R_t = 700$ to 1100 ohms and for class-C sound-channel operation, 1000 to 1300 ohms. The adjustment of Z_L may set R_t within the proper limits. The bandwidth also depends on the selection of R_t.

Sample Voltage-Distribution Calculations

The voltage distribution will now be computed for the previous example. The useful power output from the cavity P_o is 14 kilowatts at the peak of the sync pulses. The tube must deliver about one kilowatt more to cover the losses in the plate network; however, the 14-kilowatt figure is conservative, since higher useful outputs have been obtained with the 6448 tube. For the sake of simplicity, the cavity attenuation will be neglected. The computation will be made for plate-loading resistors, $R_t = 1000$ ohms, an arbitrary value. The actual load value will be determined later to meet the bandwidth requirements.

According to Equation (11)

$$E_t = \sqrt{14000 \times 1000} = 3740 \text{ volts, r.m.s.}$$

The fictitious high voltage in the first $\lambda/4$ section from Equation (12) is

$$E'_{11} = \frac{3740}{\sin 69.5^\circ} = 3990 \text{ volts, r.m.s.}$$

The voltage at the end of the anode block of the tube is, according to Equation (13),

$$E_c = 3990 \sin 78.9^\circ = 3920 \text{ volts, r.m.s.}$$

The voltage at the cavity-to-tube joint plane is, according to Equation (14),

$$E_{11} = 3990 \sin 41.4^\circ = 2640 \text{ volts, r.m.s.}$$

The fictitious high voltage in the Z_{12} line section, according to Equation (15), becomes

$$E'_{12} = 3990 \frac{\sin 41.4^\circ}{\sin 23.2^\circ} = 6690 \text{ volts, r.m.s.}$$

The cavity current at the zero-volt plane, according to Equation (16), becomes

$$I_0 = \frac{6690}{21.9} = 305 \text{ amperes, r.m.s.}$$

At the sending end of the sliding tuning-line section, from Equation (17),

$$E_{21} = 6690 \sin 0.66^\circ = 77 \text{ volts, r.m.s.}$$

and according to Equation (18), at the load-end of the cavity

$$E_{22} = 6690 \frac{\sin 0.66^\circ}{\sin 7.4^\circ} = 598 \text{ volts, r.m.s.}$$

and from Equation (19), the load which must be presented to the cavity to absorb the 14-kilowatt power at the end of the sliding tuning section is

$$Z_L = \frac{598^2}{14000} = 25.6 \text{ ohms.}$$

If this load were applied, the tube would see $R_t = 1000$ ohms as the reflected plate loading.

The voltage step-down ratio of the cavity between the α_t tube plane and the α_{22r} load plane, according to Equation (21), is

$$n = \frac{\sin 69.5^\circ \times \sin 23.2^\circ \times \sin 7.4^\circ}{\sin 41.4^\circ \times \sin .66^\circ} = 6.24.$$

Computation of the Wattless Power and the Plate-Loading Resistance

The wattless power in the cavity will now be determined. Each cavity section will be considered individually. The reactive volt-amperes in the capacitance of a line section which is shorter than a quarter wavelength and extends from the α_1 to the α_2 planes (see Figure 14C) is expressed by

$$VA = \frac{E'^2}{Z} (K_{a1} - K_{a2}) \tag{22}$$

where

$$K_{a1} = \frac{\alpha_1}{2} - \frac{1}{4} \sin 2\alpha_1 \tag{23}$$

$$K_{a2} = \frac{\alpha_2}{2} - \frac{1}{4} \sin 2\alpha_2. \tag{23}$$

The line sections from the 90° (maximum voltage plane) to the α_1 plane and from 0° (0-volt plane) to α_2 are replaced by other components producing matching reactances at the α_1 and α_2 planes. E' is the fictitious high voltage which is present if the line section is extended to 90°; Z is the surge impedance of the line. The derivations of Equations (22) and (23) are presented at the end of the paper as an Appendix. To simplify the computations the values of K_a are presented for $\alpha = 0$ to 90° in Figure 15.

The voltage E_c at the end plane of the anode block produces the wattless power in the anode-to-ground condenser C (Figure 2) of

$$VA_c = 2\pi f C E_c^2. \tag{24}$$

The capacitive wattless power in the Z_{11}, Z_{12}, Z_{21}, and Z_{22} line elements, according to Equations (22) and (23), are

$$VA_{11} = \frac{E'_{11}{}^2}{Z_{11}} (K_{a11s} - K_{a11r}) \tag{25}$$

$$VA_{12} = \frac{E'_{12}{}^2}{Z_{12}} K_{a12s} \tag{26}$$

$$VA_{21} = \frac{E'_{21}{}^2}{Z_{21}} K_{a21r} = \frac{E'_{12}{}^2}{Z_{12}} K_{a21r} \tag{27}$$

$$VA_{22} = \frac{E_{22}{}^2}{Z_{22}} (K_{90} - K_{a22s}). \tag{28}$$

The total wattless power in the cavity is

$$\Sigma VA = VA_c + VA_{11} + VA_{12} + VA_{21} + VA_{22} \tag{29}$$

and the loaded Q is expressed by $\Sigma VA/P_0$. The wattless power and the loaded Q of the cavity were computed with an arbitrarily selected plate-loading resistance, R_t. We may write, however,

$$X = \frac{E_t{}^2}{\Sigma VA}. \tag{30}$$

E_t was determined from Equation (11). X represents the lumped capacitive, or inductive, branch reactance of a fictitious parallel-tuned tank circuit which stores ΣVA wattless power with E_t tube voltage. Their ratio X, however, is independent of the value of R_t. Consequently, X can be obtained without considering R_t. From the values of the wattless-power components from Equations (24) to (28), and the voltage Equations (12), (13), (15) and (18), Equation (30) can be transformed to

$$X = \sin^2 \alpha_t \left[2\pi f C \sin^2 \alpha_{11s} + \frac{K_{a11s} - K_{a11r}}{Z_{11}} + \frac{K_{a12s} \sin^2 \alpha_{11r}}{Z_{12} \sin^2 \alpha_{12s}} + \frac{(K_{90} - K_{a22s}) \sin^2 \alpha_{11r} \times \sin^2 \alpha_{21r}}{Z_{22} \sin^2 \alpha_{12s} \times \sin^2 \alpha_{22s}} \right]^{-1}. \quad (31)$$

Obviously, Equation (31) depends only on tube and cavity geometry. VA_{21} was omitted in Equation (31) because it has a negligible low value. For practical computation of X, Equation (30) is preferable, because it is useful to obtain approximative values for the wattless powers in the cavity sections.

From the definition, the loaded Q may also be written

$$Q_L = \frac{R'_t}{X} = \frac{f}{BW}. \quad (32)$$

thus

$$R'_t = X \frac{f}{BW}. \quad (33)$$

Loading Control

R'_t is the plate loading which must be used to obtain the required bandwidth, BW. To this end the load at the α_{22r} plane, Z_L, must be selected according to Equation (20). The value of R'_t in Equation (20) must be taken from Equation (33). Note the voltage distribution in Figure 2, following the solid line. The voltage is stepped down first by the sliding Z_{22} line section to a lower value than required for the 50-ohm line. This factor helps to keep the stored wattless power low in the cavity. The tapered section (shown in Figure 1) steps the voltage up for the 50-ohm line without substantially increasing the stored wattless power. The cavity stores less than 20 per cent of the over-all wattless power and more than 80 per cent is stored in the tube.

If no impedance transformer is connected between the 50-ohm

output line and the terminating 50-ohm load (antenna), the only possible Z_L value is identical to Z_{21}. Z_{22} and β_{22} *are to be selected by the designer to approach this ideal case at the proper tube plate loading,* R_t, *and at the required bandwidth,* BW. In this ideal case, the line between the end of the Z_{22} section and the antenna is matched.

Such an ideal condition cannot be obtained for all the frequencies in a cavity where tuning within wide carrier-frequency limits is a requirement. It is possible, however, to reach a satisfactory compromise. To correct deviations from the ideal, a resistance transforming device is necessary in the 50-ohm output line. This device must intro-

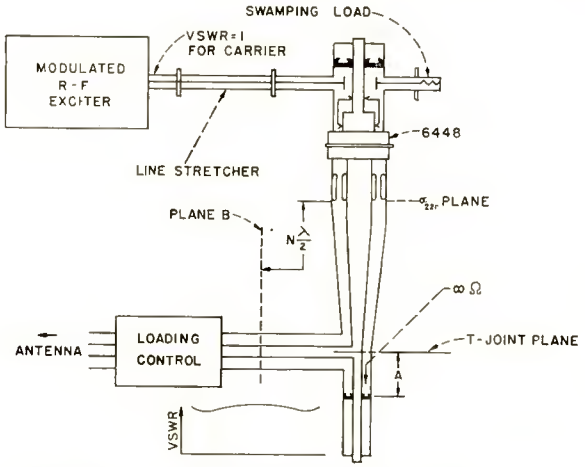

Fig. 6—Operational adjustments of the system.

duce a moderate standing wave in the tapered section, and by this means the value of Z_L at the $\alpha_{22r} = 90°$ plane can be adjusted to a value which is different from Z_{21}.

Care must be taken to ensure that the impedance transformer shows a pure resistive load to the $\alpha_{22r} = 90°$ plane of the cavity, in which case the loading control will have no detuning effects. To attain this end, it is necessary to find the first plane in the output line which is an electrical half-wave in distance from the α_{22r} plane. This plane (plane B in Figure 6) can be determined by a cold test. Before the cold test is made the distance of the short-circuiting plunger from the T-joint, A in Figure 6, must be set in an electrical $\lambda/4$ position. Any loading-control system may be used which can be preset to produce higher or lower resistance than the transmission-line surge impedance in plane B and consequently in the α_{22r} plane.[13] The loading-control

[13] See T. Moreno, *Microwave Transmission Design Data*, McGraw-Hill Co., Inc., New York, 1948, pp. 103-110.

unit serves to change the reflected antenna resistance at plane B into a higher value than the line surge-impedance if the plate cavity bandwidth must be narrowed, or into a lower value if the bandwidth is to be increased. A moderate standing wave, with a maximum or a minimum at plane B, is present in such cases between the α_{22r} plane of the cavity and the loading-control device. The wattless power in the water-inlet stub tuner may increase or decrease somewhat due to the voltage change at the cavity T-joint plane. The increase of the wattless power in the stub tuner, in the taper, and in the line is, however, negligible, compared with the wattless power in the tube and in the cavity up to the α_{22r} plane. Thus they may be neglected in computations. Experimentally, if the loading control is adjusted during a cold test to pre-set the required plate bandwidth, the R_t value of Equation (33) is automatically obtained.

Sample Wattless-Power and Plate-Loading-Resistance Computations

The wattless powers and the plate-loading resistance will be computed for the previous example, first with the arbitrarily selected $R_t = 1000$ ohms plate resistance, at $f = 650$ megacycles. A plate-cavity bandwidth of 8.5 megacycles between 3-decibel points is required; thus $Q_L = 650/8.5 = 76.5$. The necessary plate-loading resistance and the transformation factor on the $Z_{21} = 21.9$ ohms virtual load in the 90° plane of the sliding line element will be determined so as to meet this requirement.

According to Equation (24)

$$VA_c = 2\pi \times 650 \times 10^6 \times 3920^2 \times 4.5 \times 10^{-12} = 282000 \text{ volt-amperes, r.m.s}$$

In the $Z_{11} = 10.63$ ohms line in the tube, according to Equation (25) with $K_{78.9} = .59$ and $K_{41.4} = .113$ (from Figure 15),

$$VA_{11} = \frac{3990^2}{10.63} (.59 - .112) = 715000 \text{ volt-amperes, r.m.s.,}$$

and from Equation (26) with $K_{23.2} = .021$,

$$VA_{12} = \frac{6690^2}{21.9} \times .021 = 42800 \text{ volt-amperes, r.m.s.}$$

VA_{21} is neglected because the β_{21} section extends only from 0 to 0.66°, and thus the amount of the wattless power is insignificant.

From Equation (28), with $K_{90} = .784$, and $K_{7.4} = .0007$,

$$VA_{22} = \frac{598^2}{1.95} (.784 - .0007) = 144000 \text{ volt-amperes, r.m.s.}$$

The total wattless power, based on the auxiliary $R_t = 1000$ ohms, from Equation (29) is

$$\Sigma VA = 282 + 715 + 42.8 + 144 = 1183.8 \text{ kilovolt-amperes, r.m.s.,}$$

from Equation (30)

$$X = \frac{3740^2}{1183.8 \times 10^3} = 11.8 \ (\pm j) \text{ ohms,}$$

and from Equation (33)

$$R'_t = 11.8 \frac{650}{8.5} = 903 \text{ ohms.}$$

Thus the proper plate loading, to obtain a bandwidth of 8.5 megacycles, is less than the arbitrarily selected 1000 ohms. Consequently all the voltage values in the cavity and the current in the zero-volt plane, I_0, are reduced by the factor of $\sqrt{903/1000} = .95$. The output voltage at the 90° plane of the sliding line element, which was computed in the previous example, $E_{22} = 598$ volts r.m.s., becomes $.95 \times 598 = 569$ volts r.m.s.; and the loading at this plane ($Z_L = 25.6$ ohms), computed with $R_t = 1000$ ohms, becomes $Z'_L = 25.6 \ (903/1000) = 23.1$ ohms. The same value is obtained for Z'_L with Equation (20). The load resistance in the 90° plane, if no resistance transforming element is used in the antenna line, is $Z_{21} = 21.9$ ohms. Consequently, a minor load-correction is necessary and is achieved by introducing a voltage-standing-wave ratio of $23.1/21.9 = 1.055$ in the tapered section of the cavity and in the transmission line, up to the loading-control device (Figure 6).

Some Experimental Data

Experimental results indicated that 6-kilovolts d-c is a proper plate

voltage for the tube for typical operation. With $R_t = 903$ ohms plate loading, the maximum plate swing is $E_t = .95 \times 3740 = 3550$ volts r.m.s., or 5020 volts peak. The lowest instantaneous plate voltage is $6000 - 5020 = 980$ volts, which is close to the second grid voltage of 1000 volts. In a typical operation at low carrier frequencies the plate-power efficiency is about 40 per cent at the peak of sync. During picture transmission the plate current is reduced. The plate current value above .75 ampere is, as a good approximation, proportional to the square root of the instantaneous power outputs. The typical static plate-current value is .75 ampere.

Measurement of the Circuit Efficiency

The losses in the cavity and the tube can be determined by low-power bandwidth measurements on the system. The expression $P = P_0 Q_U/(Q_U - Q_L)$ gives the relation between the real output from the cavity, P_0, and the electronic output, P, produced by the tube. Q_U and Q_L are the unloaded and loaded Q values of the plate network. For the measurement of Q_U, the load and also the tapered section of the cavity (Figure 1) must be decoupled; otherwise a high standing-wave ratio is built up in the taper which operates substantially matched, when the cavity is loaded.

If it is intended to separate the circuit losses between the tube-plate system and the cavity, a low-loss dummy-tube must be built, reproducing the anode-circuit geometry of the tube. Whereas in this case Q_L will be substantially unchanged, Q_U increases somewhat. Thus the factor $Q_U/(Q_U - Q_L)$ is closer to unity, and the computed output, P, approaches more closely the real cavity output, P_0. This is a consequence of the fact that the losses in the tube-plate region are now not included in P. The circuit loss is computed by $P - P_0$ in both cases. Measurements indicate that the losses with the 6448 tube are not substantially greater than the losses measured with a dummy tube.

The net cavity losses can also be measured during high-power operation from the cooling-air temperature increase (Figure 1). For high accuracy, the radiated heat from the cavity surface should also be taken into account.[14]

Computation of the Dimensions of the Grid Cavity

The grid cavity is a $\frac{3}{4}$ λ resonator. In the 470- to 890-megacycle

[14] L. F. Blume, *Transformer Engineering*, John Wiley & Son, Inc., New York, 1938, pp. 280-282.

frequency region, the first $\lambda/4$ section of the resonator and part of the second $\lambda/4$ section are entirely within the tube. This is due to the fact that the grid-to-ground capacity is of the order of 300 micro-microfarads, so that the first $\lambda/4$ section becomes very short. Because of this and the complicated geometry of the input section of the tube, a method of computation for the grid cavity is presented which is different from the method applied to the plate cavity.

The first step was measurement of the reactances presented by the grid input to the cavity at different carrier frequencies. A coaxial cavity of $Z_0 = 12.2$ ohms uniform surge-impedance was placed on the grid (Figure 7). The cavity was tunable with a short-circuiting plunger. The distance of the plunger from a reference plane was measured at resonance, and the reactance presented by the short-

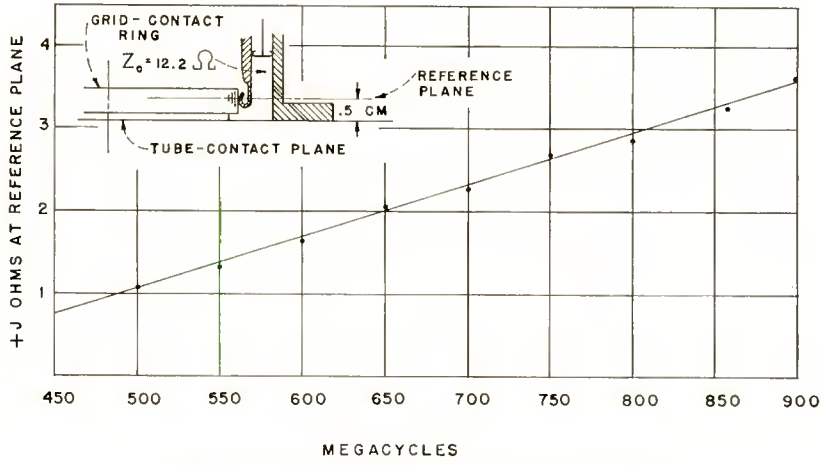

Fig. 7—Reactance curve of the grid input.

circuited cavity, which is equal to but opposite in sign from the TEM-mode tube reactance, was computed. A plane one-half centimeter above the tube ground plane was selected as reference for the reactance computation; consequently, the reactance values of Figure 7 are not absolute data for the 6448 tube, but they give good information for the design.

The cross section of a cavity design is shown in Figure 8 and the voltage distribution in the cavity, in Figure 9. The tube shows inductive reactance to the cavity; thus the cavity must represent a capacitive reactance at the grid-contact plane for resonance. A low-impedance coaxial-line element follows the coaxial grid structure outside the tube. This capacitive low-impedance section has a sliding, telescopic extension. The position of the sliding extension is set to produce the re-

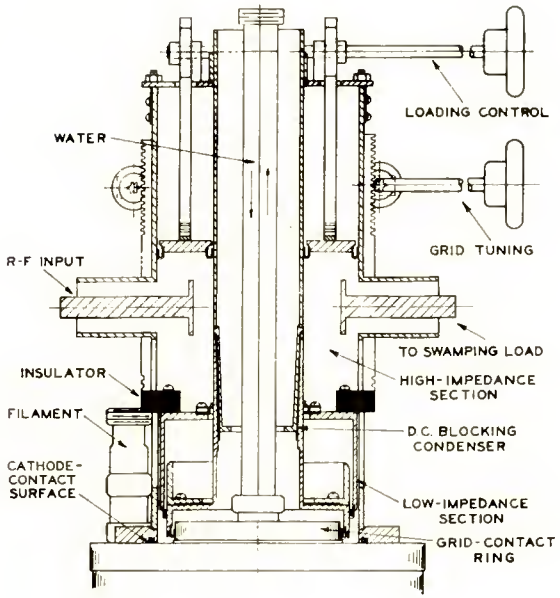

Fig. 8—Grid cavity.

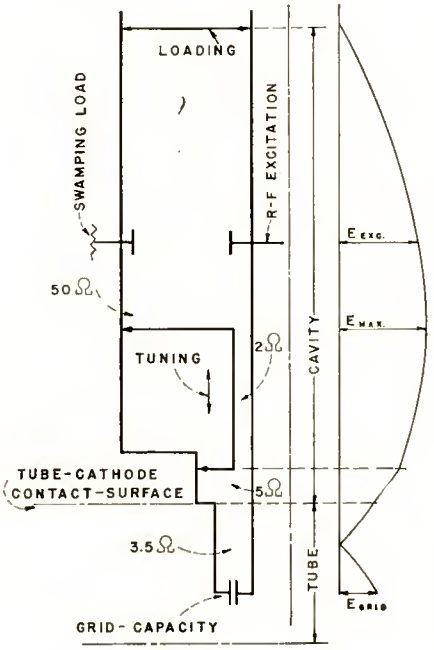

Fig. 9—Length of the line elements and voltage distribution in the grid cavity in qualitative representation.

quired capacitive reactance for grid tuning. We may write, for the shortest electrical length, β_g, of the low-surge-impedance section at the highest selected carrier frequency:

$$\cot \beta_g \approx \frac{X_g}{Z_g}$$

where X_g is the tube-reactance value from Figure 7 and Z_g is the line surge impedance of the telescopic section, when compressed. To predict the lowest carrier frequency, the reactance-versus-frequency curve should be computed for the fully extended telescopic line at the grid input plane. The intersection of the computed curve with the tube reactance line in Figure 7 determines the lowest frequency. The 90° plane of the second $\lambda/4$ is at the end of the extendible low surge-impedance line section. The low-impedance line is fed by a high-impedance line-section which is substantially a $\lambda/4$ resonator. It can be shown that the capacitive section should have the lowest possible surge-impedance and the feeding-$\lambda/4$ section the highest impedance for broad-band operation. Typical surge impedance values are 2 to 4 ohms for the low-impedance section and 50 ohms for the high-surge-impedance section.

The high-impedance section is excited from a driver stage with an adjustable capacitive coupling. If the power amplifier is in class-B service, the bandwidth of the grid circuit must be broad. A swamping resistor added to the grid cavity with another adjustable coupling is helpful in this respect. It increases the required power output from the exciter stage, generally by the factor of two. The power-amplification factor, which is the ratio of the power-amplifier and exciter-stage outputs, is 15 in linear class-B television amplifier service; in class-C service, where no swamping load is applied, the power amplification factor may reach 50.

It was observed that in the 550-megacycle region the grid system in the 6448 tube can be excited not only in the TEM mode, but also in the $TE_{1,1}$ mode. In order to avoid the latter, special care must be taken to obtain a symmetrical TEM-mode excitation in the grid, as was demonstrated by R. N. Clark of this Company. Figure 10 is a photograph of the main components of the grid cavity.

Figure 6 shows the connection of the exciter stage to the class-B power amplifier in schematic form. For picture-transmission test, a one-kilowatt UHF television transmitter was used as the modulated exciter. The grid cavity of the power amplifier must match the input line at the carrier frequency. The matching requirement is not neces-

ary for the whole television sideband spectrum. It was found rather advantageous to work with a narrower grid-cavity bandwidth and to adjust the input line-length (and thereby the voltage-standing-wave ratio for the sidebands) in such way that a peaking of the grid response up to about 2 decibels is observed at the +4.2 megacycles sideband frequency. Figure 11B shows the sideband response in the grid cavity with the typical peaks of a band-pass filter. The two tuned elements of the filter are the plate cavity of the exciter and the grid cavity of the high-power amplifier. This adjustment also permits the use of a relatively narrow plate-cavity bandwidth in the power amplifier, for ex-

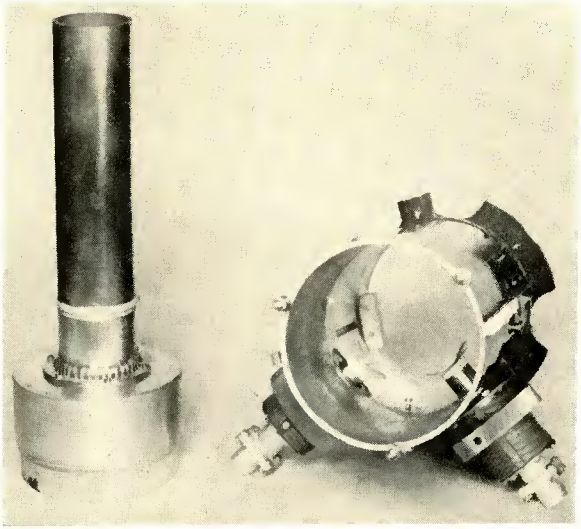

Fig. 10—Inner conductor of the grid cavity with the sliding extension (standing) and the external conductor of the grid cavity.

ample 8.5 megacycles between the —3-decibel points. If in the power-amplifier plate cavity the carrier is offset by 1 megacycle toward the lower sidebands, the over-all response becomes almost perfectly flat between the —1.5 and +4.2 megacycle sideband limits, which is satisfactory for color television.

Data on the Modulated Envelope Under Practical Amplifier Operation

Special care was taken in this developmental work to assure proper amplifier operation for color-television picture transmission. Some experimental data important for color transmission is presented in the following.

Figure 11 shows a typical sideband picture of a television amplifier

with 14 kilowatts peak sync power. Response (A) was taken from the plate output transmission line with a directional coupler, and response (B), which was discussed previously, was taken from the grid cavity with a small capacitive probe. A television sideband response analyzer[15] was used to produce the sideband pictures.

Figure 12A represents a step-wave-modulated output, sampled from the power-amplifier output line. A burst of 3.58-megacycle color subcarrier frequency is on the steps. The input signal to the modulator

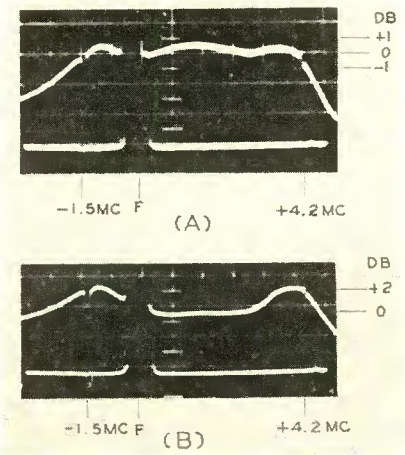

Fig. 11—Amplitude response of the sidebands; peak of sync power output 14 kilowatts. (A) response in the output line, (B) response in the grid cavity.

of the exciter stage was produced with a linearity checker.[16] The output envelope was detected with a diode. The detected signal flowed through a color signal analyzer.[17] Figure 12B represents the same information as 12A after passing it through a low-pass filter, and 12C represents the same information as 12A after passing it through a high-pass filter. The oscillograms presented in Figures 12A, B and C indicate that the transmitter has a satisfactory linearity in the low-frequency region and also at the region of the color information. The color signal analyzer gave additional information based on the demod-

---

[15] J. A. Bauer and F. E. Talmage, "The RCA-BW-5A Television Sideband Response Analyzer," *Broadcast News*, pp. 32-39, July-August, 1953.

[16] J. A. Bauer, "A Versatile Approach to the Measurement of Amplitude Distortion in Color Television," *Proc. I.R.E.*, Vol. 42, pp. 240-246, January, 1954.

[17] A. C. Luther, Jr., "Method of Verifying Adherence to the NTSC Color Signal Specifications," *Proc. I.R.E.*, Vol. 42, pp. 235-240, January, 1954.

ulated output, which was passed through the high-pass filter. The 3.58-megacycle color subcarrier bursts, modulated at different power (luminance) level, may show different phase relationship. Such a phase-versus-amplitude distortion introduces color error in the picture, and therefore this distortion must be kept very low.[18] With increasing second-grid voltage the phase-versus-amplitude distortion decreases and almost disappears at the 1000-volt second-grid-voltage region.

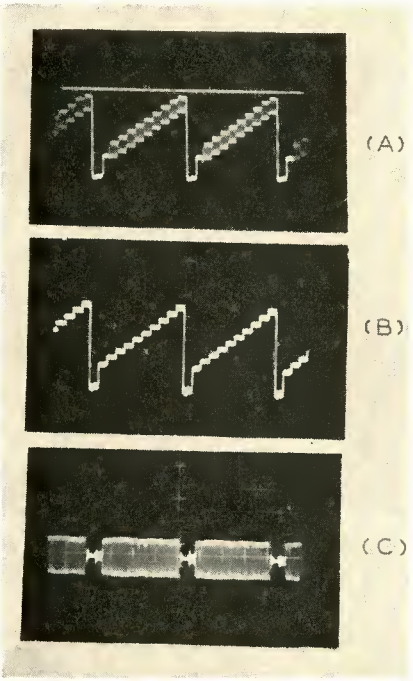

Fig. 12—(A) Step-wave modulation with 3.58-megacycle color subcarrier burst on each step. Peak of sync power 14 kilowatts at 740 megacycles. (B) The same as (A) but bursts rejected by a low-pass filter. (C) The same as (A) but step-wave rejected by a high-pass filter.

Comparative measurements on the phase relationship between the bursts in the input and output of the power amplifier indicated 3° phase difference between the bursts of the lowest and highest power level, which is satisfactory. A further control on the phase-versus-amplitude distortion can be applied at the modulator of the exciter stage. The promising test results were confirmed with practical color transmission.

Figure 13 represents a practical amplifier design with the described

[18] T. M. Gluyas, Jr., "Television Transmitter Considerations in Color Broadcasting," *RCA Review*, Vol. XV, pp. 312-334, September, 1954.

cavities and type 6448 beam-power tube, as used in the TTU-12A transmitter.[19] The power amplifier is excited by the output of a TTU-1B transmitter.[20]

Appendix—Computation of the Wattless Power in Resonant Transmission-Line Elements

It is an important step in a transmitter design to predetermine the stored wattless power in a tank circuit. Generally, a cavity reso-

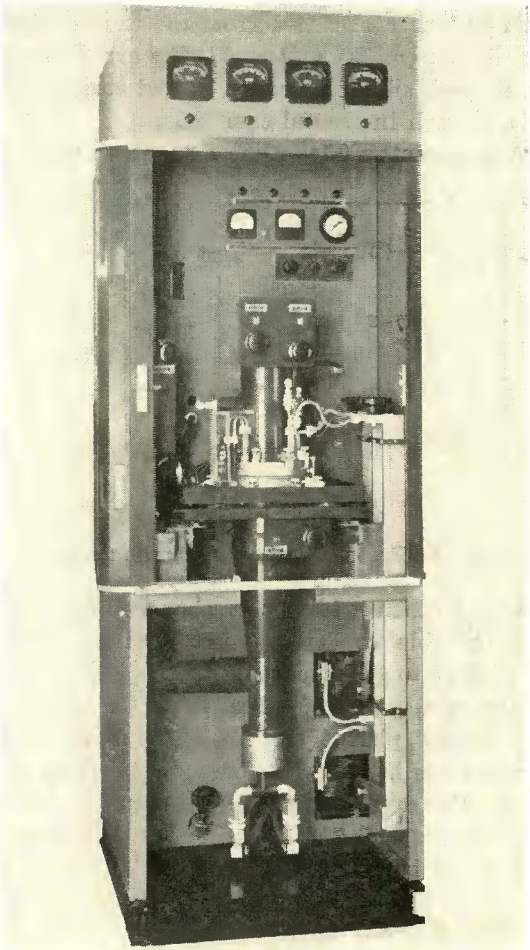

Fig. 13—A practical UHF power-amplifier design.

[19] R. L. Meisenheimer, "New 12½ Kilowatt UHF Transmitter," *Broadcast News*, pp. 22-29, May-June, 1954.

[20] T. M. Gluyas and E. H. Potter, "The TTU-1B 1-KW UHF TV Transmitter," *Broadcast News*, pp. 22-31, May-June, 1953.

nator is composed of lumped reactances and transmission-line elements, as shown in Figures 14A, B and C. Computation of the wattless power in a lumped reactance is straightforward when the voltage on the reactance is known (Figure 14D). Computation of the wattless power in the transmission-line elements, however, is somewhat more complicated. Here the voltages in the cavity are known from the design; thus it is convenient to base the computation on the stored energy in the electric field, at the instant when the current is zero. It may be supposed that the standing-wave ratio is infinite in the cavity, and therefore the real power absorbed from the cavity with loading, and also the cavity losses can be neglected. The error introduced by this simplification is small since the loaded Q, and consequently the standing-wave ratio, is high in coaxial cavities.

Figure 14A represents a 0 to α_1 line element which is short-circuited

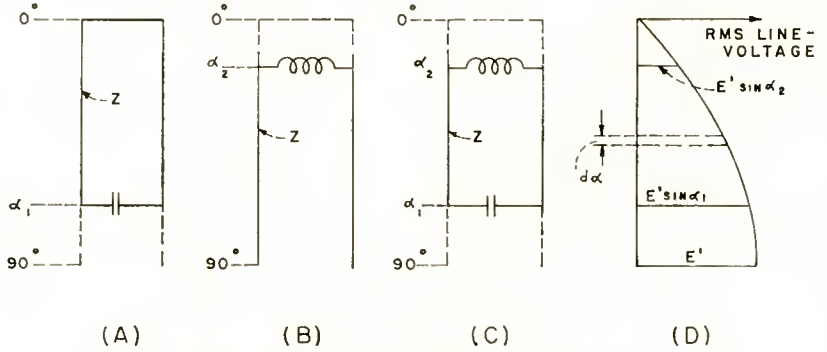

Fig. 14—Resonant transmission-line sections.

in the 0° plane and which is tuned to resonance by an added condenser. The reactance of this condenser matches the inductive reactance $(+jZ \tan \alpha_1)$ of the 0 to α_1 line-element in the α_1 plane with a capacitive reactance of the same absolute value. E' is the r.m.s. voltage which would exist in the 90° plane if the line element were a $\lambda/4$ resonator. The voltage in the line in an α plane on a short $d\alpha$ line element becomes $E' \sin \alpha$. C is the line capacity for unity line length. For an elementary dl line section, the capacity is Cdl. The wattless power in a dl line element is expressed by

$$d\ (VA) = 2\pi f C E'^2 \sin^2 \alpha\ dl. \tag{34}$$

Integrating Equation (34) and substituting

$$dl = \frac{\lambda}{2\pi}\, d\alpha,$$

it is seen that

$$VA = \int_0^{\alpha} d\,(VA) = \lambda f C E'^2 \int_0^{\alpha} \sin^2\alpha\, d\alpha. \tag{35}$$

But $\lambda = v/f$ and $C = 1/vZ$, where v is the velocity of the propagation in the Z surge-impedance line, and

$$\int_0^{\alpha} \sin^2\alpha\, d\alpha = \frac{\alpha}{2} - \frac{1}{4}\sin 2\alpha. \tag{36}$$

Thus the wattless power is expressed as

$$VA = \frac{E'^2}{Z}\left(\frac{\alpha}{2} - \frac{1}{4}\sin 2\alpha\right) = \frac{E'^2}{Z} K_a, \tag{37}$$

where

$$K_a = \frac{\alpha}{2} - \frac{1}{4}\sin 2\alpha. \tag{38}$$

Figure 15 shows the K_a values from Equation (38) for the $\alpha = 0°$ to 90° region.

For a line section extending from the α_2 plane to 90° (Figure 14B) which is tuned to the $\lambda/4$ mode resonance, we may write

$$VA = \frac{E'^2}{Z}(K_{90} - K_{a2}) \tag{39}$$

and for a resonating line section extending from the α_1 plane to the α_2 plane (Figure 14C), the capacitive wattless power is

$$VA = \frac{E'^2}{Z}(K_{a1} - K_{a2}). \tag{40}$$

If the line voltage, E', is expressed in Equations (37), (39), or (40) in r.m.s. volts, the wattless power is expressed in reactive r.m.s. volt-amperes, which, when divided by the real power in watts, gives the loaded Q of the line element. Application of Equation (40) is shown in the sample computation.

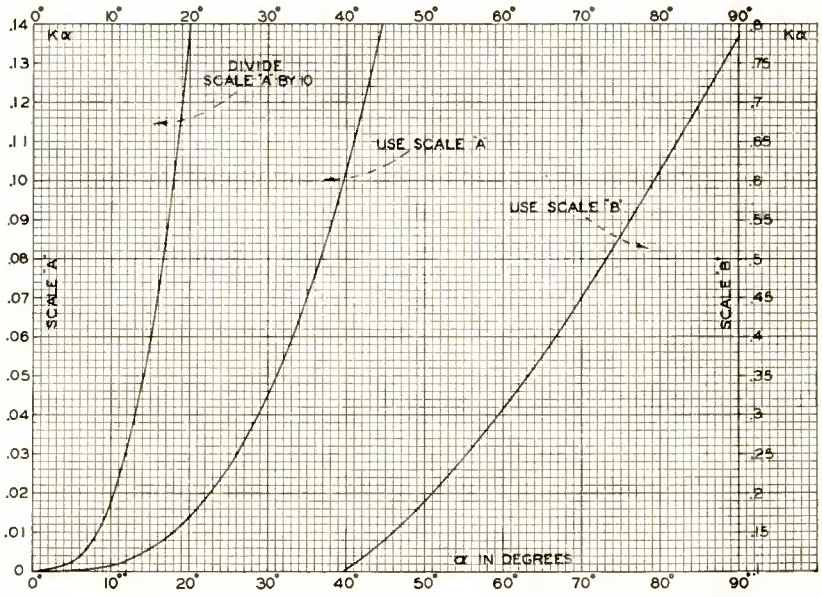

Fig. 15—K_a graph for 0 — 90° electrical line-lengths, $VA = \frac{E'^2}{Z}(K_{a1} - K_{a2})$.

Acknowledgments

The author is indebted to several engineers of the Radio Corporation of America for their cooperation during the development. Valuable discussions were held with T. J. Boerner and W. P. Bennett; M. W. Duris and R. N. Clark contributed important suggestions on electrical design questions and participated in the tests; F. C. Blancha, G. J. Rogers, and D. H. Eberlin contributed to the mechanical design of the cavity; J. W. Chasteen, T. Douma, and R. E. Wolf contributed to the different phases of the experimental work; N. J. Oman made measurements on the color performance of the system; and J. E. Joy, E. M. Coombs, and T. N. Newman were responsible for the planning of the amplifier test setup.

A UHF–VHF TELEVISION TUNER USING PENCIL TUBES*

By

W. A. Harris and J. J. Thompson

Tube Division, Radio Corporation of America,
Harrison, N. J.

Summary—*The use of pencil tubes in a television tuner covering all channels in the UHF and VHF bands is discussed. The input and output resonant frequencies of the pencil tubes are high enough to allow the use of shunt-tuned circuits in a UHF–VHF tuner, and the feedback inductance is low enough to insure stability in the required frequency ranges. The shunt-tuning method has the advantages of providing small over-all dimensions and a moderate number of switching components.*

The paper includes discussion of the measurements of the tube characteristics at high frequencies and the use of such data in the design of the tuner circuits.

Tuner Requirements

THE tuner for a modern television receiver must give satisfactory performance in all the ultra-high-frequency (UHF) and very-high-frequency (VHF) channels assigned for television broadcasting. The ranges of the three separate frequency bands allotted for television are 54 to 88 megacycles (channels 2 through 6), 174 to 216 megacycles (channels 7 through 13), and 470 to 890 megacycles (channels 14 through 83). Economic considerations suggest that television tuners employ methods similar to those used in multirange broadcast receivers, i.e., that switching be utilized between the various bands and continuous tuning within the bands. The three television frequency bands may be subdivided into smaller bands for convenience to the user or because of circuit considerations. In the tuner to be described, three VHF and three UHF bands are used.

In a UHF–VHF tuner, it is desirable that each tube be used to perform the same function in all bands. It is also desirable that as many circuit elements as possible be common to all channels so that the complete unit is a single all-band tuner rather than separate units for different frequency bands. Performance requirements for such a tuner may be summarized as follows:

(1) The noise factor, gain, selectivity, and stability in the VHF bands must be at least as good as those of the best currently available tuners.

---

* Decimal Classification: R583.5.

(2) The gain, selectivity, and stability in the UHF bands must be substantially the same as in the VHF bands.

(3) The noise factor in the UHF bands must be as good as the present state of the art permits, with due regard to over-all cost considerations.

This paper describes a tuner which uses three pencil-type triodes as r-f amplifier, mixer, and oscillator. In the shunt-tuned circuits used, variable capacitors provide continuous tuning and coils mounted on wafer switches provide for band changing. The rotary-type tuning capacitors are mounted on a common shaft. It is expected that advantages of this tuning method such as mechanical stability, compactness, and low cost already attained in multirange broadcast receivers can also be attained in television tuners.

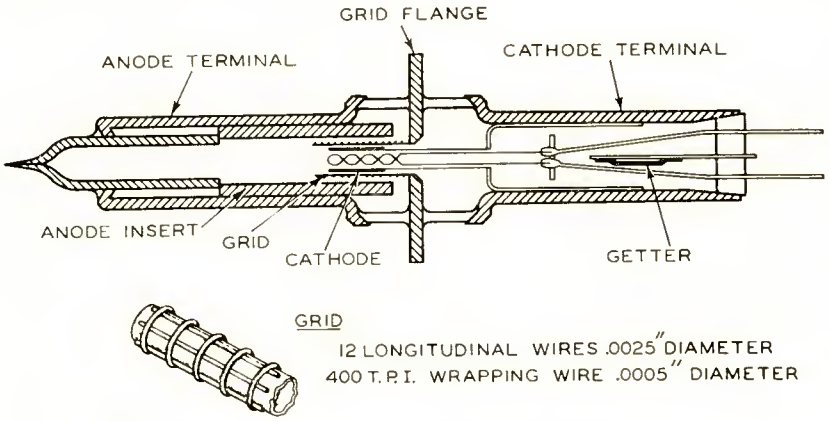

Fig. 1—Cross-sectional view of developmental pencil tube.

The purpose of this paper is to demonstrate principles and to suggest methods for the use of pencil tubes in practical television tuners. Although the tuner described is not a commercial product, it is believed that this discussion will help the designers of television tuners by suggesting better ways to solve a difficult problem.

Developmental Pencil Tube for Tuner

The pencil triode used in the UHF–VHF tuner is a developmental type similar to types 5675, 5876, and 5893. The appearance of this tube and some details of the internal structure are shown in Figure 1. In order to provide a more compact unit, the external grid disc of the developmental tube is smaller in diameter and somewhat thicker than that used in commercial types. Internally, the cathode diameter is the same as that used in the 5893. However, to improve tube performance

the grid mesh is finer and the grid-to-cathode spacing is smaller than that used in any of the standard types mentioned.

Characteristics of the developmental pencil triode including inductance and resonant-frequency data are shown in Figure 2. The inductance values shown in the table apply when short-circuiting rings are used across the glass. In a 50-ohm coaxial circuit, the cathode and plate inductances are approximately one millimicrohenry higher than those shown. The resonant frequencies for plate and cathode are calculated from the inductance values in the table and the capacitance values in the table less the capacitance across the glass, which is approximately one-half micromicrofarad. The feedback resonant frequency is the frequency at which the inductive and capacitive feedback components cancel each other.

Developmental Pencil Triode

Heater Voltage	6.3	volts	**Capacitances:**		
Heater Current	0.225	amperes	Grid to Plate	2.0	$\mu\mu$f
Maximum Ratings, *(Design-Center Values)*:			Grid to Cathode	5.4	$\mu\mu$f
Plate Voltage	250 *max.*	volts	Plate to Cathode	0.04	$\mu\mu$f
Plate Dissipation	2.5 *max.*	watts			
Plate Current	30 *max.*	ma	**Inductances:**		
Heater–Cathode Voltage	80 *max.*	volts	Plate to Grid	0.6	mμh
Seal Temperature	175 *max.*	°C	Cathode to Grid	1.2	mμh
Typical Operating Conditions:			Grid	0.05	mμh
Plate Voltage	120	volts			
Cathode–Bias Resistor	60	ohms	**Resonant Frequencies:**		
Plate Current	18	ma	Plate	5300	Mc
Transconductance	17000	μmhos	Cathode	2100	Mc
Amplification Factor	54		Feedback	2000	Mc

Fig. 2—Tentative data for the developmental pencil triode.

The low value of grid inductance is probably the primary advantage of the disc-seal type of tube at high frequencies. Tubes using wire leads, even multiple leads, exhibit grid-inductance values about 50 times higher than the value shown for the pencil tube. For such a tube having the same capacitance, therefore, the feedback resonant frequency would be reduced to about 1/7 that of the pencil tube. Because the short-circuit feedback admittance increases with the cube of the frequency at frequencies above this resonant frequency, the control of regeneration becomes a very serious problem when tubes having wire leads are used in the UHF band.

The high input and output resonant frequencies of the pencil tube make the shunt-tuning methods described in this paper possible.

Circuit Design

A top view of the television tuner is shown in Figure 3. The tuner

is divided into four sections which contain the antenna-tuning circuit, the r-f amplifier, the mixer, and the oscillator. The metal rotor shaft of the tuning capacitor extends through the four sections. The bearings for the shaft are attached to the base of the tuner. Rotor plates are used in the antenna-tuning, r-f amplifier, and oscillator sections; the rotor shaft is grounded to the side wall of the sections by means of wiping contacts. The stator plates for the tuning capacitors are supported by the switch wafers. These stator plates also support the anode contacts for the r-f amplifier and oscillator tubes. The anode resonant circuits are completed by means of short straps between the

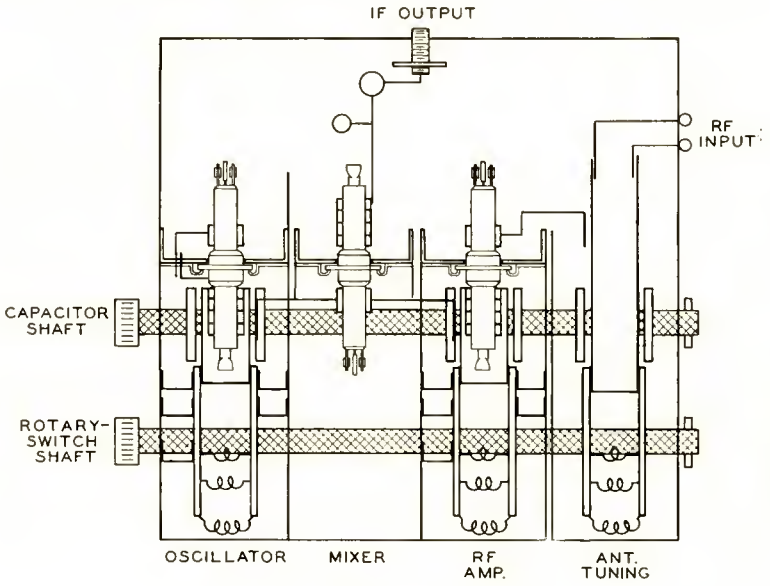

Fig. 3—Top view of tuner.

switch wafer and the side walls to obtain the highest frequencies. Four parallel paths can be used to each section to obtain the necessary low inductance. Coils for the lower frequencies are mounted on the switch wafers. The use of the switch wafers to support the stator plates minimizes the amount of dielectric material. The use of the stator plates for the support of the anode contacts for the tubes keeps the inductance low. Blocking capacitors in the form of silver–mica strips are used between the anode contacts and the stator plate assemblies.

Six switch positions are used, three for the VHF range and three for the UHF range. Because six bands are used, the required tuning-capacitance ratio in any band is only 1.5 to 1. The required capacitance

is readily obtained by the use of two rotor plates in each section, provided a suitable plate spacing is used.

Tuner Construction

Figure 4 shows the construction used in the mounting of the tube. The mounting arrangement is practically identical for the oscillator and r-f amplifier sections. In the mixer circuit, however, the plate contact is mounted on a dielectric strip similar to that used to support the cathode contact. Only the switch contacts used for the highest

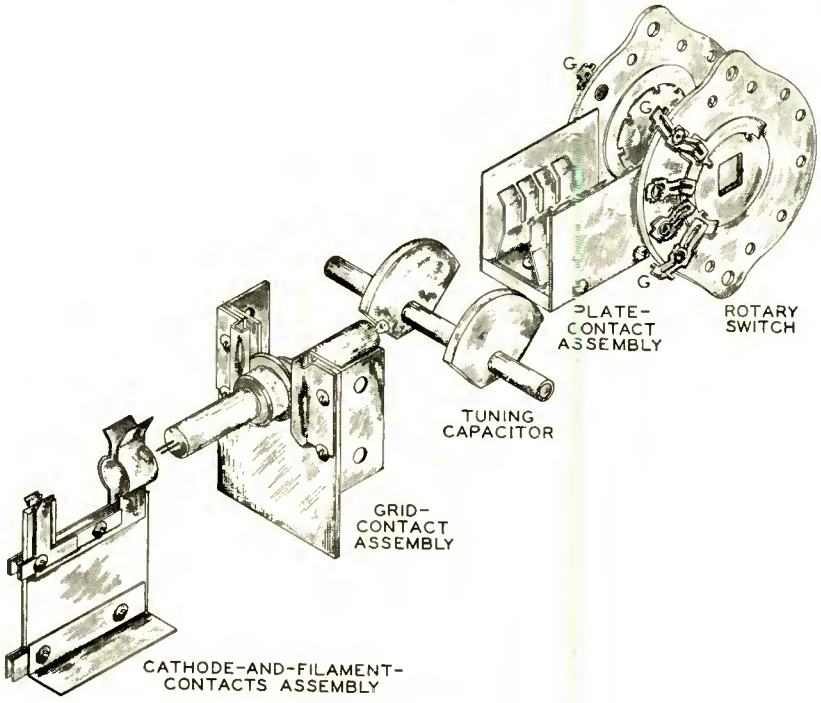

Fig. 4—Tube-mounting details.

frequency are shown. The switch points marked G are connected to the side walls by means of short straps. When minimum lengths are used, the maximum oscillator frequency is over 1000 megacycles. Since the required maximum frequency for the oscillator is approximately 930 megacycles, some latitude for adjustment is available.

The principal support for the tube is the grid-contact assembly, which is fastened between the side walls to form a shield between anode and cathode spaces. Insulation is used between the grid assembly and the side walls to provide d-c isolation. In the oscillator section, the

insulation consists of Teflon* sheets thick enough to reduce the capacitance between grid and ground to a value below 20 micromicrofarads. Capacitance higher than this value may cause blocking of the oscillator. In the r-f amplifier and mixer sections mica insulation is used to provide sufficient capacitance for adequate bypassing.

The cathode and heater contacts are assembled on a strip of dielectric material, and bypass capacitors are built into the assembly. A bifilar or trifilar coil is used to complete the heater and cathode circuits.

For the UHF bands and the highest VHF band, feedback for the oscillator is provided by the addition of capacitance between cathode and plate. For the two lowest VHF bands, feedback is obtained by the connection of taps on the bifilar or trifilar coil to the cathode.

The switch includes means for short-circuiting the plate choke provided for the VHF bands when the UHF bands are in use. In this way, the "suck-out" difficulties frequently encountered in a multirange oscillator are avoided. The cathode coil is small enough so that all of its self-resonant frequencies are above the highest operating frequency used.

Performance Data

Besides having the high self-resonant frequencies needed for tuning, the pencil triode exhibits relatively little frequency drift during warmup. This advantage becomes increasingly important for color-television applications. A series of frequency-drift tests was made at 970 megacycles in a special oscillator test circuit in which the external circuit was held at substantially constant temperature so that only the effects of tube behavior would be observed. The average frequency change for the pencil triodes was only 93 kilocycles, and the random variation among tubes was ± 20 kilocycles. In practical circuit design the drift can be compensated to some extent by the use of temperature-compensating elements. The excellent performance obtained from pencil tubes probably is a result of the tube structure, which contains no constraining elements such as micas at the upper ends of the grid and cathode. It is also possible that the change in spacing due to expansion from the time at which emission is sufficient for oscillation to the time at which equilibrium is established is quite small in the cylindrical type of structure used in pencil tubes.

When a low-noise high-gain amplifier is used, a triode mixer offers advantages over a diode mixer. The triode mixer provides some gain, about 3 decibels, whereas the diode mixer has a conversion loss of 8 to 12 decibels. An advantage in uniformity is also obtained. The one

* Registered trade mark of the E. I. DuPont Co.

disadvantage of the triode mixer is that more oscillator input power is required. Figure 5 shows some typical results obtained from a pencil tube in the mixer circuit used in the tuner at a frequency of 870 megacycles. The power values shown represent the plate input power to the pencil-triode oscillator.

The oscillator and r-f amplifier signals are coupled into the cathode of the mixer. As previously mentioned, the grid is kept close to r-f ground potential by the insertion of thin sheets of mica between the grid-contact assembly and the side walls. Bias is obtained by means of a grid resistor. The plate circuit is tuned to the intermediate frequency, which is about 41 megacycles, and the signal is available at the output terminals of the mixer section.

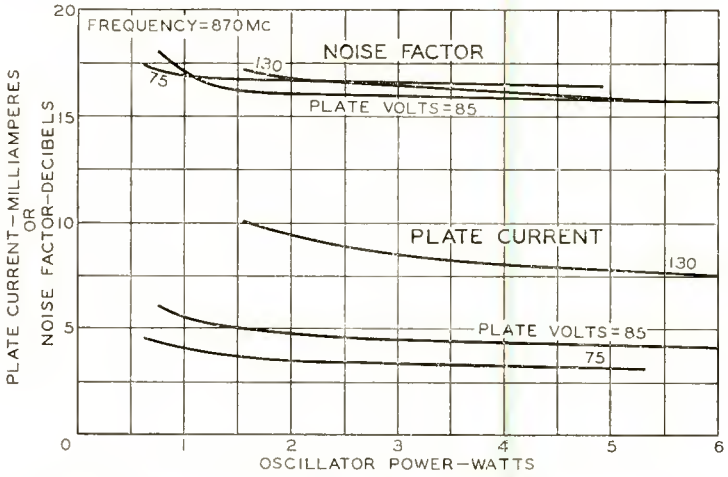

Fig. 5—Performance of mixer circuit at 870 megacycles.

The design of coupling elements in a tuner requires knowledge of the way the input admittance of a tube varies with the plate loading and tuning. Figure 6 shows the relation between input susceptance and input conductance for different values of plate load conductance when the load susceptance, i.e., the plate tuning, is varied. Measurements for Figure 6 were made at 870 megacycles. The point common to all the circles represents the short-circuit input admittance of the tube. The angle between the common axis of the circles and the constant-susceptance lines is the sum of the phase angles of the forward and feedback admittances. The points diametrically opposite the common point represent the input admittances when the plate load is tuned to resonance.

Although the largest circle represents zero coupling to the load, some circuit losses are present. If the losses were lower, the diameter

would be sufficient to extend the circle into the region of negative input conductance and, consequently, the tube would oscillate. An adequate margin of stability is indicated for the circles corresponding to loads giving suitable bandwidths. Any material increase in feedback would seriously reduce this margin, however, because the diameters of the circles are directly proportional to the magnitude of the feedback admittance.

There has been some misconception about the effect of transit time on short-circuit input conductance of a grounded-grid or cathode-drive amplifier. Actually, the conductance remains constant through the UHF band for pencil tubes as well as for other close-spaced tubes because grounded-grid triodes have the same type of characteristic as

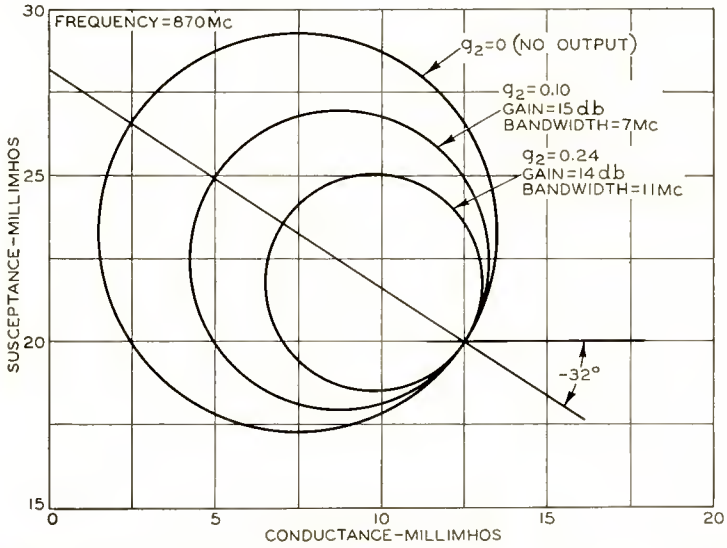

Fig. 6—Variation of input admittance with output tuning and load.

that of a diode. At higher frequencies, it may be expected that the conductance will decrease. Because of cathode inductance, the actual measured conductance at the input of the tube when the output is short-circuited is not constant. The input conductance of the tube under loaded conditions is less than the short-circuit input conductance, and is not constant with frequency unless the load and feedback admittance are kept constant.

Because losses in the external circuitry have a tendency to increase with frequency, it might be expected that the gain would decrease with frequency. However, transit-time effects in the tube help to counterbalance the increasing losses because the phase shift in the output

admittance causes the conductance component to decrease with frequency.

Figure 7 shows values of gain and noise factor as a function of frequency for a developmental pencil tube in a coaxial test cavity. During test, the load was adjusted for a bandwidth of 10 to 11 megacycles. The values of gain shown are not the maximum possible for this bandwidth because the coaxial circuit was not ideal with respect to circuit capacitance. The maximum gain–bandwidth product may be obtained by the use of plate tuning consisting of lumped inductance or a coaxial element having substantially higher characteristic impedance than the 50 ohms used in this case.

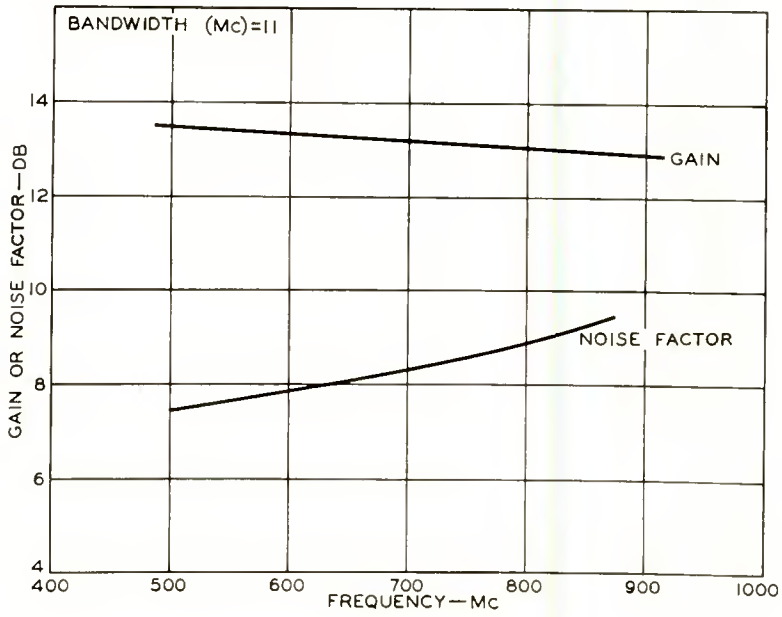

Fig. 7—Amplifier performance of pencil tube versus frequency.

The circuit of the r-f amplifier is very similar to that used for the oscillator. In the r-f amplifier circuit, however, the anode is coupled to the mixer cathode rather than to its own cathode, the grid is at r-f ground potential, and bias is obtained by means of a cathode resistor.

Figure 8 is a circuit diagram of the complete tuner. The antenna-tuning section is constructed and supported in the same manner as the anode-contact assembles for the r-f amplifier and oscillator. The antenna-tuning section serves two purposes: (1) it is a stage of preselection; (2) it serves as the coupling network for the amplifier cathode.

Different coupling methods are employed for VHF and UHF channels. For the UHF channels, interstage coupling is accomplished by means of a fixed capacitance provided by flat straps of silvered copper soldered to the cathode support of the amplifier and mixer tubes. The unsoldered ends of the straps are brought close to the appropriate stages to provide the required capacitance. For the VHF channels, inductive coupling is provided by coils switched in by means of the wafer switches. No tuning is employed in the cathode circuits of the amplifier or mixer stages.

The specific channel groupings used in the tuner are as follows: channels 2, 3, and 4 in the first band; channels 5 and 6 in the second band; channels 7 to 13 inclusive in the third band; and channels 14 through 32, 33 through 55, and 56 through 83 in the UHF bands. Although relatively large numbers of channels are included in the UHF

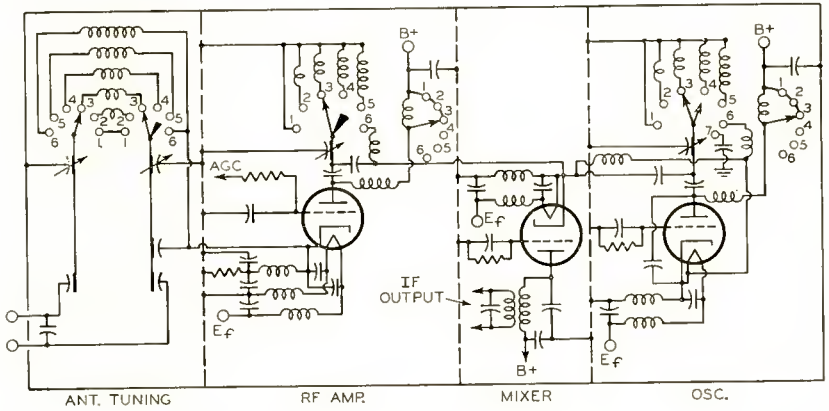

Fig. 8—Circuit diagram of tuner.

bands, it is probable that a fairly small number of well-separated channels will be available in any particular locality. The general tuning procedure is similar to that encountered in tuning in broadcast stations. Mechanical indexing may also be provided if the precision attained in the product warrants it.

Figure 9 shows the performance obtained in the circuits used in the tuner and results obtained in the coaxial measuring circuits. The failure of the coaxial-cavity gain curve to rise at the loads which provide minimum bandwidths indicates the presence of skin-effect losses.

The lower gain at the wide-bandwidth end of the curve for the lumped-constant circuit indicates the presence of higher circuit capacitance than that in the cavity circuit. Also, the lower gain at the narrow-bandwidth end of the curve indicates somewhat higher losses. Although

a separate amplifier chassis essentially the same as that in the tuner was used for these tests, it may be found that the tuner coupling elements cause slightly greater reduction in gain or bandwidth than in the test chassis.

The over-all dimensions of the tuner are 5 inches by 4 inches by 2 inches. The only parts which project outside these dimensions are the tuning shafts. The tubes are mounted completely inside.

Other Considerations

The tuner discussed in this paper is incomplete in a number of respects. One serious lack is the absence of conventional alignment and trimming adjustments for the various bands. Trimmer capacitors may be added to each of the stator sections of the main tuning capaci-

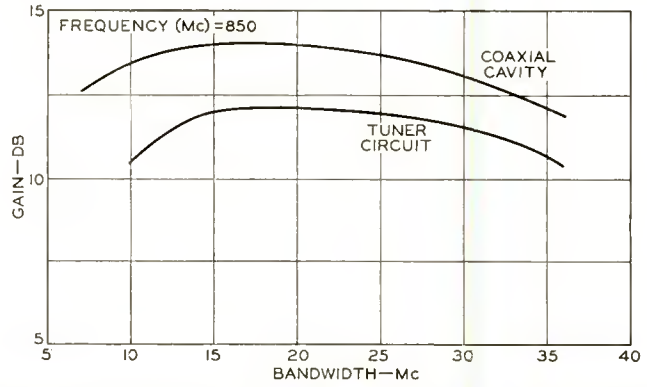

Fig. 9—Comparison of amplifier performance in tuner circuit and coaxial test circuit.

tors to compensate for variations in tube output capacitance. A capacitor for frequency adjustments should also be added on each of the oscillator switch positions. Trimming capacitors for r-f alignment are also needed. It would also be preferable to provide for inductance adjustment on the oscillator in addition to the capacitors. These added elements probably can be supported by the switch wafers, particularly if special punchings are designed. The parts used in the tuner as shown are standard punchings from a switch-assembly kit.

Measurements made separately on tubes and components can be used to estimate the over-all performance to be expected from the tuner. The noise factor of the r-f amplifier tube is approximately 9.5 decibels in the highest UHF channels. Although an over-all noise factor of 10 decibels has been observed in special test circuits, this may become 10.5 or 11 decibels because of lower r-f gain and higher mixer noise

factor in the complete tuner. The noise factor may also be increased as a result of the insertion loss of the antenna-tuning circuit.

For an insertion loss of 1 decibel at a frequency of 890 megacycles, the unloaded Q of this circuit must be approximately 350 if the bandwidth is 10 megacycles, or 175 if the bandwidth is 20 megacycles. It seems that these values, or values considerably higher, can be achieved, although it may be necessary to substitute better dielectric materials for the phenolic wafers used. Special attention should also be given to the design of the switch contacts and the wiping contacts for the tuning-capacitor rotor shaft.

Subject to these considerations, it should be possible to achieve an over-all noise factor for the tuner of 11 decibels or better at the highest UHF frequencies and 8 or 9 decibels at the low end of the UHF band. Noise factors of 4 to 6 decibels are expected in the VHF bands. The over-all gain of the tuner is the sum of the r-f and mixer gains in decibels, minus the antenna-circuit insertion loss; the expected values are 14 or 15 decibels at 890 megacycles per second and 17 or 18 decibels in the low UHF and VHF bands.

It appears that a tuner design functionally similar to the one described in this paper will be a logical development for future television receivers. Because tubes having resonant frequencies of the order of those described will be required, and because of the advantages inherent in the use of tubes employing cylindrical construction, pencil triodes appear to offer the best prospects for television-tuner use.

DEVELOPMENT OF THE PREMIUM ULTRA-HIGH-FREQUENCY TRIODE 6J4-WA*†

By

George W. Barclay

Tube Division, Radio Corporation of America,
Harrison, N. J.

Summary—*This paper describes the development of the 6J4-WA‡, a premium version of the 6J4 UHF amplifier triode for military applications. The electrical and mechanical features of the 6J4-WA are discussed, together with design modifications which increase interelectrode insulation, reduce heater-to-cathode leakage, and minimize temporary grid-to-cathode shorts. The manufacture of the close-wound grid for this close-spaced type is also discussed. Considerable emphasis is placed on the quality-control procedures and special processing used in the production of the premium tube. Electrical specifications and performance data for the 6J4-WA are compared with those for its prototype.*

Introduction

THE 6J4-WA, a "premium" version of the commercial 6J4 for military applications, is an ultra-high-frequency (UHF) amplifier triode in a seven-pin miniature bulb. Having a very high transconductance-to-plate-current ratio and a frequency range up to 500 megacycles, the 6J4-WA is used primarily as a grounded-grid amplifier in military equipment.

Because of the high degree of reliability under unusual conditions required in modern military equipment, modified versions of many existing tube types have been developed to meet the specific requirements of the new applications. The objective of the work described here was the development and production of a tube which would be capable of withstanding prolonged periods of shock and vibration, would have reasonably long life, stability of characteristics, and a low early-life inoperative rate, and could replace the 6J4 in existing equipment.

Development Program

Analysis of Rejects

The first step in the development of the 6J4-WA was the analysis

---

* Decimal Classification: R331.

† Presented at the National Electronics Conference, Chicago, October 4-6, 1954.

‡ Developed under Bureau of Ships Contract NOBSR-57568.

of commercial 6J4 tubes which failed to meet the extreme performance requirements of field equipment. The majority of the rejects fell into three categories. The first category included grid-to-cathode shorts, of both a temporary and a permanent nature, which were caused by sagging grid lateral wires, lint, and other foreign particles. The second category included rejects caused by heater failure; the principal cause of these rejects was open heaters and heater-cathode shorts. The third and probably most important category included tubes rejected because of leakage between electrodes. This leakage developed very early in life, and, because of the critical nature of the application, caused the equipment to become inoperative.

Tube Structure

The work that had been done on the 6J4 was very beneficial in setting up the program for the 6J4-WA. Because of the extremely small interelectrode spacings used in the 6J4, many of the practices used in its manufacture approach premium-tube techniques.

It was decided initially that the same basic structure would be used in the 6J4-WA as in the 6J4. This decision was based on two factors: (1) the 6J4 has several desirable features including a rugged mount structure; (2) a great deal of manufacturing experience is available on this structure.

The rugged mount structure of the 6J4 was further strengthened for the 6J4-WA by the addition of several features. These features are illustrated in the side view of the 6J4-WA structure in Figure 1. In this structure, the number of swages per grid is increased from two to four to minimize movement or shifting of the grids. The swaging operation provides burrs on the grid side rods which hold the grids in place against the micas. Plate stops of metal are welded to the plate ears to anchor the plate firmly and thus eliminate distortion of the plate and enlargement of the mica holes. The thickness of both the cathode tab and the grid connector is increased from 0.001 inch to 0.002 inch for increased strength. Ribbon heater connectors are also added to prevent tungsten embrittlement at the heater-to-stem-lead weld. In addition to these design improvements, the 6J4-WA uses a special grade of mica which is less likely to flake or to decompose during tube operation.

Quality-Control Procedures

In the fabrication and assembly of the 6J4-WA, stringent process controls and quality-acceptance procedures are used on every important part in the tube. The more critical the part, the stricter the quality-acceptance criteria. All bulbs and stems are inspected visually for

defects such as cracks, seal holes, and surface cuts. A sample group of stems is also taken each hour from the stem machine as a process control. Grids, plates, cathodes, and heaters are all sampled in accordance with rigorous quality-acceptance criteria. Each tray of parts is sampled to a 2.5-per-cent AQL (acceptable quality level) for major defects and to a 6.5-per-cent AQL for minor defects.

Cages, mounts, and finished tubes are inspected on a 100-per-cent basis. In addition, mounts and finished tubes are sampled to a 1.0-per-cent AQL for major defects and to a 6.5-per-cent AQL for minor defects. Major defects include open welds, poor grid–cathode align-

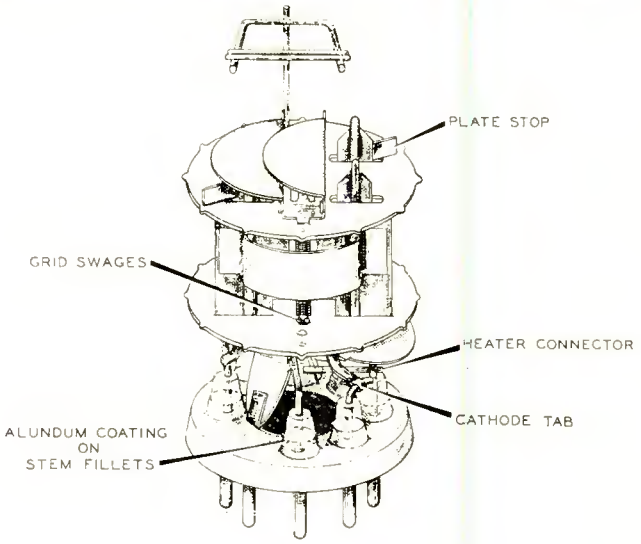

Fig. 1—Mount structure.

ment, split micas, micas not tight and parallel, getter touching the bulb wall, and lint and particles. Minor defects include crooked plate straps, crooked getter, bent outer stem leads, and less than the desired four stem leads touching the bottom mica.

Quality-control procedures are also used in the inspection of the work of operators in the mounting section. Ten mounts of each operator are checked per hour; corrective action, if necessary, is taken immediately.

Lint Control

Because of the close spacing between electrodes in this tube, it was necessary to set up a lint-control program. Lint is listed as a major defect on such parts as plates, grids, and cathodes, and extra care is exercised in handling these parts. They are transported in lint-free,

covered trays, and all parts are blown in a high-pressure air stream just prior to mount assembly. Tables in the mounting unit are kept as clean as possible, and operators use either rubber finger cots or nylon gloves when handling parts, cages, and mounts. All mounts are carefully blown in a high-pressure air stream just before they are placed in bulbs.

Grids

From the manufacturing standpoint, the grid presented the greatest challenge because of the high number of turns per inch (240), the small lateral-wire diameter (0.0012 inch), the wide side-rod spacing (0.220 inch center-to-center), and the close grid-to-cathode spacing (0.001 inch to 0.0015 inch).

In order to obtain a flat grid within the required tight tolerances, it is necessary that the grid be sized or formed. The sizing operation is necessary for three major reasons: (1) to obtain the proper grid diameter; (2) to obtain the correct center-to-center spacing; (3) to elongate the grid lateral wires enough so they acquire a permanent set. One of the major problems in the fabrication of the grids has always been a high percentage of broken lateral wires during the sizing operation. It has also been very difficult to obtain good grid-lateral-wire-to-cathode spacing; improper spacing results in temporary grid-to-cathode shorts and cutoff failures.

In the development of the 6J4-WA, an extensive investigation of the grid problems was undertaken. Because of the winding difficulties, special lathes were set aside for the sole purpose of winding the 6J4-WA grid. Spools of lateral wire were also selected for a particular lathe setting. The acceptance procedure for spools of lateral wire is as follows. Sample grids are produced from each spool of lateral wire. These grids are then sized, put into cages, and inspected. The number of breaks during sizing and the inspection of the finished cages determine whether a particular spool can be used.

One of the most useful and indicative measurements used to determine the suitability of the grids is the "taut" measurement. In this measurement, the unsized grid is placed on the sizing blades and the blades are expanded just enough to take the slack out of the grid lateral wires. The distance from the center of one grid side rod to the center of the other grid side rod is the "taut" measurement. It has been found that grids whose taut measurement is too high have a high percentage of collapsed turns. Grids whose taut measurement is too low have a high percentage of breaks in the lateral wires at sizing. This measurement is so critical that it must be controlled to within one and a half thousandths of an inch.

An extensive study of the grid-sizing operation revealed several interesting facts. It has been observed that the sizing operation not only "sets" the proper grid-to-cathode spacing, but in all cases improves the grid-lateral-wire spacing. Although the speed at which a grid is sized does not influence the number of breaks appreciably, in general the slower the speed the lower the percentage of failures.

Tests were made to determine whether the sharp offsets put in the grid lateral wire during the sizing operation caused breaks and weak grids. For the fabrication of a sample lot of tubes, the relatively sharp shoulders of the sizing blades were rounded off so that a more nearly elliptical grid which would have a naturally stronger structure was produced. The use of the nearly elliptical grid, however, produced a definite increase in breaks during sizing and in grid-to-cathode shorts.

The greatest single item that decreased temporary and permanent grid-to-cathode shorts and lateral-wire breaks at sizing was the addition of strict quality controls. In addition to the method of checking the spools already mentioned, sample grids from each lathe are checked periodically visually, microscopically, and on a comparator to a tight AQL. If the grids fail to meet this AQL at any check, all the grids produced since the last successful check are inspected on a 100-per-cent basis for the item or items for which the sample failed, and the lathe is shut down until the trouble is corrected.

These controls have been developed as a result of many months of experience in the manufacture of this grid. As a result of the effectiveness of these controls, this tube now passes a short-and-continuity test to a 0.4-per-cent AQL, which is equal to requirements for other premium tubes.

It was found by experience that Dowmo wire (50-per-cent molybdenum, 50-per-cent tungsten alloy) was much stronger than the grid-lateral wire previously used. The grid side rods are made of chrome copper because the high heat conductivity of this material reduces the possibility of grid emission. As an added precaution, the lateral wire is plated with either gold or rhodium. Both of these plating materials provide low grid emission when the wires are properly plated. Although rhodium-plated wire has always produced about 10 per cent more breaks at the sizing operation than gold-plated wire, more uniform characteristics are obtainable with rhodium plating. Because both platings work quite satisfactorily, both are used in production.

Electrode Insulation

Although electrode insulation on the 6J4-WA was high during initial operation, the tube developed very low insulation resistance during the early hours of life. Reports from the field indicated that

the leakage was between the grid and the heater. The only place for this leakage to develop was across the stem, which provides the only continuous path between the grid and the heater. A special lot of tubes in which the cathode tabs were omitted still had heater-cathode leakage as tested externally, indicating that the leakage path existed between the heater and cathode leads in the stem.

Inspection of the stem revealed a noticeable deposit between the grid and heater stem leads. A chemical analysis of the deposit showed that nickel (probably from the cathode) and aluminum (probably from the heater insulation) were present. The location of the deposit suggested that the material was coming from the vicinity of the cathode; no parts of the stem that were shielded from the cathode had any deposit.

Further investigation revealed that the basic difficulty was the high cathode temperature (1100 degrees Kelvin with 6.3 volts on the heater). This temperature causes certain cathode materials to evaporate (cathode sublimation) on the cooler parts of the tube. Several possible ways of reducing cathode sublimation or its effects were considered. One such possibility is to lower the power input to the cathode by reducing the heater current. However, tests showed that tubes having lower-power heaters also had lower emission and, consequently, unsatisfactory characteristics.

Because it did not appear practical to cool the cathode and still maintain a satisfactory emission level, other means of slowing down or preventing the formation of a low-resistance leakage path were investigated. The next expedient considered was the use of a stem shield made of either mica or metal. The metal shield was not suitable because of its effect on tube capacitances and because of the difficulty of locating such a shield mechanically. The mica shield also presented severe mounting difficulties.

After the use of a shield was found impractical, it was decided to coat the stem with Alundum* between the stem fillets. The Alundum, acting like the spray on micas, serves to increase the length of the leakage paths. This Alundum is put on the stems by hand to insure coating of the stem between all the leads. This process does not prevent the formation of leakage paths, but it definitely delays the development of low-resistance paths. Stem "painting" or Alundum coating of the stems has been used in production for nearly a year with excellent results.

At the time it was discovered that the leakage was caused by cathode sublimation, tests were also run on three different types of cathode

* Registered trade mark of The Norton Company, Worcester, Mass.

materials to determine which was least subject to sublimation. The three cathode materials could be classified as follows: (1) "normal" cathode material having a small percentage of silicon and magnesium; (2) "intermediate" cathode material having a high percentage of cobalt and a percentage of silicon and magnesium similar to that of the "normal" material; (3) "passive" cathode material having a very low percentage of silicon.

Tubes were made using each of these cathode materials with and without "painted" stems. These tubes were life-tested with both 6.3 and 7 volts on the heater. The results of these tests indicated that the poorest material for cathode sublimation was the "normal" cathode. The "passive" cathode material was satisfactory for sublimation, but very poor for emission. It was decided that the "intermediate" cathode material would be used in production for two reasons: first, this material was the best for electrode insulation; second, the activation level was satisfactory although not as high as the "normal" cathode material.

The tests conducted on the electrode-insulation problem were evaluated by life tests of the tubes having various constructions during which only heater voltages were applied. Because the rate of cathode sublimation depends on the cathode temperature, the tests were conducted with 7.0 volts instead of the rated 6.3 volts on the heater to accelerate the test and duplicate equipment operating condition.

Figure 2 shows electrode insulation between the grid and all other electrodes of 6J4-WA tubes on a 6.3-volt life test before the use of Alundum-coated stem fillets and the "intermediate" cathode material. Each line represents the reading on some particular tube at a specific test point. The number at the head of each column represents the number of tubes having insulation resistance above 200 megohms. In the last column, for example, it can be seen that 50 of the original 120 tubes were below 200 megohms at 500 hours.

Figure 3 shows similar electrode-insulation measurements for tubes having Alundum-coated stems and the "intermediate" cathode material. It can be seen that only one tube out of 120 dropped below 200 megohms at 500 hours.

Figure 4 shows a comparison of electrode insulation between the grid and the heater on 7.0-volt life tests before and after the use of Alundum-coated stem fillets and the "intermediate" cathode material. It can be seen that 29 tubes having the old construction and only 7 tubes having the new construction were below 200 megohms at 67 hours.

Test Specification

The 6J4-WA test specification has been written in the Military Control form. Several of the ratings for the 6J4-WA differ from those

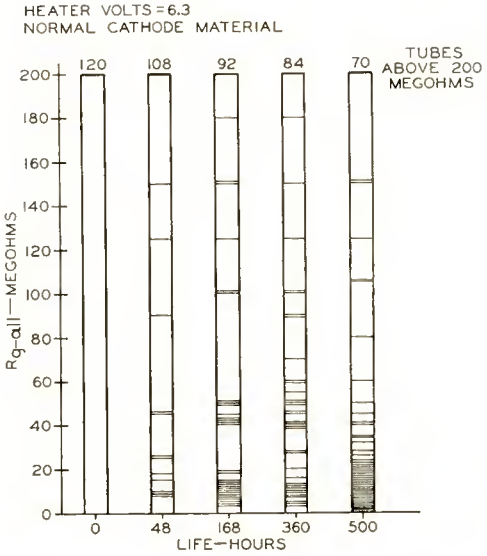

Fig. 2—Electrode insulation on 6.3-volt life test on old construction.

of the 6J4, the changes having been made to satisfy the special requirements of military applications and to define the new tube more accurately.

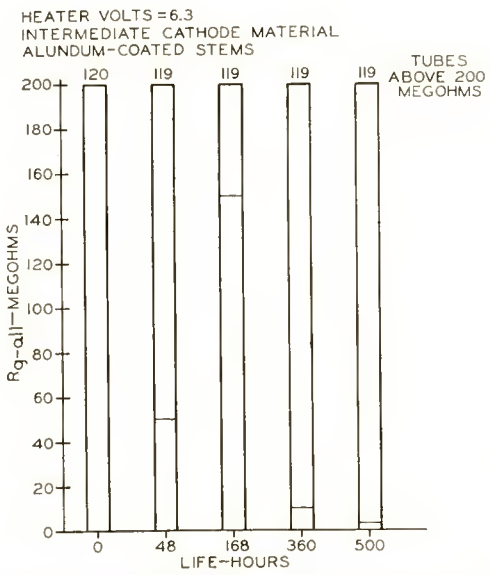

Fig. 3—Electrode insulation on 6.3-volt life test on new construction.

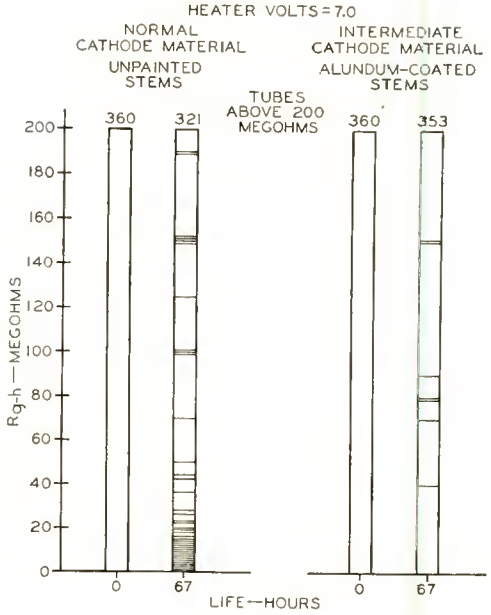

Fig. 4—Electrode insulation on 7.0-volt life test on old and new construction.

Figure 5 shows a comparison of initial limits for the 6J4 and the 6J4-WA. The ranges for both plate current and transconductance are reduced for the 6J4-WA, and the maximum limits for plate current and the maximum and minimum limits for transconductance are lowered. The lowering of these limits was found necessary because of the less

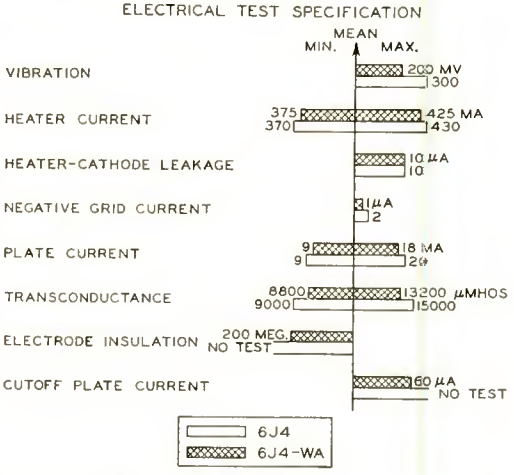

Fig. 5—Comparison of 6J4 and 6J4-WA specification limits on initial characteristics.

active cathode material now used. The less active cathode material, as explained previously, was found necessary in the 6J4-WA to prevent early-life equipment failures because of low electrode insulation. It should be noted that the 6J4-WA has a minimum electrode-insulation limit of 200 megohms.

The test specification for the 6J4 calls for a 250-hour test having one end point. The 6J4-WA specification calls for four individual life tests, including stability, survival, heater-cycling, and intermittent life tests.

The stability life test is conducted for one hour on a sample group of tubes to determine the stability of the tube characteristics. A maximum shift in transconductance of 10 per cent is allowed, and tubes are tested to a 1.0-per-cent AQL.

The survival-rate life test is conducted for one hundred hours on a sample group of tubes to determine the early-life inoperative rate. The sample must meet a 0.65-per-cent AQL for inoperatives. In addition, the 6J4-WA specification includes a 100-hour transconductance limit.

The heater-cycling life test consists of 2000 cycles of one-minute-on, one-minute-off operation. In addition to the usual heater-cycling life-test end points of heater-cathode leakage and heater failure, the 6J4-WA also has an electrode-insulation end-point criterion. The heater-cycling test is an excellent accelerated test for electrode insulation because a heater voltage of 7.0 volts is used.

The intermittent life test is cycled on the basis of 100 minutes on and twenty minutes off for 500 hours. This life test has nine end-point criteria plus a test for inoperatives. Included among the end-point criteria are limits on average transconductance change, individual transconductance change, and slump transconductance. There is also a life-test end-point criteria of 100 megohms for electrode insulation.

The test specification also includes a 500G-acceleration impact test and a fatigue-vibration test of 2.5G acceleration at 25 cycles for 96 hours to insure a mechanically strong tube. Five end-point criteria are specified for these tests, including one for the maximum allowable shift in transconductance.

Acknowledgment

The author wishes to express his appreciation for the cooperation of the personnel of the Bureau of Ships and Aeronautical Radio Incorporated who were associated with this development and to the personnel at Collins Radio Incorporated for their cooperation in evaluating structural changes.

THE TRANSFLUXOR — A MAGNETIC GATE WITH STORED VARIABLE SETTING*

By

Jan A. Rajchman and Arthur W. Lo

Research Laboratory, RCA Laboratories,
Princeton, N. J.

Summary—*The Transfluxor comprises a magnetic core made of material with a nearly rectangular hysteresis loop and having two or more apertures. The control of the transfer of flux between the three or more legs of the magnetic circuits provides novel means to store and gate electrical signals as well as a means to transmit according to a stored setting.*

The Transfluxor can control, for an indefinitely long time, the transmission of a-c power according to a level established by a single setting pulse. This level can have any value in a continuous range, from almost zero to some maximum, thus affording either "on-off" or "continuous" stored control.

The operation of a two-aperture Transfluxor is described. The device has high efficiency of power transmission, short setting time, negligible coupling between setting and output circuits and sharp setting thresholds. These properties of the Transfluxor, possessed by no other passive element, make it useful in a great many applications in various fields of electronics.

Introduction

THE recent advent of magnetic materials with nearly rectangular hysteresis loops, particularly of "ferrites," has opened a new era in storing and switching devices. Arrays of memory cores are presently the best known means to obtain selective address memories of large storage capacity and short access time. Magnetic shift registers and magnetic combinatorial switches are the basis of many computing and controlling devices. In all these applications toroidal or ringed-shaped cores which have single apertures and unique flux paths are used.

This paper describes a novel device which is based on the fact that completely new switching and storing functions become possible when two or more apertures are made in the rectangular hysteresis loop cores, thereby creating a number of distinct legs and flux paths in the magnetic circuit. The new device operates by the controlled transfer of flux from leg to leg in the magnetic circuit and was consequently named "Transfluxor."

The most important property of the Transfluxor is its ability to control an indefinitely long flow of alternating electric power according

* Decimal Classification: R282.3.

to the setting established by a single electric pulse. The energizing a-c drive will or will not produce an a-c output depending upon the nature of the last setting pulse to which the Transfluxor was subjected. Furthermore, intermediate setting is possible for which an output of any desired level in a continuous range between the blocked (almost zero) and unblocked levels will be produced according to the amplitude of a single setting pulse. The Transfluxor may be thought of as being a transformer in which the effective amount of magnetic material coupling the primary and secondary can be adjusted by a single pulse. In its on-off operating mode, the Transfluxor is a one-bit storage element whose state can be ascertained any arbitrary number of times without altering that state, i.e., a storage element with "nondestructive" read-out.

The setting and output electric circuits need not be coupled in the Transfluxor as they necessarily are in the single-apertured core. This property of isolation of the input and output circuits renders the Transfluxor most useful even in those applications where only a single output pulse is required for a given setting.

The storage and switching capabilities of the Transfluxor outlined above render it potentially most important for many applications, and make possible entirely new devices and systems. This paper describes the principle of the Transfluxor and the behavior of a typical model comprising a core with two circular apertures of unequal diameter molded from square-loop ferrite.

Principle of the Transfluxor

Consider a core made of magnetic material such as a molded ceramic ferrite which has a nearly rectangular hysteresis loop and consequently a remanent induction B_r substantially equal to the saturated induction B_s. Let there be two circular apertures of unequal diameter which form three distinct legs, 1, 2, and 3 in the magnetic circuit, as illustrated in Figure 1. The areas of the cross sections of the legs 2 and 3 are equal and the cross section of leg 1 is equal to, or greater than, the sum of those of legs 2 and 3. There are windings W_1 on leg 1 and W_3 and W_0 on leg 3, shown with single turns for the sake of simplicity.

The operation of the device may be explained as follows: Assume that at first an intense current pulse is sent through winding W_1 in a direction to produce a clockwise flux flow which saturates legs 2 and 3. This is possible since the larger leg 1 provides the necessary return path. These legs will remain saturated after the termination of the pulse since remanent and saturated inductions are almost equal.

Consider now the effect of an alternating current in winding W_3 linking leg 3, producing an alternating magnetomotive force along a path surrounding the smaller aperture, as shown by the shaded area in Figure 1. When this magnetomotive force has a clockwise sense, it tends to produce an increase in flux in leg 3 and a decrease in leg 2. But no increase of flux is possible in leg 3 because it is saturated; consequently there can be no flux flow at all, since magnetic flux flow is necessarily in closed paths. Similarly, during the opposite phase of

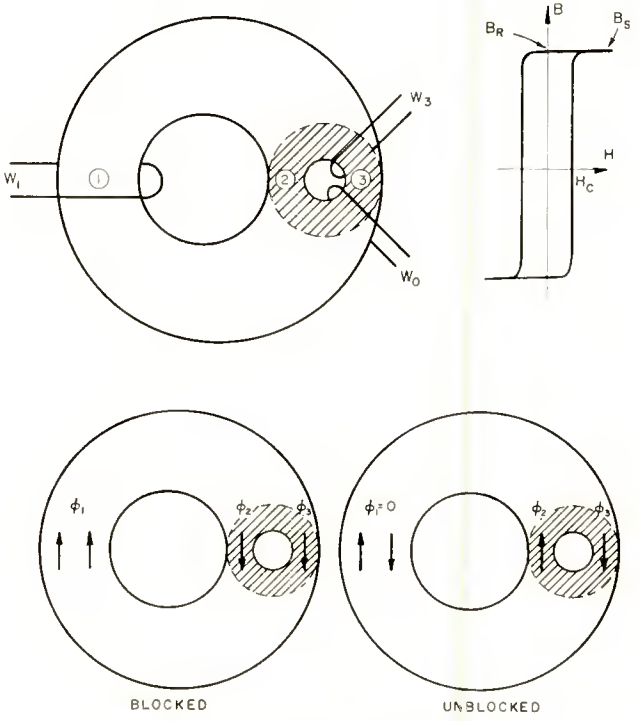

Fig. 1—Principle of Transfluxor.

the a-c, the magnetomotive force is in a counter-clockwise sense and tends to produce an increase of flux in leg 2, which is again impossible since that leg is saturated. Consequently, flux flow is "blocked" as the result of the direction of saturation of either leg 2 or 3. The Transfluxor is in its "blocked" state and no voltage is induced in an output winding W_0 linking leg 3.

Consider now the effect of a current pulse through winding W_1 in a direction producing a counter-clockwise magnetomotive force. Let this pulse be intense enough to produce a magnetizing force in the

closer leg 2 larger than the coercive force H_c but not large enough to allow the magnetizing force in the more distant leg 3 to exceed the critical value. This pulse, called hereafter the "setting pulse," will cause the saturation of leg 2 to reverse and become directed upwards (Figure 1) but will not affect leg 3 which will remain saturated downward. In this condition, the alternating magnetomotive force around the small aperture resulting from the alternating current in winding W_3 will produce a corresponding flux flow around the small aperture. The first counterclockwise phase of the a-c will reverse the flux, the next clockwise phase will reverse it again, etc., indefinitely. This flow may be thought of as a back-and-forth transfer of flux between legs 2 and 3. The alternating flux flow will induce a voltage in the output winding W_0. This is the "unblocked" or "maximum set" state of the Transfluxor.

It is seen that the Transfluxor is blocked when the directions of remanent induction of the legs surrounding the smaller aperture are the same and unblocked when they are opposite. In the blocked state the magnetic material around the small aperture provides essentially no coupling between the primary (W_3) and secondary (W_0) windings, while it provides a relatively large coupling between these two windings in the unblocked state.

There is a possibility that, in the blocked condition, a sufficiently large a-c in the phase tending to produce counterclockwise flux flow could in fact change the flux in leg 3 by transferring flux to leg 1. There is therefore a limit to the permissible amplitude of the a-c which is imposed by the possibility of "spurious unblocking." This limit is increased by the use of unequal hole diameters rending the flux path via legs 1 and 3 much longer than via legs 2 and 3. There is no danger of spurious unblocking by the a-c in the phase tending to produce a clockwise flux flow, since in this phase leg 3 is being magnetized in the direction in which it is already saturated. Therefore there is a considerable advantage in using asymmetric alternating current or a train of interlaced relatively large "driving" pulses (clockwise) and relatively small "priming" pulses (counter clockwise). The driving pulses, which cannot possibly spuriously unblock a blocked Transfluxor, can be arbitrarily large, with the result that when the Transfluxor is unblocked by proper setting, these pulses may not only provide the required minimal reversing magnetizing force around the small aperture but also provide substantial power to deliver large output currents. The priming pulses must be of sufficient magnitude to provide the required magnetizing force around the small aperture but insufficient to provide it around both apertures.

The Transfluxor can also be set to any level in a continuous range

in response to the amplitude of a single setting current pulse. Once set, it will deliver indefinitely an output proportional to the setting. This operation may be explained with simplifying idealizations as follows: Consider first the Transfluxor in its blocked condition. Let there be a setting current pulse through winding W_1 of a chosen amplitude and, of course, of a polarity opposite that of the original blocking pulse. A magnetizing force H, proportional to this current, is produced around the large hole. This force is greatest at the periphery of the hole and diminishes gradually with distance. In the case of a circular aperture it is inversely proportional to the radius. Therefore, for the given selected amplitude of the setting current pulse, there will be a critical circle separating an inner zone, in which the

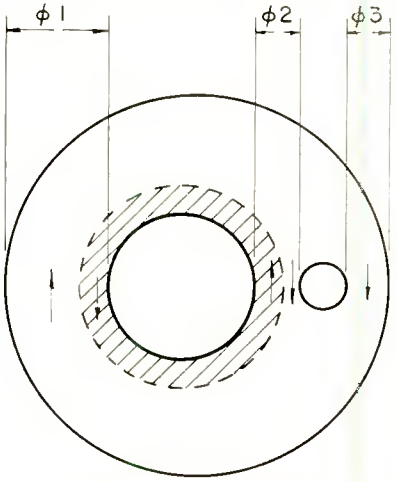

Fig. 2—Setting the Transfluxor to a level in a continuous range.

magnetizing force is larger than the threshold magnetizing force H_c required to reverse the sense of flux flow, and an outer zone, where this field is smaller than the threshold value. These two zones are shown in Figure 2. Consider now an indefinitely long sequence of priming and driving pulses. The priming pulse, applied to leg 3 in a direction to produce downward magnetization in leg 2, can change only that part of the flux in leg 2 which is directed upwards, namely, that part which has been "set" or "trapped" into that leg by the setting pulse. This changing part of the flux will flow through leg 3 until leg 2 reaches its original downward saturation. The amount of flux set into leg 2 is therefore transferred to leg 3. The next driving pulse, which follows the priming pulse, applied to leg 3 in a direction to produce a downward magnetization, will saturate leg 3 to its original downward

direction and retransfer the trapped amount of flux back to leg 2. There is no danger of any transfer of flux to leg 1, since the magnetizing path is much longer through that leg, and once leg 3 is saturated no further flux flow is possible however intense the driving pulse. It is apparent therefore that the succession of priming and driving pulses will cause an interchange between legs 2 and 3 of an amount of flux just equal to that initially set into leg 2. This will produce across the output winding W_0 an indefinitely long train of voltage pulses.

When priming and driving, the flux in leg 1 is not affected by the interchange of flux between legs 2 and 3, so that there is no coupling between the output and input circuits. When setting, there is also no coupling between the input and output circuits because no flux is changed in leg 3, but only in legs 1 and 2. The same applies when blocking occurs after driving, rather than priming, since the drive pulse has already saturated leg 3 in the direction of blocking and no further flux change is possible.

Departures from Idealized Magnetic Properties

The operation of the Transfluxor is substantially as explained above even when the magnetic properties of its core deviate considerably from the idealized ones assumed for the sake of simplicity.

The magnetic properties of a homogenous material can be characterized by the relation between the magnetic induction B and the magnetizing force H of an elementary volume of the material. These characteristics are usually given in the form of a family of hysteresis loops whose outer envelope is the major loop and which includes a set of symmetrical minor loops as well as sets of minor unsymmetrical loops. The entire family of loops is necessary for the complete specification of all reversible and irreversible flux flow properties.

The distribution of the magnetic induction B in a homogenous body of given geometry having a certain family of hysteresis loops is determined by the history of the electrical currents which have linked and are linking the apertures in the body. This distribution is determined by two fundamental laws:

(1) Continuity of magnetic flux flow requires that the lines of magnetic induction be closed on themselves, and

(2) The line integral of the magnetizing force along any closed path is proportional to the electric current flowing through the area enclosed by that path ($Ni = \oint \mathrm{Hds}$).

The exact general solution of the distribution of magnetic induction for the geometry and material of the Transfluxor is difficult to obtain. However, the essential behavior of the device can be obtained from phenomenological considerations and is as follows:

(1) A gradual diminution of flux interchanged back-and-forth between legs 2 and 3 would occur if, for every transfer, a small amount of flux was irreversibly lost to leg 1. One might at first suppose that very rectangular loops are required to prevent such cumulative losses and make the "Transfluxor action" possible.

Analysis shows that this is not the case even with very nonrectangular loops, provided there is appreciable remanence. When leg 3 is a-c driven, it describes a relatively large closed hysteresis loop and this causes legs 2 and 1 to describe loops that are closed as well, leg 2 describing a larger loop than leg 1. The fact that the loop of leg 1 is closed indicates that there is no irreversible loss of flux to it. The reversible flux excursion of leg 1 is reduced when that leg is spaced further from legs 2 and 3.

In general, the steady-state closed loops are not reached during the first cycle of the a-c, but require several cycles. However with materials having nearly rectangular hysteresis loops, used in practical Transfluxors, the steady state loops are substantially reached by the end of the first cycle.

(2) The amount of flux interchangeable between legs 2 and 3 is determined by the setting pulse on leg 1 and does not depend upon whether all the setting flux from leg 1 was originally transferred to leg 2 only or whether it was shared between legs 2 and 3. The first priming pulse will concentrate all of the set flux in leg 3 no matter what the original distribution between legs 2 and 3 might have been. Subsequent drive and prime pulses will interchange an amount of flux which will reach a steady-state value after a few cycles during which a negligibly small amount will be lost by retransfer to leg 1 as mentioned under (1).

(3) While any appreciable hysteresis is sufficient for Transfluxor action, hysteresis loops as rectangular as possible are still desirable because:

(a) The undesirable interchangeable flux in the blocked condition due to imperfect saturation of legs 2 and 3 is less.

(b) The coupling between legs 1 and 3 is smaller, increasing the isolation of the control and output circuits.

(c) The threshold of the setting current pulse is sharper and therefore the device is more useful in switching applications.

Transfluxor Action

The Transfluxor exercises control by means of the amount of flux which can be transferred for an indefinitely long time between legs 2 and 3, and which can be set by a single pulse to any desired value in a continuous range. This back-and-forth transfer of flux between legs 2 and 3 can be considered also as a back-and-forth reversal of flux around the small aperture along a path which is effectively the output magnetic circuit and may be characterized by a conventional hysteresis loop relating the flux flow and the magnetomotive force on leg 3 producing it. Figure 3 shows a photograph of oscilloscope traces of a family of such loops, each obtained for a different setting including the blocked and maximum settings. For a setting magnetomotive force below a threshold value, the amount of reversing flux is negligible and

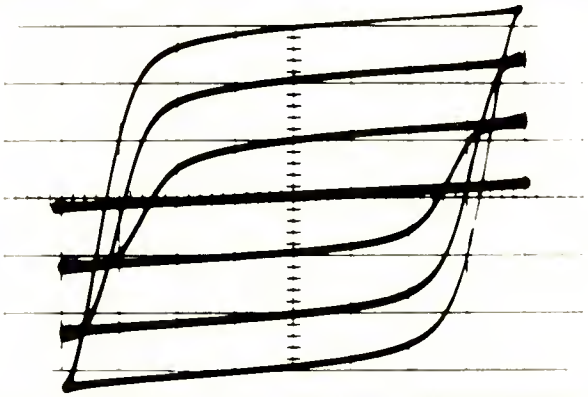

Fig. 3—Hysteresis loops of the output magnetic circuit for various settings.

the hysteresis loop approaches a horizontal line. Above the threshold the change of the amount of reversing flux with respect to the setting magnetomotive force is linear. The sharp threshold and the subsequent linear range are important features of the Transfluxor.

It is apparent that the Transfluxor operates as if the output magnetic circuit consisted of a conventional one-apertured core with the essential property that the effective cross-sectional area of that core can be adjusted by a single set pulse to any desired value from practically zero to a maximum value equal to the physical cross-sectional area of its smallest leg.

The two-aperture Transfluxor has been discussed to illustrate the principles of operation and the general properties of the device in one of its simplest forms. The use of more than two apertures creates many new modes of flux transfer and broadens the kind and number of switching and storing functions, making possible many applications. This was demonstrated in a number of test models.

Conclusion

The Transfluxor has the unique property of being able to control the transmission of electrical power according to a stored level established by a single setting pulse. On-off or intermediate settings can be established in microseconds without producing any output by themselves. The transmission of power is efficient and does not feed back into the setting circuit.

In contrast to the magnetic amplifier in which the input is not stored and must be present at all times, the Transfluxor requires only a single setting. In contrast to the conventional memory core, the Transfluxor is not only capable of storing a given amount of set-in flux but also is capable of furnishing on demand, and for an indefinite length of time an output according to the stored setting without affecting that setting in the least. In a sense, the Transfluxor combines the functions of a magnetic amplifier and a memory core.

The Transfluxor is a solid-state passive device of simple construction. It is rugged and stable in operation; no permanent deterioration can occur by overdriving any of the associated circuits.

The Transfluxor has unique properties, useful in many fields, and may well become a basic component of electronic circuits.

Acknowledgment

George R. Briggs of these Laboratories has greatly contributed to the understanding of the operation of the Transfluxor and helped in many experimental phases of the work.

RCA TECHNICAL PAPERS†

First Quarter, 1955

Any request for copies of papers listed herein should be addressed to the publications to which credited.*

"Beam Focusing by Periodic and Complementary Fields," K. K. N. Chang, *Proc. I.R.E.* (January) 1955

"Calculation of Radiant Photoelectric Sensitivity from Luminous Sensitivity," R. W. Engstrom, *RCA Review* (March) 1955

"Class B Operation of Audio-Frequency Junction Transistors," K. E. Loofbourrow, *RCA Industry Service Laboratory Bulletin LB-975* (March 25) 1955

"Color Equipment Planning," L. E. Anderson, *Broadcast News* (February) 1955

"Color Servicing," W. W. Cook and C. E. Lasswell, *Radio-Electronics* (January) 1955

"Comparative High-Frequency Operation of Junction Transistors Made of Different Semiconductor Materials," L. J. Giacoletto, *RCA Review* (March) 1955

"Decilog," J. B. Moore, *Elec. Eng.* (March) (Letter to Editor) 1955

"Deflection and Convergence of the 21-Inch Tri-Color Kinescope," M. J. Obert, *RCA Review* (March) 1955

"Delayed Collector Conduction, a New Effect in Junction Transistors," M. C. Kidd, W. Hasenberg, and W. M. Webster, *RCA Review* (March) 1955

"Development of a 21-Inch Metal-Envelope Color Kinescope," H. R. Seelen, H. C. Moodey, D. D. VanOrmer, and A. M. Morrell, *RCA Review* (March) 1955

"Direct Titration Method for Determination of Barium," S. B. Deal, *Analytical Chemistry* (January) 1955

"The Effect of Superposing a Small Alternating Excitation on the Steady Excitation of a Luminescent Material," K. F. Stripp and R. H. Bube, *Jour. Appl. Phys.* (February) (Letter to the Editor) 1955

"An Electron Tube for High-Speed Teleprinting," W. H. Bliss and J. E. Ruedy, *RCA Review* (March) 1955

"Energy Levels of a Disordered Alloy," R. H. Parmenter, *Phys. Rev.* (February 1) 1955

"Equipment for Evaluating Lenses of Television Systems," E. Hutto, Jr., *Jour. S.M.P.T.E.* (March) 1955

"Evaluation of High-Fidelity Phono Pickups," J. M. Salani, *Audio* (March) 1955

"A Fifteen-Kilovolt Beam Power Tube for UHF Service," W. P. Bennett, *I.R.E. Transactions* BTS (March) 1955

"Ground State of Impurity Atoms in Semiconductors Having Anisotropic Energy Surfaces," M. A. Lampert, *Phys. Rev.* (January 15) 1955

† Report all corrections or additions to RCA Review, RCA Laboratories, Princeton, N. J.
* *RCA Industry Service Laboratory Bulletins* are not published and are issued only as a service to licensees of the Radio Corporation of America.

"How to Plan for Color Television Broadcasting—Part I," L. E. Anderson and W. O. Hadlock, *Tele-Tech* (February) 1955

"How to Plan for Color Television Broadcasting—Part II," L. E. Anderson and W. O. Hadlock, *Tele-Tech* (March) 1955

"Large-Area High-Current Photoconductive Cells Using Cadmium Sulfide Powder," S. M. Thomsen, B. Kazan, and F. H. Nicoll, *RCA Industry Service Laboratory Bulletin LB-967* (January 19) 1955

"On the Measurement of the Average Time Delay in Secondary Emission," M. H. Greenblatt, *RCA Review* (March) 1955

"Methods for Revealing p-n Junctions and Inhomogeneities in Germanium Crystals," J. I. Pankove, *RCA Industry Service Laboratory Bulletin LB-971* (February 18) 1955

"National Television Servicemen's Week," D. Y. Smith, *Rad. and Tele. News* (March) 1955

"New Developments in Electronics," D. Sarnoff, *Elec. Eng.* (March) 1955

"A New Method for Magnifying Electron Beam Images," W. R. Beam, *RCA Industry Service Laboratory Bulletin LB-970* (February 17) 1955

"New TV and Radio Test Equipment," R. Samuel, *Rad. and Tele. News* (March) 1955

"Nomographs for Rectangular Waveguides," T. S. Chen, *Electronics* (January) 1955

"Optimum Design of Periodic Magnet Structures for Electron Beam Focusing," K. K. N. Chang, *RCA Review* (March) 1955

"Pattern Measurements of RCA UHF TV Antennas," E. H. Shively and L. D. Wetzel, *Broadcast News* (February) 1955

"A Phase Rotation Single-Sideband Generating System," J. R. Hall, *RCA Review* (March) 1955

"Photoconductivity and Crystal Imperfections in Cadmium Sulfide Crystals. Part I. Effect of Impurities," R. H. Bube and S. M. Thomsen, *Jour. Chem. Phys.* (January) 1955

"Photoconductivity and Crystal Imperfections in Cadmium Sulfide Crystals. Part II. Determination of Characteristic Photoconductivity Quantities," R. H. Bube, *Jour. Chem. Phys.* (January) 1955

"Polaragraphic Determination of Cadmium and Zinc in Zinc-Sulfide–Cadmium Sulfide Phosphors," S. B. Deal, *Analytical Chemistry* (January) 1955

"Pole Mount Microwave Station," P. A. Greenmeyer, *Radio-Electronic Engineering* (January) 1955

"Properties of Ohmic Contacts to Cadmium Sulfide Single Crystals," R. W. Smith, *Phys. Rev.* (March 15) 1955

"Recombination Processes in Insulators and Semiconductors," A. Rose, *Phys. Rev.* (January 15) 1955

"Reduction of Spurious Signals in Image Orthicon Cameras," A. A. Rotow, *Broadcast News* (February) 1955

"Reliability Starts at the Materials Level," C. Eddison, *Electrical Manufacturing* (March) 1955

"A Sandwich-Type Metal-to-Ceramic Vacuum-Tight Seal," N. E. Pryslak, *Ceramic Age* (March) 1955

"Saturation Current in Alloy Junctions," W. M. Webster, *Proc. I.R.E.* (March) 1955

"Selectivity and Transient Response Synthesis," R. W. Sonnenfeldt, *RCA Industry Service Laboratory Bulletin LB-968* (January 24) 1955

"Semiconductors and the Transistor," E. W. Herold, *Jour. Frank. Inst.* (February) 1955

"Space-Charge-Limited Currents in Single Crystals of Cadmium Sulfide," R. W. Smith, *Phys. Rev.* (March 15) 1955
"Space-Charge-Limited Currents in Solids," A. Rose, *Phys. Rev.* (March 15) 1955
"Staple Problem," J. Pastor, Jr., *Electronics* (March) (Letter to the Editor) 1955
"Studies of Externally Heated Hot Cathode Arcs," E. O. Johnson and W. M. Webster, *RCA Review* (March) 1955
"Studio Amplifier Design for Color Television," J. O. Schroeder, *Electronics* (March) 1955
"Technique for Fabricating Small Cylindrical Grids of Novel Design for Use in Pencil Tubes," H. J. Ackerman, *RCA Industry Service Laboratory Bulletin LB-973* (March 4) 1955
"Television and Electronics," D. Sarnoff, *Radio-Electronics* (January) 1955
"Transistorized Portable Receiver," G. B. Herzog and R. D. Lohman, *Radio-Electronics* (January) 1955
"Transistorized Sync Separator Circuits for Television Receivers," H. C. Goodrich, *RCA Industry Service Laboratory Bulletin LB-974* (March 25) 1955
"Traveling-Wave Tube System Having Multiplied Gain," F. R. Arams, *Proc. I.R.E.* (January) (Letter to the Editor) 1955
"TS-11A Switcher Offers New 'Preview' and 'Rehearsal' Features," C. R. Monro, *Broadcast News* (February) 1955
"A UHF–VHF Tuner Using Pencil Tubes," W. A. Harris and J. J. Thompson, *I.R.E. Transactions* BTR (January) 1955
"Unusual Assembly Methods Used in Developing a New Thyratron," N. R. Goldstein, *RCA Industry Service Laboratory Bulletin LB-972* (March 4) 1955
"Variation of the Conductivity of the Semitransparent Cesium-Antimony Photocathode," W. Widmaier and R. W. Engstrom, *RCA Review* (March) 1955
"The Variation of Current Gain with Junction Shape and Surface Recombination in Alloy Transistors, Part II," K. F. Stripp and A. R. Moore, *RCA Industry Service Laboratory Bulletin LB-966* (January 17) 1955
"Wide Screens in Drive-in Theaters," R. H. Heacock, *Jour. S.M.P.T.E.* (February) 1955
"Wind Velocity and its Effect on Transmitting Antennas and Towers," D. W. Balmer, *Broadcast News* (February) 1955

AUTHORS

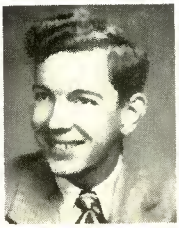

GEORGE W. BARCLAY received the B.S. degree in Electrical Engineering from the University of Vermont in 1952. After graduation, he joined the RCA Specialized Training Program for a period of one year. Upon completion of this program, he joined the Receiving Tube Development Group of the Tube Division at Harrison, New Jersey. Mr. Barclay's work is concerned primarily with the development of pencil-type and premium tubes.

WALTER R. BEAM received the B.S. degree in Electrical Engineering from the University of Maryland. He pursued graduate work while serving as Instructor in Electrical Engineering at the same university, and received the M.S. degree in 1950. During part of this period he was also engaged in development of radio sounding instruments at Washington Institute of Technology. He joined the Microwave Tube group at RCA Laboratories in 1952. In 1953 he was awarded the Ph.D degree from the University of Maryland. Since joining RCA he has been engaged in research on microwave amplifiers and electron guns. Dr. Beam is a member of Institute of Radio Engineers, Tau Beta Pi, and Sigma Xi, and is a licensed Professional Engineer.

STANLEY BLOOM received the B.S. degree in Physics and Mathematics from Rutgers University in 1948. In 1949 he received the M.S. degree in Physics and in 1952, the Ph.D. degree in Physics from Yale University. In 1952 he joined the RCA Laboratories where he has engaged in research on noise problems in traveling-wave tubes. Dr. Bloom is a Member of the American Physical Society, Sigma Xi, and Phi Beta Kappa.

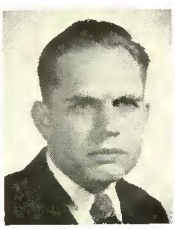

GEORGE W. GRAY attended Princeton University as a civilian and in the Navy V-12 Program until 1943 when he was assigned to active duty in the Navy. After release to inactive duty in 1946, he returned to Princeton University and received the B.A. degree in Physics. In March of 1947 he joined the technical staff of RCA Laboratories Division at Princeton, N. J. He is at present a member of the Electronic Research Laboratory engaged in television research. Mr. Gray is a member of Sigma Xi.

WILLIAM A. HARRIS received the B.S. degree in Electrical Engineering from Rose Polytechnic Institute, Terre Haute, Indiana in 1927. From 1927 to 1929, he was employed by the General Electric Company, first in Lynn, Massachusetts and later in the Radio Department at Schenectady, New York. He transferred to RCA in 1930, and has been with the Tube Division at Harrison, N. J. since 1931. He is now a member of the Advanced Development Group. Mr. Harris is a Fellow of the Institute of Radio Engineers.

ARTHUR S. JENSEN received the B.S. degree in 1938, the M.S. degree in 1939, and the Ph.D degree in 1941 in Physics from the University of Pennsylvania where he was a research fellow from 1939 to 1941. After a short period as a research physicist at the Naval Research Laboratory, he reported for active duty with the U. S. Naval Reserve in August, 1941. From then until 1946 he served as an officer-instructor in physics and aviation physics at the U. S. Naval Academy with the rank of Commander. At the end of 1945, he joined RCA Laboratories where he has been engaged in research on storage tubes, switching tubes and associated circuits. Dr. Jensen is a Senior Member of the Institute of Radio Engineers and a member of the American Physical Society, the American Association of Physics Teachers, the American Association for the Advancement of Science, Pi Mu Epsilon, and Sigma Xi.

L. L. KOROS graduated in 1925 from the Royal Joseph Technical University, Budapest, Hungary, as an Electrical and Mechanical Engineer. He then joined a European associate of the International Telephone and Telegraph Company of New York and in 1932 he became the managing Director of the Stabilovolt Company within the same organization. He joined the Radio Corporation of America in 1943. Up to 1948 he was Chief Design Engineer of the Transmitter and Special Products Department in charge of engineering and production of the RCA Victor Argentina Company in Buenos Aires. While in Argentina, he taught a postgraduate course on transformer design at the La Plata University. Since 1948 he has been working in the Engineering Products Division, Camden, N. J. During the last six years he has been in charge of developmental projects on magnetrons, klystrons, and grid-controlled tubes for high-power UHF transmitter applications. Mr. Koros is a Senior Member of the Institute of Radio Engineers.

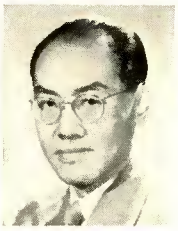

ARTHUR W. LO received the B.S. degree in 1938 from Yenching University and taught at West China Union University and Yenching University in China. He received the M.S. degree in Physics from Oberlin College in 1946, and the Ph.D. degree in Electrical Engineering from the University of Illinois in 1949. He was an assistant professor at Michigan College of Mining and Technology and a lecturer at the City College of New York before joining RCA in 1951. His work in RCA has been in the field of transistor and magnetic circuits. Dr. Lo is a member of Sigma Xi, Phi Kappa Phi, Pi Mu Epsilon, Eta Kappa Nu, and the Institute of Radio Engineers.

JAN A. RAJCHMAN, received the diploma of Electrical Engineering in 1934 and the degree of Doctor in Technical Sciences in 1938 from the Swiss Federal Institute of Technology. In 1936 he joined the Research Department of the RCA Manufacturing Company in Camden, New Jersey. In 1942 he was transferred to the RCA Laboratories Division in Princeton, New Jersey. Dr. Rajchman is a Senior Member of the Institute of Radio Rajchman is a Fellow of the Institute of Radio Engineers, a Member of the American Physical Society, Sigma Xi, and the Association for Computing Machinery, and co-recipient of the Levy Medal of the Franklin Institute 1946.

JOHN J. THOMPSON received the B.E.E. degree from Pratt Institute, Brooklyn, New York in 1950. From 1943 to 1946, he served as a Radar Technician in the United States Marine Corps. In 1950, he joined the Specialized Training Program of the Radio Corporation of America. After completing this program, he was assigned to the Advanced Development Group of the Tube Division in Harrison, N. J. Mr. Thompson is a member of Tau Beta Pi.